ABSTRACT

SONG, YI. A Numerical Modeling Study of the Coupled Variability of Lake Victoria in Eastern Africa and the Regional Climate. (Under the direction of Dr. Fredrick H. M. Semazzi.)

The objective of this investigation was to investigate and study the coupled atmosphere-lake climate system over the Lake Victoria basin, and determine the corresponding physical mechanisms that are involved. The primary research vehicle for the investigation is a fully coupled model of the regional climate of Eastern Africa and Lake Victoria which has been developed and applied in this study. The atmospheric component of the model is the NCAR Regional Climate Model (RegCM2). The lake component of the model is based on the Princeton Ocean Model (POM) configured for Lake Victoria by replacing the open boundaries in the standard version of the model with a closed coastline and adopting the bythemetry of Lake Victoria. The horizontal resolution is 20 km for both the atmosphere and lake model components.

The results show that the bythemetry and geometry of the lake play a fundamental role in determining the climatology of Lake Victoria. There exists Kelvin-like waves in the thermocline trapped along the coast and they propagate clockwise around Lake Victoria with periodicity of about 30 days. The oscillations entirely disappear in the case of the isothermal conditions. The 3-dimensional model produces a surface temperature pattern indicative of horizontal lake water mixing associated with the horizontal spiral pattern that is not present in the 1-dimensional model. Preliminary comparison of the coupled RegCM2-POM model simulation results with the observations indicates that the model

produces more realistic lake surface temperatures (LST) and rainfall over and around the lake than the standard version of RegCM2 in which a simple one dimensional thermal diffusion lake model is used.

Over Eastern Africa, the regional climate variability is significantly influenced by the circulation over the Lake Victoria basin. Moisture advection contribution is important but secondary to evaporation in explaining the heavy rainfall over the lake. The interaction between the lake-land breeze and the prevailing northeasterly flow accounts for the asymmetry in the distribution of the diurnal rainfall variations and the southwestward movement of the dominant bands of divergence/convergence.

During the 1982 El Nino when the averaged LST over the lake was higher than that during the normal year, the LST gradient was weakened along the SW-NE axis over the lake by the strong lake circulation. This results in LST distribution whereby the southwestern region of the lake is cooled while the region of maximum LST moves to the central-eastern region of the lake from the southwestern region of the lake. The net change in rainfall distribution over the lake during the 1982 El Nino is a combination of the effect associated with the large-scale convergence pattern and the meso-scale climate changes associated with the shift of the region of maximum rainfall toward the central-eastern part of the lake from the western part of the lake in response to the LST redistribution. Conversely, the weaker lake circulation enhances the LST gradient over the western part of the lake, especially over the northwestern region, and the rainfall maxima is still found over the northwestern sector of the lake. Therefore, the hydrodynamics of the lake play an important role in determining the coupled variability

of the lake circulation and the lake basin-wide climatic conditions. This outcome based on the use of the coupled 3-dimensional lake model is not reproducible from the corresponding simulations based on the coupled 1-dimensional lake model. It is therefore apparent, that neglecting the lake's hydrodynamics and basing the lake model only on thermodynamical considerations deprives the coupled regional climate model of the ability to transport heat efficiently within the lake and thereby degrades the simulation of the climate downstream over the rest of the lake and the surrounding regions.

The potential climate change resulting from total clearing of the tropical rain forests in Africa was also investigated by the standard version of the NCAR CCM3 global climate model. Over Eastern and Western Africa the impact of deforestation is primarily characterized by reduction in rainfall, however the CCM3 resolution of T42 which we have adopted may not be adequate to resolve the large contrasts in terrain and vegetation types. A striking result is that the strong remote response of the Southern Africa region to deforestation over Central Africa. This may be attributed to the role of the trapped large amplitude Rossby waves which transmit the response signal a long distance away from the source region.

Based on the present results we infer that, the downscaling would be highly beneficial not only for the immediate region of Eastern and Central Africa where significant removal of tropical forest vegetation cover could occur in the coming decades, but also for the region further south to infer the projected detailed response of the Southern Africa region to remote deforestation effects.

A Numerical Modeling Study of the Coupled Variability of Lake Victoria in Eastern Africa and the Regional Climate

by

YI SONG

A thesis submitted to the Graduate Faculty of
North Carolina State University
in partial fulfillment of the
requirements for the Degree of
Doctor of Philosophy

MARINE, EARTH AND ATMOSPHERIC SCIENCES

Raleigh, North Carolina, USA
2000

APPROVED BY

Dr. Adel F. Hanna

Dr. John Morrison

Dr. Lian Xie
Co-Chair of Advisory Committee

Dr. Fredrick H. M. Semazzi
Co-Chair of Advisory Committee

DEDICATION

The author dedicates this work to his parents Quanshen Song and Qingmei Gao, his wife Ying Zhang, his brother and sisters for their patience, support and encouragement through the years.

BIOGRAPHY

Yi Song was born in Handan, Hebei Privince, P. R. China and spent the first eighteen years of his life there. He began to study Meteorology at Peking University in 1984 and received his B.S. in Meteorology from Department of Geophysics in July 1988. He continued his graduate studies at Chinese Academy of Meteorological Sciences and earned a M.S. in Climate Dynamics in May 1991. Thereafter he worked at the academy as an assistant professor for two and half years, and then moved to National Climate Center to work as an assistant professor for two and half years. Beginning Fall 1996, Yi embarked on a doctoral degree in Atmospheric Science at North Carolina State University under the sponsorship of his advisor's National Science Foundation (NSF) research grants. The development of a fully coupled three-dimensional atmosphere-lake regional climate model was the focus of his research.

ACKNOWLEDGEMENTS

I would like to express my sincerest thanks and highest appreciation to my advisor Dr. Fredrick H. M. Semazzi for his kindness, patience, guidance and motivational support during my study at North Carolina State University. I would also like to thank Dr. Lian Xie, co-chairman of my advisory committee, for his encouragement and helpful discussions during this research. I would also like to express my sincere appreciation to Dr. John Morrison and Dr. Adel Hanna for their valuable advice and assistance, which greatly improved the research, and manuscripts of this dissertation.

I would also thank Dr. Ping-Tung Shaw who provided me with much help on Kelvin waves. I further extend my deep appreciation to my colleagues, particularly those at the Climate Research Laboratory and the Facility for Atmospheric Modeling and Visualization ($FOAM^V$) at North Carolina State University: Richard Anyah, Ray Burton, Dr. Feng Ding, Dr. Hao Jin, Dr. Yi Jin, Xiaoming Liu, Ling Mao, Dr. Indeje Matayo, Dr. Ramachandran Nair, Gilbert Ouma, Machuan Peng, Dr. George Pouliot, Dr. Jianhua Qian, Nelson Settumba, Dr. Shaohua Shen, Yukuan Song, Dr. Liqiang Sun, Dr. Kejian Wu, Bowei Xu, Tingzhang Yan, Chen Zhang, Dr. Fuqing Zhang, Dr. Jing Zhang and Li Zhao for their general assistance.

This work was supported by National Science Foundation under grant ATM-9113511. The model integrations were performed on the North Carolina Supercomputing Center on the T90 supercomputer and NCAR Cray-J90 supercomputer. The post-processing of the model output was carried out at FOAMV visualization and parallel computing facility at NCSU.

TABLE OF CONTENTS

Page

LIST OF TABLES

LIST OF FIGURES

Chapter 1

Introduction

The African continent (Fig. 1.1) is the only one that straddles the equator with roughly equal landmasses within both hemispheres. It is one of the three major tropical land masses (along with South America and Indonesia-Borneo or the so-called maritime continent). Africa is also surrounded by two of the three tropical oceanic basins. As a consequence of its vast size and proximity to the equator, Africa experiences a wide variety of climate regimes ranging from deserts to tropical rain forests (Nicholson et al., 1988; and Krishnamurti and Ogallo, 1989). The poleward extremes of the continent experience winter rainfall associated with the passage of the middle-latitude synoptic disturbances. Across the Kalahari and Sahara desert regions, precipitation is inhibited by sinking motion virtually throughout the year. In contrast, the equatorial and tropical regions are characterized by abundant precipitation concentrated along the Inter-Tropical Convergence Zone (ITCZ). Since the movement of the ITCZ trails the position of maximum surface heating associated with the north/south displacement of the overhead position of the sun, the near equatorial regions have two rainy seasons while most of the other regions of the continent get only one distinct rainy period during the year (Fig. 1.2). The climate of Africa is further modified by the presence of orography. The influence of the large-scale mountain barriers is well known and it is essentially characterized by

relatively drier conditions to the leeward side while wetter climate prevails on the windward slopes of the mountains. Evidence suggests that large-scale orography and the existence of lakes across the continent could be playing an important role in modulating the continental climate (Semazzi 1980 a, b; Semazzi and Sun 1997). This basic mean climate state is further significantly modified by the asymmetry of the continent, the adjacent ocean basin circulation, and the global Walker circulation. (Hastenrath, 1998).

Equatorial eastern African has complex topographical features, which include the Ethiopian highlands to the northeast and East African highlands to the southwest, the Great Rift Valley Lakes (Malawi, Tanganyika, and Victoria) and the west Indian Ocean sector. The eastern African climate is one of the most complex sectors of the African continent. The large-scale tropical climate regimes, which include several major convergence zones, are superimposed upon regional factors associated with complex terrain, extreme contrasts in vegetation type, the existence of large inland lakes and the proximity of the Indian Ocean (Fig. 1.1). As a result, the climate patterns over eastern Africa are extraordinarily complex, and change rapidly over short distances. The atmospheric dynamical and physical forcing varies on a scale of less than a few hundred kilometers (Ininda 1994). Land rainfall exhibits a high degree of spatial variability (Nicholson et al., 1988).

In the past, most investigations concerning the climate of eastern Africa were based on empirical analysis (e.g., Farmer 1988; Ogallo 1988). Despite the valuable insight gained through this approach, it has limited potential in clarifying the cause-effect relationships

associated with the climate variability of this region. Perhaps, the most effective and comprehensive tools used in the climate research are Global Climate Models (GCMs).

Current GCMs have attained a high level of sophistication, and simulated the main characteristics of general circulation reasonably well, but their performance in reproducing regional climate details is rather deficient (Giorgi et al., 1991). The effects of local forcing such as Lake Victoria are poorly resolved in GCMs. The failure to resolve the important local features of the forcing results not only in lack of regional detail of the simulated climate but also in marked inaccuracies in the large-scales resolved by the GCMs. The main constraint in using the GCMs to simulate regional climate is the limitation in the availability of computer resources. Computer speed and CPU memory required to run GCMs increases approximately with the second power of the horizontal grid point spacing (Giorgi. et al., 1991). Even with this rapid growth in computing power, in the foreseeable future, it will still not be feasible to conduct GCMs climate studies at sufficient resolution to deal adequately with meso-scale climate phenomena. Thus nested models with high resolution at a specific region of interest have a role to play in improving our understanding of the effects of local topography, vegetation, and hydrological forcing.

Recently, a collaborative effort among North Carolina State University, National Center for Atmospheric Research (NCAR), University of Nairobi (Kenya), and Drought Monitor Center (Kenya) has been initiated aimed at the development of a Seasonal Climate Prediction System (SCPS) for eastern Africa. Under this project, NCAR RegCM2 has

been successfully customized for the region of eastern Africa to form the RegCM2-EA version, and its performance in simulating the intra-seasonal and interannual climate variability has been examined (Sun, Semazzi, Giorgi, and Ogallo (1999a,b), hereafter, SSGO99ab). These studies have clearly demonstrated the feasibility of applying the nested modeling approach, based on RegCM2, for climate simulations. Given realistic large-scale lateral boundary conditions, the model is capable of simulating a realistic climatology in the interior of the domain as affected by the lateral boundary large-scale forcing and the internal high-resolution forcing characteristic of the region's geomorphology over eastern Africa, and able to reproduce the observed intraseasonal and interannual variability of precipitation over most of eastern Africa. This current study is a continuation of the work by SSOG99ab.

Lake Victoria (Fig. 1.1) is the largest freshwater lake in the tropics and it is the second in the world following the Great Lakes in the USA. The lake is situated in a major depression in eastern Africa. The lake straddles the Equator and it is approximately located at the center of the East Africa (Kenya, Tanzania and Uganda). Its rectangular coastline extends from 2.5°S to 0.5°N in the north-south direction and from 32°E to 34°E in the east-west direction, thus approximately 400 km long and 240 km wide, and its only major outlet is the river Nile which is the longest river in the World. Lake Victoria is one of the shallowest in eastern Africa with average (maximum) depth of about 45m (92m). The altitude of the lake surface is about 1135km above MSL (Anyamba, 1983; and IDEAL, 1996).

On longer time scales, several studies (Stager et. al 1986, Kendall 1969, have shown that lake Victoria has experienced large surface water level fluctuations during the past 25,000 years. Stager and et al (1986) have estimated that the water level was only 26m between 14,750 and 13,700 BP, thus nearly 50% of the present depth. Their estimates show that a 60m drop in lake level would result in a 20% decline in surface area and a 45% drop in the circumference. These paleoclimatic conditions need to be incorporated in recent regional modeling activities to infer the corresponding changes in the catchment rainfall and lake circulation, and thereby provide enhanced interpretation of the paleoclimate theories which have been proposed over the years.

Lake Victoria is facing a number of climate-related environmental problems which need immediate and concerted effort to halt the rapid environmental damage that is threatening its existence and that of its people. This onslaught is coming from all directions. The water Hyacinth is the most visible of all the problems. This weed (Eichornia Crossipes) is reported to have made its entry into the lake from Rwanda during the late 1980's (Muwonge, 1994). There are a number of methods of controlling the water Hyacinth which have been applied in other countries, but all the methods would benefit from improved ability to predict the conditions of the lake and the spread of the water Hyacinth by the its water currents using reliable numerical simulation models.

Deforestation around the shores of the lake and beyond is another major problem. Trees have been cut to provide local fuel for fish smoking and brick making activities along the lake shores. Improper cultivation has also flourished in some areas where trees have

been cleared thereby exposing the soil. Therefore, lack of vegetation cover has accelerated the runoff of top soil into the lake. Moreover, the increase in surface albedo, the reduction in evapotranspiration and surface roughness (Sud and Smith 1985, Sud et al. 1988, Nobre et al. 1991, and Williams 1990) associated with the degradation of vegetation could have a positive feedback on future rainfall.

Understanding of the climate variability and predictability of the lake at all time scales has important potential social-economic benefits. The lake Victoria basin is one of the three most agricultural productive areas in East Africa. The hydroelectric power station, at the source of the Nile supplies most of the commercial and domestic energy for Uganda and a significant amount for Kenya. The lake level and hence the productivity of the power plant are sensitive to the fluctuations in the local and regional climate and particularly to the occurrence of the global El Nino climate events. Lake Victoria is the primary source of municipality-water for domestic use as well as serving the major industrial cities of Kampala, Jinja, Kisumu, Musoma, Masaka, Musoma, Mwanza and Bukoba on the perimeter of the lake. The lake transport plays a key role in supporting the commercial needs of its catchment region. Furthermore, fishing from Lake Victoria contributes over 30% of the food supply for the population in the urban cities surrounding the lake. Any variations in the timing and intensity of rainfall over the lake basin tend to have diverse effects on agriculture and other social-economic planning in the region. During the 1982-1983 ENSO event alone, Africa suffered from economic losses estimated at well over US $ 3 billion over eastern and southern African (Indeje, 2000).

The losses associated with the 1997/98 ENSO surpassed that of 1982/83 in the countries of eastern Africa. To avert climate-related losses and act to help mitigate or even exploit the abnormal conditions, understanding the physical aspects and mechanisms of the climate variability is a critical prerequisite forward improving the accuracy of the regional climate prediction of eastern Africa.

The objectives of this investigation are: 1. to develop a three-dimensional (3-D) primitive equation dynamical model for Lake Victoria. 2. to couple this lake model with the regional climate model (RegCM2-EA). 3. to investigate the mechanism involved in modulating the coupled Lake-Regional climate system. 4. to study the intraseasonal and interannual variations of the short rain season of eastern Africa, and investigate the mechanisms that determine the impact of ENSO on the climate over the Lake Victoria basin, and 5. to investigate the role of the deforestation, as an example of large-scale flow changes, that in future could warrant exploration of how they may be coupled with the lake basin climate and provide a background for the regional deforestation study over eastern Africa.

Some of the potential applications of the results in this study are: (i) prediction of fish environments and population dynamics, (ii) prediction of lake transportation of potentially highly toxic chemical affluent from the food processing, textile production, and cement industries around the shores of Lake Victoria, (iii) prediction of the migration patterns of the Water Hyacinth (Eichornia Crossipes), which begun invading the lake during the late 1980s, (iv) provision of marine and meteorological advisories for ship

navigation considering a series of previous lake circulation and weather-related catastrophic accidents, (v) provision of guidance in the design and management of hydroelectric power plants, (vi) provision of guidance in the design of future observational platforms for monitoring the variability of climatic conditions in Lake Victoria and its surrounding region, and (vii) climate change studies. It is therefore a matter of high priority to acquire comprehensive understanding of the climate of Lake Victoria and its coupling with the regional atmospheric circulation and hydrology.

The outline of this thesis is as follows: In chapter 2, we develop a coupled regional climate simulation model for the Lake Victoria basin. First we customize the Princeton Ocean Model (POM) to Lake Victoria. Second we investigate role of the upper boundary forcing and the lake wave activities. Then we develop a fully coupled atmosphere-lake (RegCM2-POM) model and verify the model results with the data from published literature. In chapter 3, we simulate the climate conditions during the short rainy season for 1982 (wet conditions), 1987 (dry conditions) and 1988 (normal conditions) by using the coupled RegCM2-POM model. Then we analyze the mechanism modulating the climate over Lake Victoria basin during ENSO climate conditions. In chapter 4, the NCAR CCM3 global climate model (GCM) is used to investigate deforestation over the primary region of interest in this study and other regions over Africa. We investigate the potential climate change which could result from the total clearing of the tropical rain forests in Africa and replacing it with savanna vegetation. In chapter 5, we present the summary of the study.

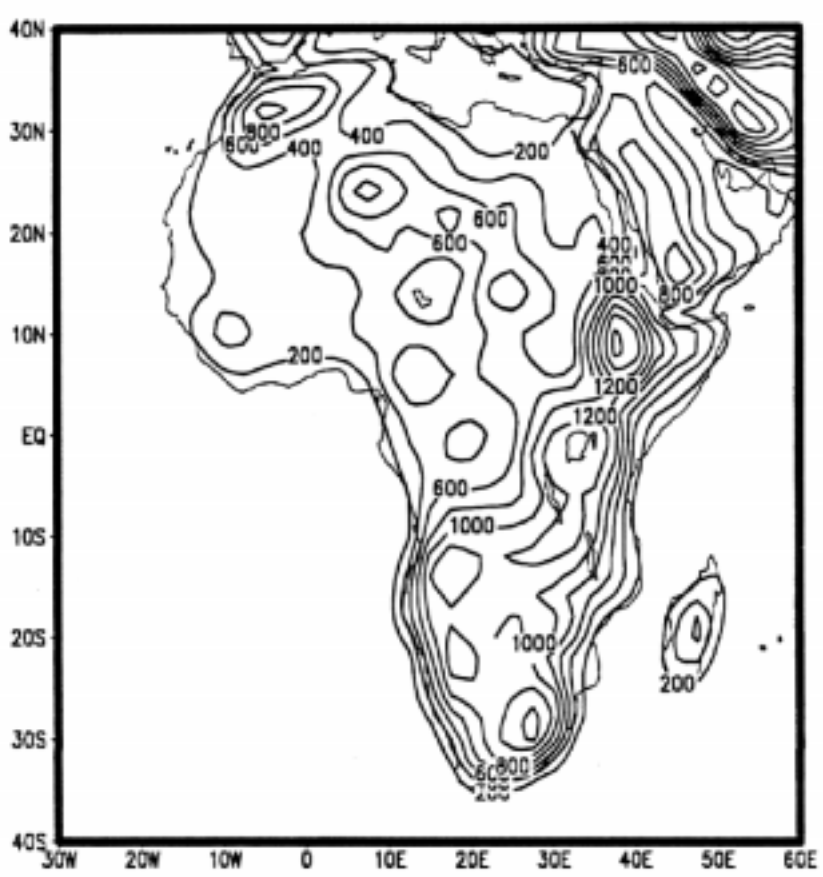

Fig. 1.1. Orography of Africa. Contour interval 200m

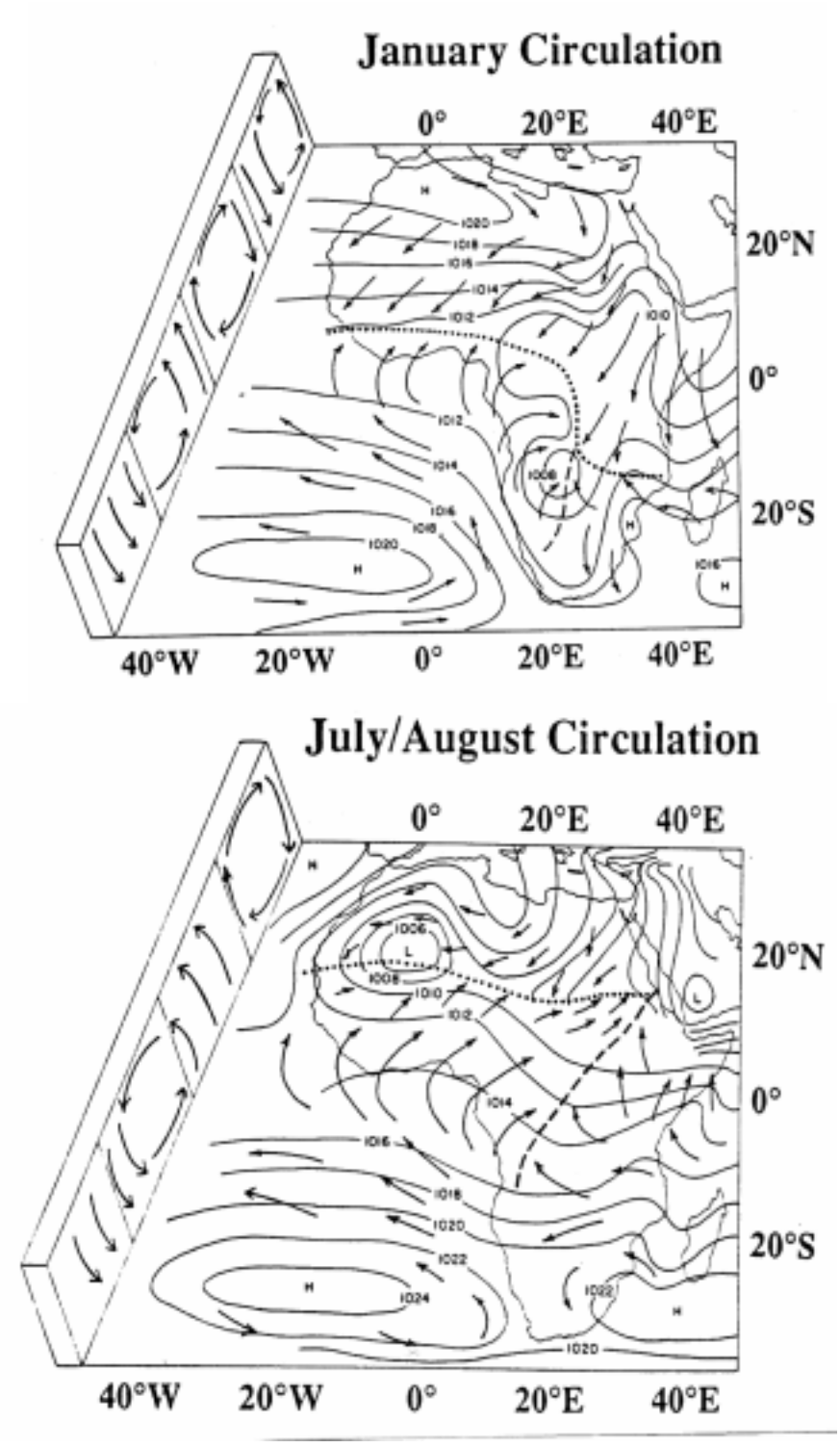

Fig. 1.2. Mean position of the ITCZ over Africa for (a) January, and (b) July/August (Nicholson 1986). Dotted and dashed lines show the location of the ITCZ

Chapter 2

Development of a Coupled Regional Climate Simulation Model for the Lake Victoria Basin

2.1 Background

The seasonal climate over the Lake Victoria basin is primarily governed by the passage of the intertropical convergence zone (ITCZ). The ITCZ separates the NE and SE monsoons (Nicholson, et al., 1996). The ITCZ crosses East Africa twice every year, once during April-May and again during October-November. This migration of the ITCZ is responsible for the two main rainfall peaks, each year in most regions of eastern Africa, which occur in March to May, and Mid-October to early December. These seasons are commonly known as long rains and short rains of Eastern Africa, respectively. Lake Victoria also experiences the two-rainfall maxima (Faris 1997). In this investigation we focus on the short rains season (October to December) of 1988. The short rains season has been chosen because it has greater spatial coherence than the long rains of March through May. In this inquiry we focus on 1988 because it exhibited near normal climate conditions (Ininda 1994). Furthermore, the short rains are closely linked to the ENSO global climate anomaly conditions than the long rains (Semazzi and Indeje 1999; Indeje et al 2000). Since the ENSO climate signal is strong over Eastern Africa, we envisage

that Lake Victoria has strong response to it. This chapter discusses some of our work toward the goal of adopting the modeling approach in investigating the predictability of the ENSO signal and other teleconnection climate signals within the lake and the surrounding regions of Eastern Africa.

There are three types of wave motion associated with lakes, namely, the Poincare free internal waves, the Kelvin internal waves, and the topographic waves (Csanady (1967 and 1968). The Poincare waves extend across the entire lake basin within the thermocline. The largest scale of this type of waveform has maximum wave amplitude on opposite sides of the lake with a node at the center. The internal Kelvin waves are coastally trapped in the thermocline and progress cyclonically in the Northern Hemisphere and in the opposite direction in the Southern Hemisphere. The topographic waves have a barotropic response. These are vorticity waves occurring only in the presence of significant earth's rotation and sloping bathymetry. In this chapter, we also discuss model evidence of wave motion in Lake Victoria which we believe is important in the development comprehensive understanding of the variability and predictability of the regional climate of Eastern Africa.

A fully coupled model of the regional climate of Eastern Africa and Lake Victoria has been developed in this chapter. The atmospheric component of the model is the NCAR regional climate model (RegCM2). The lake component of the model is based on the Princeton Ocean Model (POM) configured for Lake Victoria by replacing the open boundaries in the standard version of the model with a closed coastline and adopting the

bythemetry of Lake Victoria (Fig.2.1). The lake model has 9 equal vertical sigma levels and the horizontal resolution is 20 km. The model's upper boundary conditions are based on momentum, sensible heat and radiative energy fluxes derived from the simulations of the nested NCAR regional climate model (RegCM2) with 20km resolution or idealized surface wind forcing. In these experiments we apply selective and systematic suppression of radiation, heat and momentum fluxes contributions to the upper boundary forcing to determine their relative importance.

2.2 Description of the Atmospheric and Lake Models

2.2.1 Regional Climate Model

In this section we briefly describe the main attributes of the North Carolina State University (NCSU) version of the National Center for Atmospheric Research (NCAR) regional climate model (RegCM2; Semazzi, 1999; Sun et al, 1999ab). RegCM2 has been adapted for Eastern Africa using the 60-km horizontal resolution. In the vertical, the atmosphere is stratified into 15 layers. The model's initial and lateral boundary conditions are taken from European Center for Medium Range Weather Forecasting (ECMWF), 6-hourly, analyzed atmospheric observational data. To evaluate the regional climate model's performance in reproducing the observed precipitation over eastern Africa, Indeje et al. (1999) compared regional averages of simulated and observed precipitation over nine homogeneous climate subregions using cluster analysis techniques. A striking feature of the comparison between the model and the observed

rainfall (not shown) is that the model reproduces the month-to-month changes (increase or decrease) of the rainfall for all the 9 regions. This demonstrates the ability of the model to resolve the complex migration patterns of the Inter-Tropical Convergence Zone (ITCZ) over such complicated terrain, vegetation, and land-water contrasts over eastern Africa. Contemporary global climate models cannot produce such geographical details because of their coarse resolution. We consider this performance of the regional climate model as an important step toward the application of RegCM2 in the prediction of the climate of the region. The model also reproduces the day-to-day and year-to-year changes (not shown) in rainfall over the catchment region of Lake Victoria (SSGO99a, b). Furthermore, we have also compared the diurnal variations of the rainfall at several locations around the lake (not shown). Fig. 2.2 shows the simulated hourly precipitation in November 1988 interpolated from the simulation in which the RegCM2 model is coupled to the 1-dimensional lake model. Over the west (Kishanda, Masaka and Entebbe) and central region (Kahunda) of the lake, the precipitation occurs mostly during early morning and little or no precipitation during the afternoon and evening. Over the eastern part of the lake (Muhuru Bay and Kadenge), the maximum precipitation occurs around midnight, and thereafter rainfall decreases sharply with minimum precipitation around noon. In qualitative terms, the diurnal cycle of the simulated rainfall (Fig. 2.2) along the lakeshore and Island locations compares well with the observed rainfall (Fig. 2.3). The former which is model rainfall expressed in mm/month while the latter, is based on (Datta, 1981), and corresponds to frequency of rainfall occurrences per month. This comparison suggests that the RegCM2 model coupled to the one-dimensional lake model

accurately reproduce the observed diurnal asymmetries in the rainfall distribution over and around Lake Victoria**.** This indirect evaluation of the RegCM2 model performance in reproducing the precipitation over and around the perimeter of the lake is significant because the momentum, radiation, and heat fluxes from RegCM2 have been used, as proxy for atmospheric forcing in the construction of the upper boundary conditions for the dynamical model of lake Victoria. In future, we hope comprehensive meteorological data and marine observations for Lake Victoria will become available for evaluating the high-resolution models used in this study for simulating the climate over eastern Africa and the circulation in Lake Victoria. Consequently, several inferences made in the investigation will be based on the outcome from sensitivity mechanistic model simulations. Recent results based on remote sensing in the estimation of the rainfall over lake Victoria (Ba and Nicholson, 1998; and Yin and Nicholson, 1998) have been used in this study to validate our numerical model integration results.

The representation of Lake Victoria in the standard version of the RegCM2 regional climate model is based on the 1-dimensional lake formulation (Hostetler et al, 1993). In this treatment, heat from the Sun's radiation, which is incident at the lake surface, penetrates and exits the lake along vertical columns of water. A major deficiency in this formulation is that this energy does not mix horizontally. As demonstrated later in this chapter, we have found that upgrading the RegCM2 model to incorporate the 3-dimensional dynamical effects in the representation of Victoria, and hence allow for horizontal mixing of heat and momentum, results in positive impacts on the performance

of the regional climate model.

The nested RegCM2 model simulations in the fine resolution were used to generate the upper boundary conditions for the 3-D lake model described in section 2.2.2. This involves taking output from a coarse resolution (60 km) model run to generate the initial and boundary conditions for the 20km horizontal resolution nested simulation. In the fine resolution nested simulations, the inner domain is centered at (33°E, 1°S), and covers a region of 1660 km by 1480 km compared to 5580 km by 5040 km of the coarse mesh. This high resolution domain covers the Lake Victoria catchment. All the other parameters are the same as those of the 60-km resolution model runs.

2.2.2 Lake Model

The Lake model in this study is based on the Princeton Ocean Model (POM) 1997 version (Mellor 1998). It is a three dimensional, nonlinear, primitive equation finite difference hydrodynamic ocean model. The model employs a mode splitting technique that solves for the barotropic mode for the free surface and vertically averaged horizontal currents, and the baroclinic mode for the full three-dimensional temperature, turbulence, and current structure. The governing equations (1-4) are written in a terrain following $\sigma = (\eta - h)/(H + h)$ vertical coordinate system, where H (x, y) is the bottom topography and η(x, y, t) is the surface elevation, and includes a turbulence closure submodel with an implicit time scheme for vertical mixing (Mellor and Yamada, 1974). The equation of state (Mellor, 1991) is used to calculate the density as a function of temperature, salinity,

and pressure. A three-time level leapfrog scheme is used for the temporal differencing. The basic equations of the σ coordinate system may be expressed as follows:

$$\frac{\partial UD}{\partial t}+\frac{\partial U^2D}{\partial x}+\frac{\partial UVD}{\partial y}+\frac{\partial U\omega}{\partial \sigma}-fVD+gD\frac{\partial \eta}{\partial x}+\frac{gD^2}{\rho_0}\int_\sigma^0\left[\frac{\partial \rho'}{\partial x}-\frac{\sigma'}{D}\frac{\partial D}{\partial x}\frac{\partial \rho'}{\partial \sigma'}\right]d\sigma' = \frac{\partial}{\partial \sigma}\left[\frac{K_M}{D}\frac{\partial U}{\partial \sigma}\right]+F_x \tag{2.1}$$

$$\frac{\partial VD}{\partial t}+\frac{\partial UVD}{\partial x}+\frac{\partial V^2D}{\partial y}+\frac{\partial V\omega}{\partial \sigma}+fUD+gD\frac{\partial \eta}{\partial y}+\frac{gD^2}{\rho_0}\int_\sigma^0\left[\frac{\partial \rho'}{\partial y}-\frac{\sigma'}{D}\frac{\partial D}{\partial y}\frac{\partial \rho'}{\partial \sigma'}\right]d\sigma' = \frac{\partial}{\partial \sigma}\left[\frac{K_M}{D}\frac{\partial V}{\partial \sigma}\right]+F_y \tag{2.2}$$

$$\frac{\partial TD}{\partial t}+\frac{\partial TUD}{\partial x}+\frac{\partial TVD}{\partial y}+\frac{\partial T\omega}{\partial \sigma}=\frac{\partial}{\partial \sigma}\left[\frac{K_H}{D}\frac{\partial T}{\partial \sigma}\right]+F_T-\frac{\partial R}{\partial \sigma} \tag{2.3}$$

$$\frac{\partial UD}{\partial x}+\frac{\partial DV}{\partial y}+\frac{\partial \omega}{\partial \sigma}+\frac{\partial \eta}{\partial t}=0 \tag{2.4}$$

where u, v are, respectively, the velocity components along the x and y axes in the lake, and $D=H+\eta$. The vertical coordinate σ ranges from σ = 0 at $z=\eta$ to σ = -1 at z= -H; ω is the velocity component normal to σ surfaces; T is potential temperature; f is the Coriolis parameter; ρ_0 is reference density; ρ' is density at sigma level σ'; g is gravitational acceleration, t is time; K_M and K_H are vertical eddy viscosity and eddy thermal diffusivity, respectively; F_x, F_y and F_T are horizontal viscosity terms for u, v and T, respectively. The surface boundary conditions for the momentum are given by,

$$\omega=0 \quad at \quad \sigma=0;\ \frac{K_M}{D}\left(\frac{\partial U}{\partial \sigma},\frac{\partial V}{\partial \sigma}\right)=-(<wu(0),wv(0)>) \quad at \quad \sigma=0 \tag{2.5}$$

where $wu(0)$ and $wv(0)$ are the x and y components of surface wind stresses. The first equation specifies no flow normal to the lake surface and the second equation expresses the boundary condition of the shear stresses at the lake surface. The upper boundary condition for temperature is given by,

$$\frac{K_H}{D}\frac{\partial T}{\partial \rho} = -(< w\theta >) \qquad at \quad \sigma = 0 \tag{2.6}$$

where $< w\theta >$ is the input value of the surface turbulence heat flux. At the lake bottom, the boundary conditions are as follows:

$$\omega = 0 \qquad at \quad \sigma = -1; \; \frac{K_M}{D}\left(\frac{\partial U}{\partial \sigma}, \frac{\partial V}{\partial \sigma}\right) = C_Z[U^2 + V^2]^{1/2}(U,V) \qquad at \quad \sigma = -1 \tag{2.7}$$

where

$$C_Z = MAX\left[\frac{k^2}{[\ln\{(1+\sigma_{KB-1})H / z_0\}]^2}, \quad 0.0025\right] \tag{2.8}$$

The coefficient k=0.4 is the Von Karman constant, z_0 is the roughness parameter, and σ_{KB-1} stands for the σ value at the level just above the bottom boundary. Equations 2.7 and 8 specify no flow through the bottom and the boundary condition of shear stresses at the bottom. For the temperature field, the following no-flux bottom condition is used.

$$\frac{K_H}{D}\frac{\partial T}{\partial \sigma} = 0 \qquad at \quad \sigma = -1 \tag{2.9}$$

The POM model has been widely used to study major lakes, such as Lake Michigan (O'Connor et al., 1995) and Lake Erie (Kelly et al., 1998). Water temperature and circulation of Lake Michigan and Lake Erie are generally predicted well by POM. In this study, we configure the POM model for the simulation of Lake Victoria, the largest lake

in the tropics. A significant difference of freshwater lakes compared to coastal ocean is that they are not influenced by salinity effects and tides.

In applying POM model for Lake Victoria, several simplifications have been made. First, the model domain is assumed to be completely enclosed by land so that open boundary conditions are not required. Second, we ignore the effects of river runoff, evaporation and precipitation on the elevation of the lake. Finally, salinity is set to a constant value of 0.2ppt, which corresponds to freshwater lakes (O'Connor et al., 1994).

As seen from the lake topography (Fig. 2.1), the deepest region is located around (33.4°E, 0.7°S). The slope is steeper on the eastern side than on the western side of the lake. A rectangular grid system is adopted. The horizontal grid spacing is 20 km in both the x and y directions which gives 191 grid points covering the entire lake. The model employs 9 sigma levels in the vertical and layer thickness of approximately 8m over the deepest region of the lake and 0.5m over the shallowest locations. The internal and external time steps are 1800s and 60s, respectively. The fluxes of the surface momentum were calculated from the 10-m height winds over lake Victoria, and heat fluxes were calculated by using the 2-m height heat flux parameters based on the output of the fine resolution nested RegCM2 runs. To calculate the surface wind stress, a constant drag coefficient $C_d = 0.0015$ was adopted.

2.3 Design of experiments

Table 2.1 Summary of Numerical Experiments

	Wind Stress	Heat Flux and Radiation	Initial Temperature Structure
Experiment 1a	Uniform easterly wind	None	Warmer water over the upper layers and colder water with increasing depth
Experiment 1b	Uniform northeasterly wind	None	Same as Exp.1a
Experiment 1c	Uniform southeasterly wind	None	Same as Exp. 1a
Experiment 2a	The direction of wind stress-shear was reversed during experiment	None	Isothermal
Experiment 2b	Same as Exp. 2a	None	Same as Exp. 1a
Experiment 3	Simulated wind based on RegCM2	Simulated heat flux and radiation based on RegCM2	Simulated temperature structure based on 1-D lake model in RegCM2
Experiment 4a	Same as Exp. 3	None	Same as Exp. 3
Experiment 4b	None	Same as Exp. 3	Same as Exp. 3

A total of eight experiments have been designed and performed to investigate the circulation and thermodynamics of Lake Victoria based on the 'stand alone' lake model. The corresponding discussion regarding the coupled RegCM2-POM model experiments is presented in section 2.5. Table 2.1 is a summary of numerical experiments. The

details of the primary attributes of the eight experiments are described in section 2.4.

2.4 Lake Victoria model simulation results

2.4.1 Idealized surface wind stress forcing without horizontal shear

The POM model has been employed in the Great Lakes Forecast system for short-term integration, but it has not been extensively applied over tropical lakes and in the climate mode. First, we investigate the simple solutions which arise from applying idealized forcing to understand of the basic response to wind forcing at the top of the lake.

Since the basic wind structure in the tropics is easterly, in Exp. 1a we prescribed simple idealized upper boundary forcing comprised of easterly flow without horizontal shear. The surface wind stress was set to $W_u = 0.0001 m^2 s^{-2}$ (approximately equivalent to 10 m/s wind). Fig. 2.4a-c shows the simulated circulation of Lake Victoria at the surface, 10-m depth, and 20-m depth respectively. The lake circulation within the upper 20m is basically barotropic. The mass continuity dynamical constraint imply that upwelling is initiated along the eastern coastline and downwelling along the western coastline of the lake (Fig. 2.4d). At 20m depth, the eastward undercurrent splits into two cells, with the anti-clockwise cell to the north and the clockwise cell to the south of the undercurrent (Fig. 2.4c).

As noted earlier (section 2.1) the lake Victoria region is primarily associated with

northeasterly monsoon flow during Northern Hemispheric winter, and southeasterly monsoon flow during Northern Hemispheric summer. Thus, two further experiments (Exp. 1b and 1c) forced by northeasterly and southeasterly wind stress were carried out with zero heat fluxes at the top. In Exp. 1b, the horizontal orientation of northeasterly surface wind stress was set to 30° relative to the x-axis and its components are, $W_u = 0.0000866 m^2 s^{-2}$ and $W_v = 0.00005 m^2 s^{-2}$ respectively. The total wind stress is approximately $0.0001 m^2 s^{-2}$. In Exp. 1c, the southeasterly wind stress components were set to $W_u = 0.0000866 m^2 s^{-2}$ and $W_v = -0.00005 m^2 s^{-2}$, thus, only the direction of the wind stress on the y-axis was reversed relative to the northeasterly case. Fig. 2.5a-d is the simulated circulation of Lake Victoria driven by the northeasterly wind (Exp. 1b). The main features of the lake circulation are similar to those of the easterly wind, but the circulation is asymmetric with a broader counter clockwise circulation over the northern part of the lake, and a stronger eastward undercurrent (Fig. 2.5c). On the other hand, with southeasterly surface wind stress forcing (Exp. 1c) the simulated circulation is stronger over the southern basin and eastward undercurrent is weaker (Fig. 2.6a-d).

In this set of simulations the geometry of the lake plays a significant role. It is wider in the meridional direction than the zonal direction (Fig. 2.1) and it is oriented in the northeast-southwest direction thus almost parallel to the northeasterly wind stress in Exp. 1b. Therefore, the northeasterly wind stress exerts greater forcing on the lake flow than the southeasterly wind stress. The resulting lake circulation in Exp. 1b is therefore stronger than that in Exp. 1c. The asymmetric shape of the lake, which is characterized

by greater depth and width over the northern sector, may, in part, also account for the differences in the simulated circulation in the three experiments. Since Lake Victoria is situated in the vicinity of the equator (0.3°N-2.4°S) the Coriolis effect is small and the circulation changes noted in this section are mainly due to wind stress and bottom topography. The accuracy of the bythemetry data therefore plays an important role in customizing the POM model for Lake Victoria.

2.4.2 Idealized surface wind stress forcing with horizontal shear

The large heat capacity and density of water tends to cause the temperature of oceans to vary relatively slower and retain larger memory of past conditions than the land and therefore affect the climate on seasonal and longer time-scales. The oceans store large amounts of heat during the summers and release it during the winter. Therefore, the oceans have longer thermodynamic memory than the atmosphere. Lake Victoria is the largest fresh lake in the tropics and considering its spatial scale it would be valuable for prediction purposes to determine if it also exhibits significant ability to retain heat and momentum anomalies which can influence the local and regional climate anomalies during subsequent seasons. In this preliminary inquiry we investigate the ability of Lake Victoria to retain past memory about its circulation. A similar study concerning the role of heat content of the lake will be undertaken in the future.

Two 360-day numerical simulation experiments starting from motionless flow have been designed and conducted. In each of the two "memory" experiments (Exp. 2a and 2b) the

surface wind stress varies only in the north-south direction. In Exp. 2a the basic forcing is easterly along the southern perimeter of the lake, linearly decreases northward to zero near the center and attains maximum westerly intensity along the northern boundary of the lake (Fig. 2.7). The value of the wind stress varied from $0.0001 m^2 s^{-2}$ to 0. The lake model was run for 180 days with this upper boundary forcing. For the rest of the numerical integration the direction of the surface wind stress forcing was reversed to investigate the response of the water circulation to abrupt changes in surface momentum forcing.

In Exp. 2a the initial temperature over the entire volume of the lake was set to 24°C (Fig. 2. 8a) which is approximated from the equilibrium temperature of the lake in our recent numerical simulation study (Semazzi, 1999; Sun et al 1999ab) based on the RegCM2 regional climate model coupled to a 1-dimensional lake model. Motionless flow was prescribed for the initial conditions of the lake circulation. We can see in Fig. 2.9 (a and b) that the simulation rapidly attains equilibrium in about 7 days. When the direction of the upper boundary surface wind stress forcing is reversed at day-180, the lake's circulation also reverses direction from cyclonic to anticyclonic. Although this is expected because of the reversal in the forcing, it is rather surprising that the new circulation readjusts to a new steady state within only 2 weeks of simulation, around day-194. The isothermal conditions of the lake are maintained throughout the entire 360-day simulation and exhibit virtually no response to the reversal in the surface wind forcing (Fig. 2.9c). Therefore, it is apparent that under isothermal conditions, the memory of the

lake is short, on the order of 2 weeks.

In Exp. 2b the initial temperature of the lake was changed from isothermal conditions by introducing vertical temperature stratification. In the modified initial conditions, the temperature varies from 21.4°C at the bottom to 24.6°C at the surface (Fig. 2.8b), which indicates a thermodynamically stable profile. The other considerations in the design of the experiment are identical to those in Exp. 2a. The simulated temperature, u component and v component of the flow at 5m depth of the lake around (33.5°E, 0.5°S) are shown in Fig. 2.10a, 10b and 10c respectively. Starting from the motionless initial conditions the simulation takes about two months to reach steady state, thus much longer than the one week in Exp. 2a where isothermal initial conditions were employed. Although the physical explanation for this difference is not entirely clear at this time, we envisage that the more stable temperature stratification associated with the non-isothermal conditions and the larger vertical temperature gradient in the shallow water regions in Exp. 2b tend to inhibit initiation of the upwelling and downwelling. Once warm water descends through downwelling and the cold water is raised by upwelling, the stratification of the vertical lake temperature gradient becomes strongly unstable. These unstable conditions promote the developments of wave motion in the lake. The oscillation amplitudes were very large during the strong mixing stage. Since the initial prescribed vertical temperature gradient is large it prolonged the duration of adjustment to reach equilibrium. Following the reversal in the direction of the upper boundary surface wind stress forcing, a new steady state is achieved in about 14 days and the equilibrium temperature did not change

as expected, thus in this respect similar to the results in Exp. 2a where isothermal conditions were assumed. These results indicate that once thermal equilibrium has been established adjustment to changes in the upper boundary wind forcing occurs rapidly, and the memory in the momentum field of the lake is short on the order of 2 weeks.

An important feature of the results which are clearly evident in Figs. 10a-10c is the existence of a 30-45 day oscillation in the u, v, and temperature at 5m depth. The oscillation is synchronous in all the three variables. In the deeper layers, such as at 40m (not displayed), the sign of the oscillation has the opposite sign to the 5m depth signal. This suggests that the oscillations have a coherent three-dimensional structure over the entire volume of the lake. To the contrary, we do not observe the oscillation in Exp. 2a where the temperature stratification is isothermal.

Wave motion has been extensively investigated in lakes. Csanady (1967 and 1968) developed a simplified linearized analytical model of the Great Lakes based on a two-layer circular basin to model the internal baroclinic waves and the surface modes. In the resulting solutions the phase velocity for the surface waves is given by,

$$c_1^2 = g(h + h') + O(\varepsilon) \tag{2.10}$$

for the surface modes. The parameter ε is the baroclinic factor which becomes zero under isothermal conditions. The variables, h and h' correspond to the height perturbation for the top and bottom layers, respectively. The corresponding phase

velocity for the internal modes is given by,

$$c_1^2 = \varepsilon g \frac{hh'}{h+h'} + O(\varepsilon^2) \qquad (2.11)$$

The latter corresponds to the waves observed in our simulations of Exp. 2b which disappear when if $\varepsilon = 0$, under isothermal conditions (Exp. 2a). Fig. 2.11a and b are the vertical cross section of the water temperature along 0.5°S at day 181 (wind direction reversed) and day 360, respectively. In the POM model, the water density is a function of temperature, salinity, and pressure. The salinity was set to a constant value of 0.2ppt, which corresponds to freshwater lakes (O'Connor et al., 1995). Thus, water density depends primarily on temperature. The vertical temperature settles down well to a quasi-stationary state by day 181 (Fig. 2.11a). With the continuous mixing due to upwelling and downwelling, the lake stratification becomes nearly isothermal except at the deeper layers of the lake (below 30 m) at day 360 (Fig. 2.11b). Meanwhile, the corresponding oscillations progressively become weaker (Fig. 2.10), which indicates that the lake stratification plays a crucial role in the development and maintenance of the wave oscillations.

Csanady's theoretical solutions predict that in the southern hemisphere, the wave patterns travel around the circular basin in a clockwise direction as we observe in Exp. 2b (Fig 12), since most of Lake Victoria is situated in the southern hemisphere. Taking the geometry of the lake into account, we plotted the anomalous temperature latitude–time

cross sections at 5 m depth from day 181 to day 360, along the 32°E (Fig. 2.12a) and 33.9°E meridians (Fig. 2.12b). The opposite direction in the wave propagation along the east and west coastal regions of the Lake Victoria is clearly evident. Along the west border near 32°E, the oscillation with periodicity of about 30 days travels northward. On the contrary, along the east border near 33.9°E, a wave with the same periodicity travels southward.

Beletsky et al (1997) performed a series of numerical experiments to investigate the numerical simulation of internal Kelvin waves and coastal upwelling fronts. They employed the POM and DIECAST ocean models to study the response of an idealized middle-latitude large circular lake and Lake Michigan to an impulsive wind stress imitating the passage of a weather event. Under steady state conditions resulting from uniform wind forcing, the balance of forces in the region of upwelling is between the wind stress, Coriolis force, and the internal pressure gradient. However, when this balance is disturbed, new balance is established giving rise to the Poincare waves, Kelvin waves and topographic waves. In the northern middle latitudes, Poincare waves are characterized by anticyclonic phase progression with periodicity slightly less than the inertial period, which corresponds to 17.5 h for central Lake Michigan. Poincare waves exhibit a basinwide response with oscillations in the thermocline across the entire lake. The lowest order Poincare wave has maximum amplitude on opposite sides of the lake, with a node at the center. To the contrary, Kelvin wave disturbances in the thermocline are trapped in the coastal region. They progress cyclonically around the lake. The period

of Kelvin wave in Lake Ontario is 25 days (Schwab, 1977). In the Exp. 2b, we note the existence of wave motion with similar features to the numerical solutions obtained by Beletsky et al (1997).

2.4.3 Upper boundary forcing based on RegCM2 fluxes

In (Exp. 3) we adopted the fluxes generated by the RegCM2 regional climate model to construct the upper boundary forcing for the lake Victoria model. The fluxes are the hourly surface wind stress, short wave radiation, longwave radiation, sensible heat flux and latent heat fluxes from the simulation of the 20km resolution nested RegCM2. Fig. 2.13 shows the RegCM2 simulated monthly mean 10-m height wind for December 1988, which is employed as the surface wind stress forcing. As noted earlier the RegCM2 is coupled to a 1-D lake model. The simulated diurnal surface wind stress is characterized by the divergent motion during the latter part of the day 18UTC (Fig. 2.13a) and convergent motion during the night 24UTC (Fig. 2.13b). Starting from motionless initial state with uniform water temperature of 24°C the lake model was integrated from 01UTC October 1, 1988 to 24UTC December 31, 1988.

2.4.3.1 Control experiment (Upper boundary forcing based on RegCM2 heat and wind fluxes)

Fig. 2.14 shows the monthly mean diurnal variation over the lake surface in December 1988. The contours represent the lake surface temperature pattern and the arrows

represent the surface water flow. The surface circulation is stronger during daytime than nighttime. The lake surface temperature is warmer at 12UTC and cooler at 24UTC. The results show that the warmer region is located over the southwestern part of Lake Victoria and the cooler region is located in the northwest region of Lake Victoria. The lake surface circulation is characterized by anti-clockwise circular motion in response to the predominantly easterly surface wind stress that is shown in Fig. 2.13. The close agreement between the surface water circulation pattern and the topography of the lake (Fig. 2.1), indicates that the depth of the lake may play a significant role in determining the climatology of Lake Victoria.

Comparison of the diurnal surface winds and surface water circulation reveals an important phenomena. Although the surface winds reverse direction during the course of the day (Fig. 2.13 a and b) in association with the land/lake breeze, and also dominate the total wind field, the water circulation maintains the same anti-clockwise circulation throughout the day, similar to the mean flow displayed in Fig. 2.15. This observation re-enforces the proposition that the circulation of the lake is primarily controlled by the prevailing wind pattern rather than the component associated with the land/lake breeze. We postulate that the large inertia associated with the water is responsible for the relatively weaker response to diurnal cycle, which dominates the near-surface wind regime. The surface flow transports warmer water northward over the eastern part of the lake and colder water southward in the western part of the lake. This advection helps to mix the warm and cold water horizontally and thus significantly modifies the spatial

distribution of the surface water temperature.

It is instructive to note that the largest warming of the lake takes place over the shallowest regions of the lake along the southern and eastern shoreline. These are the regions likely to be responsible for the formation of warm water which then funnels out to influence the temperature in the rest of the lake. Over these regions we envisage that any significant increase in the elevation of the lake could result in extensive increase in the surface area of the lake and induce positive feedback that could, in part, also help to explain the dramatic maintenance of high lake levels observed in connection with the aftermath of abnormally wet rain episodes. The sequence of events that we hypothesize in this mechanism would operate as follows. The initial trigger is an intense rain season e.g., 1898, 1961/62, or 1997/98; this is followed by large increase in the elevation of Lake Victoria; colonization of new coastal territory by the lake occurs likely over the plains regions in the south and east of the lake; this is accompanied by increase in the area of the lake occupied by shallow coastal waters. The water over the swampy coastal region originally stagnant could rise high enough to become part of the rest of the lake circulation; this would be followed by formation of warm coastal water due to insolation and the low thermal capacity of the shallow column of water; the new coastal warm pools of water would then be transported toward the interior of the lake and northward where the water is generally colder, by advection driven by surface wind forcing; this would be followed by increase in lake surface temperature (LST) and subsequent increase of precipitation over the lake; this would result in the maintenance of the expanded lake area

and close the positive feedback loop until a new level of quasi-equilibrium is attained by the lake. Preliminary evidence based on this and other studies that we have undertaken seem to support this hypothesis. However, much work remains to be done to verify it.

Fig. 2.16 shows departures from the monthly mean diurnal cycle at the surface in December 1988. The results are obtained by abstracting the entire monthly mean surface temperature and circulation from the monthly mean 06UTC, 12UTC, 18UTC and 24UTC surface temperature and circulation. We can see that the surface water responds strongly to the variations in surface atmospheric forcing, whereby the divergent circulation departures occur during daytime (12UTC and 18UTC) and convergent anomalous circulation during nighttime (24UTC and 06UTC). The surface temperature along the lake lateral boundary increases dramatically at 12 UTC, and decreases at 24 UTC. From daytime to nighttime, the variation in the water temperature at the center of Lake Victoria is relatively insignificant.

Fig. 2.17 is the monthly mean diurnal variations at the 20m depth in December 1988. The circulation patterns and thermal structures are similar to those at the surface. An anti-clockwise circulation occupies the entire lake, and the water circulation transports the warm water northward over the eastern parts and the cold water southward over the western parts of the lake. However, the water is colder and the water currents are weaker. Also, the diurnal cycle is weaker at the 20-m depth than at the lake surface. The experiments described above show that the 3-D lake model produces an active diurnal cycle of Lake Victoria.

Next we explored the ability of the model to simulate the seasonal variations of Lake Victoria. Fig. 2.18 (upper panels) shows the simulated monthly mean surface water circulation and temperature distribution over Lake Victoria (October-November-December 1988). The contours depict the lake surface temperature and the arrows represent the surface water currents. Fig. 2.18 (lower panels) display the corresponding results based on the 1-D thermal lake model in the standard RegCM2 version of the model. Comparison between the results from the 1-D and the 3-D lake model simulations clearly shows that the latter produces much more realistic results. In particular, the 3-D model shows a surface temperature pattern indicative of dynamic mixing characterized by a horizontal spiral pattern, in the temperature field, which is associated with a spreading pool of warm water across the northern section of the lake. This pattern is not present in the 1-D model. These results underscore the need to replace the 1-D formulation of the lake in RegCM2 by the new 3-D formulation. Since the 3-D lake model generates more realistic lake water surface temperature patterns than the 1-D model, it is reasonable to speculate that the coupled RegCM2/3-D lake model would produce more realistic rainfall patterns over and around the lake than the simulations based on the coupled RegCM2-1D lake model. This question is examined more fully in section 2.5 of this chapter.

2.4.3.2 Upper boundary forcing based on RegCM2 wind only (no heat fluxes contribution)

In order to investigate the influence of the wind stress a sensitivity experiment (Exp. 4a)

was carried out by using hourly wind stress forcing without heat fluxes. The wind stress forcing is same as that in the control experiment (Exp. 3; section 2.4.3.1). Fig. 2.19 shows the simulated monthly mean diurnal variation of the lake surface currents in December 1988. The arrows represent the surface currents. Similar to that of the control experiment, an anti-clockwise circulation dominates the lake surface flow field. The diurnal cycle still exists in the lake surface water circulation, but it much weaker than the case when heat flux forcing is included in the boundary forcing (not shown). Hence, the mean surface water circulation is primarily determined by wind stress, however heat flux forcing plays the primary role in modulating its diurnal cycle.

2.4.3.3 Upper boundary forcing based on RegCM2 sensible heat, short wave radiation, and long wave radiation fluxes (no wind stress contribution)

To investigate the contribution of the heat fluxes in the lake simulation, the hourly short wave radiation, long wave radiation, sensible and latent heat fluxes, which are the same as those in the control experiment (Exp. 3), were employed to force the lake model (Exp. 4b). The wind stress was turned off, so that we can isolate the effect of heat fluxes. The results of the fourth month (December) of the simulation are shown in Fig. 2.20. The contours indicate the lake surface temperature and the arrows represent the surface water current. The lake surface temperature is warmer at 18UTC and cooler at 24UTC which a manifestation of the diurnal cycle. In December, the warmer region is located over the southwestern part of the lake and the cooler region is located in the northeast region of the lake, which is consistent with the results based on the 1-D lake model (Fig. 2.18f).

However, the corresponding to transport of warmer water northward over the eastern region of the lake and colder water southward over the western part of the lake in the control experiment does not exist here. Therefore, the results show that although surface lake temperature is strongly influenced by radiation and heat fluxes at the surface, it is evident that advection by water circulation plays a primary role in determining its spatial structure.

2.5 Coupled RegCM2-POM model simulation results for Lake Victoria

To couple the lake model (section 2.2.2) with the regional climate model (RegCM2, section 2.2.1), the most important processes are the surface turbulent flux exchanges of momentum, sensible heat, latent heat and short wave radiation incident across air-lake interface. In the lake model, the upper boundary conditions in equation 6 for the momentum may be expressed as follows:

$$-\rho_0\left[wu(0)\right]=\overline{\rho}_a C_{dm} V_a u_a \tag{2.12}$$

$$-\rho_0\left[wv(0)\right]=\overline{\rho}_a C_{dm} V_a v_a \tag{2.13}$$

The upper boundary condition in equation 2.7 for the temperature is given by,

$$-\rho_0\left[w\theta\right]=F_s+F_l+F_{LW}+F_{SW} \tag{2.14}$$

F_s and F_l are respectively the sensible heat flux and the latent heat flux from the surface. F_{LW} and F_{SW} are net long-wave radiation and shortwave radiation from the surface. F_{SW} is calculated by the atmosphere model. F_{LW} is calculated by

$$F_{LW} = \gamma\sigma T_L^{\ 4} + F_{Lanet} \tag{2.15}$$

γ is the reflective index and it is set as 0.97 here. σ is the Stephan-Boltzmann constant. T_L is the lake surface temperature. F_{Lanet} is net long-wave radiation from the atmosphere and it is calculated by the atmosphere model.

F_l is calculated by

$$F_l = \frac{L_v}{C_p} F_q \tag{2.16}$$

F_q is the evaporation from the surface. F_s and F_q can be calculated as,

$$F_s = \overline{\rho}_a C_{dh} V_a (\theta_a - \theta_0) \tag{2.17}$$

$$F_q = \overline{\rho}_a C_{dq} V_a (q_{va} - q_{v0}) \tag{2.18}$$

where u_a and v_a are the surface wind speed in the x and y direction respectively.

$V_a = \sqrt{u_a^{\,2} + v_a^{\,2}}$ is the resultant speed. The other dependant variables are, ρ, θ and q which denote the density, temperature and water vapor respectively. In the above equations, subscript, "a" denote quantities at the lowest model level of the atmosphere; subscript, "o" refer to quantities at the uppermost level of the lake. Since the speed of the surface water flow is much less than that of wind at the surface, it is ignored in the coupled model. The drag coefficient C_{dm}, C_{dh} and C_{dq} are functions of surface roughness, temperature and wind speed. In the RegCM2-POM coupled model, C_{dm} is simply set to 0.0015 in this study. C_{dh} and C_{dq} are calculated by the atmosphere model. Sensitivity of the numerical results on the specification of the drag coefficients is not addressed here. However we recognize that it may be a legitimate research question that deserves greater attention in the future.

Since the lake model does not have as many physical processes as the climate model it is simpler and may be integrated more efficiently. Moreover, the water has greater inertia than the atmosphere. Therefore, the physical components of the lake, such as velocity and temperature do not change as quickly as that of the atmosphere. Consequently, the surface fluxes exchange across the air-lake interface are updated every hour in the lake model. The same frequency was adopted in the coupling of RegCM2 and the 1-D lake model. The predicted lake surface temperature is kept constant within the one hour interval, and it is used as the lower boundary condition for the atmosphere model.

Although the methodology for coupling the atmosphere models to ocean models (a lake

model here)is well established (Bryan et al 1996), here, for the sake of completion, we outline the primary features of the procedure. Equation 2.12-2.18 give the flux exchange and figure 2.21 schematically summaries the various attributes of the coupling.

To investigate the coupled air-lake climate variability over the basin of Lake Victoria a 4-month simulation was conducted from September 1, 1988 to December 31, 1988, thus in this sense similar to the treatment for the uncoupled model simulation. Both the model domain and resolution were kept the same as those of the uncoupled model. The initial and lateral boundary conditions of the atmosphere model were taken from the output of the coarse resolution (60km) model run. The initial lake temperature was set to isothermal conditions of 24°C and the lake model was integrated from motionless initial conditions.

The simulated lake surface water temperature, surface water circulation and rainfall for the fourth month (December 1988) are shown in Fig. 2.22. The patterns of the surface temperature and currents simulated by the coupled model (Fig. 2.22a) are similar to the results based on the "stand-alone" lake model (Fig. 2.18c). The solution is characterized by a horizontal spiral pattern in the temperature field which transports the warm water to the northern section and the cold water to the southern section. The net result is a warm tongue in the northeastern part and a cold tongue over the northwestern part of the lake. A distinct warm pool of water is located over the southwestern part of the lake in both the coupled 3-D lake model (Fig. 2.22a) and 1-D lake model results (Fig.2.18f), but the size

of the warm pool is diminished in size due to the 3-D mixing in the 3-D lake model. This warm pool is much weaker in the simulation of the "stand-alone" lake model (Fig.2.18c). On the average the LSTs in RegCM2-POM simulation is a degree warmer than the corresponding area average for the RegCM2-1D model. The simulated rainfall from RegCM2-POM is similar to the pattern produced by the RegCM2-1D model (not shown).

Fig. 2.23 displays the difference (RegCM2-POM minus RegCM2-1D) for the simulated rainfall, LST, and surface water circulation. The rainfall difference (Fig. 2.23a) is largest over the southwestern sector of the lake. It is instructive to observe that although the LST is generally higher in RegCM2-POM (Fig. 2.23a) than RegCM2-1D (Fig. 2.18f) the corresponding rainfall is generally lower. This suggests that there is significant decrease in rainfall associated with horizontal moisture flux advection that offsets the expected increase due to the higher evaporation in response to the higher LST. In Fig. 2.23b we display the LST departures based on the formula $[3D-1D]-ave[3D-1D]$ which highlight the horizontal gradient pattern. We postulate that this LST pattern is determined by the advection of warm water from the shallow region of the lake in southern and western sectors to the northeastern region. By contrast the RegCM2-1D does not support advection and upwelling or downwelling processes because it does not have hydrodynamics in its formulation. Moreover, this also means that the RegCM2-1D model cannot simulate upwelling and downwelling which plays an important role in determining the surface structure of LST. Fig. 2.23c shows that the corresponding low-level (850mb) circulation is direct response to the LST gradient in Fig. 2.23b and

consistent with the simulated difference between the rainfall simulated by the RegCM2-POM and RegCM2-1d models.

These results indicate that the hydrodynamics of the lake play an important role in determining the coupled variability of the lake circulation and the lake basin-wide climatic conditions. Neglecting the lake's hydrodynamics and basing the lake model only on thermodynamical considerations deprives the coupled regional climate model of the ability to transport heat efficiently within the lake and thereby degrades the simulation of the climate downstream over the rest of the lake and the surrounding regions.

Over the years, several studies have provided assorted observational data of the temperature of the lake at different locations and for different years. Spigel and Coulter (1996) found that the surface temperature of lake Victoria in December is about 25.4°C for the period 1960-1961 and 25.2°C for 1990-1991, about 32 km south of the source of River Nile, at Jinja in Uganda. Ochumba (1996) described observed monthly mean surface temperature at numerous locations in the northeast part of the lake, ranging from 25.2°C to 26°C in December 1992. Spigel and Coulter (1996) found that the surface temperatures range between 24.5°C and 26°C during the course of the year based on Talling's data (Talling, 1968). However, the locations of observational stations used to obtain these data are offshore. Yin and Nicholson (1997) have argued that Talling's surface temperatures probably best represented the temperature during the period of 1956-78 and used it to calculate the water balance of Lake Victoria using their

hydrological model. Since more suitable observational data is not readily available, Talling's surface temperature is also used in this study to validate the performance of the coupled RegCM2-POM and RegCM2-1D models.

Table 2.2 Model simulated lake surface water temperatures averaged over the entire lake in December 1988 and Talling's observational data.

	RegCM2-POM	POM	RegCM2-1D Lake	obs (Talling, 1976)
Mean LST	24.4 °C	22.4 °C	23.3°C	25.2°C
model-obs	-0.8 °C	-2.8 °C	-1.9 °C	0
% (difference/obs.)	-3.17%	-11.11%	-7.54%	0

Table 2.2 summarizes the comparison of the lake surface temperature based on Talling's observed data, RegCM2-1D model, and the RegCM2-POM model. The lake maximum surface temperature simulated by the coupled RegCM2-POM is 25.5°C and it is located over the southwest sector of the lake, which is the shallowest region of the lake. The area averaged simulated lake surface temperature over the entire lake is 24.4C which is 0.8°C (3.17%) cooler than Talling's observed temperature. The results show that the surface temperature averaged over the lake, in the "stand-alone" lake model is 22.4°C which is 1°C-2°C cooler than in the case of the coupled RegCM2-POM model and 2.8°C (11.11%) cooler than Talling's averaged surface temperature. We attribute the large negative temperature bias associated with "stand-alone" lake model to the absence of

coupled lake-atmosphere processes that are responsible for maintaining the higher temperatures of the lake surface. Back scatter radiation due to the presence of clouds, downward cloud blackbody radiation, and other positive feedback mechanisms associated with air-lake coupling are likely to play a significant role in maintaining the higher lake surface temperatures associated with the coupled RegCM2-POM model results. We believe such mechanisms may also be responsible for the peculiar occurrence of the abnormally high elevations of lake Victoria following intense episodes seasonal rains, for example the 1961-62 East African Short rains that led to the dramatic increase in the level of Lake Victoria (Flohn, 1987).

In summary, we find that the simulation of lake surface temperature based on the coupled RegCM2-POM model is superior to the "stand-alone" 3-D lake model and the coupled RegCM2-1D model. The coupled RegCM2-1D model produces better simulation of the area average surface temperature for the entire lake that the uncoupled POM model. However, as pointed out in section 2.4.3.1, the “stand-alone” 3-dimensional lake model generates more realistic water surface temperature patterns than the 1-dimensional model.

Characterization of the rainfall over Lake Victoria and its catchment has attracted much research interest over the years. Spigel and Coulter (1996) found that the monthly rainfall annual range is about 80mm to 225mm with about 130mm in December. Ochumba (1996) pointed out that the monthly rainfall varies from 10mm to 135mm over the northeastern region of Lake Victoria and the rainfall in December is about 130mm. Ba and Nicholson (1998) investigated the rainfall over the lake and its catchment, and

estimated the monthly area-averaged rainfall in 1988 to be in the range of 48mm to 185mm and with about 137mm in December 1988. However, as noted earlier, the observational stations are not located over the lake. Moreover, observation data with satisfactory spatial and temporal resolution that extend over a sufficiently long period of time are not yet available. Therefore, it is not feasible at this time to evaluate the performance of the coupled RegCM2-POM model over Lake Victoria in satisfactory detail. Based on these considerations, the precipitation data of Spigel and Coulter (1996), and Ba and Nicholson (1998) will be used to carry out preliminary assessment of the performance of the coupled RegCM2-POM model in simulating rainfall over the lake basin.

Table 2.3 Comparison of observed and simulated rainfall using the RegCM2-POM and RegCM2-1D models for December 1988.

	RegCM2-POM	RegCM2/1-D	Observed
Region based on Bugenyi et al (1996)/entire lake basin	143.5/140.0 mm	157.75 /146.7mm	130/135 mm
difference (simulation-observed)	13.5/5.1 mm	27.75/11.7 mm	0
percentage (difference/observed)	10.38%/3.77%	21.35%/8.67%	0

Table 2.3 is a comparison of the model simulations and the observations. Spigel and Coulter (1996) averaged the rainfall over the stations of Entebbe, Kisumu, Mwanza and Bukoba along the perimeter of Lake Victoria and produced an estimate of 130mm for

December. The corresponding monthly precipitation simulation based on the RegCM2 model averaged over the same four stations is 143.5mm for December 1988. This is 13.5mm (10.38%) more than the observed average. In comparison, the corresponding estimate of rainfall based on the RegCM2/1-D model is 27.75mm (21.35%). Ba and Nicholson (1998) estimated 135mm for December 1988 over their study area (5°N-10°S, 25°-40°E) which covers Lake Victoria basin. We computed the simulated rainfall averaged over the model domain (Fig. 2.22), which is smaller than their study region. For December 1988 we obtained 140.1mm for RegCM2-POM and 146.7mm for RegCM2/1-D. The corresponding rainfall bias is +3.77% (RegCM2-POM) and +8.67% (RegCM2/1-D) compared to the observed rainfall, thus indicating that the performance of RegCM2-POM is superior to RegCM2/1-D in the simulation of rainfall over the basin of Lake Victoria. However, these results must be considered as preliminary until more appropriate observed data becomes available for the assessment of the model results. In particular, we note that the regions considered in the comparison of the model performance and the estimates given by in Ba and Nicholson (1998) are slightly different. Furthermore, the time period used by Spigel and Coulter (1996) is different from the one adopted in our study. Despite these differences, the balance of evidence indicates that the performance of RegCM2-POM is very encouraging as a vehicle for investigating climate variability over Eastern Africa in general, and the climate over the basin of Lake Victoria, in particular.

2.6 Conclusions

In this study, we have configured the POM model for Lake Victoria, and coupled it with the regional climate model (RegCM2) for Lake Victoria and its catchment. A number of simulations have been conducted to investigate the dynamics and thermodynamics of Lake Victoria, and its sensitivity to different forcing specifications. The results show that (i) the memory in the momentum of lake Victoria is about two weeks, (ii) there exists a 30-day oscillation in Lake Victoria and the stratified water temperature plays a critical role in the development of the oscillations, (iii) these oscillations are trapped in the thermocline along the coast and progress clockwise, (iv) the depth of the lake plays a significant role in determining the climatology of Lake Victoria, (v) the lake surface circulation is characterized by counter clockwise motion in response to the predominantly easterly surface winds, (vi) with time-dependent wind forcing based on the RegCM2 model, although the diurnal component of the surface winds reverse direction in association with the land/lake breeze, the water circulation maintains the same anti-clockwise circulation throughout the day. This observation re-enforces the proposition that the circulation of the lake is primarily controlled by the large-scale wind pattern rather than the component associated with the land/lake breeze. We postulate that the large inertia associated with water is responsible for the weak response to diurnal cycle that dominates the near-surface wind regime. We find that the mean surface water circulation is primarily determined by wind stress, however heat flux forcing plays the primary role in modulating its diurnal cycle. Furthermore, the results show that although surface lake temperature is strongly influenced by radiation and heat fluxes at the surface, it is evident that advection by water circulation plays a primary role in determining its

spatial structure.

The 3-dimensional model produces a surface temperature pattern indicative of horizontal lake water mixing characterized by a horizontal spiral pattern in the temperature field. This is associated with the spreading of the pool of warm water across the northern section of the lake. This pattern is not present in the 1-dimensional model. Based on preliminary comparison of the coupled RegCM2-POM model simulation results with the observations, we find that it produces more realistic lake surface temperatures and rainfall over and around the lake than the standard version of the model (RegCM2-1D) which employs simple one dimensional thermal diffusion to represent lakes. We find that the dynamics of the lake play an important role in determining the coupled variability of the lake circulation and the ambient climatic conditions. Neglecting the lake's hydrodynamics and basing the lake model only on thermodynamics deprives the coupled regional climate model of the ability to transport heat within the lake and affect the climate over other parts of the lake and perhaps the land regions surrounding the lake. Shallow nearshore regions of the lake are breeding areas for warm water and could be a critical factor in the chain of processes which link the fluctuations in the lake level and area with its surface temperature and influence on the variability of the climate over the lake basin.

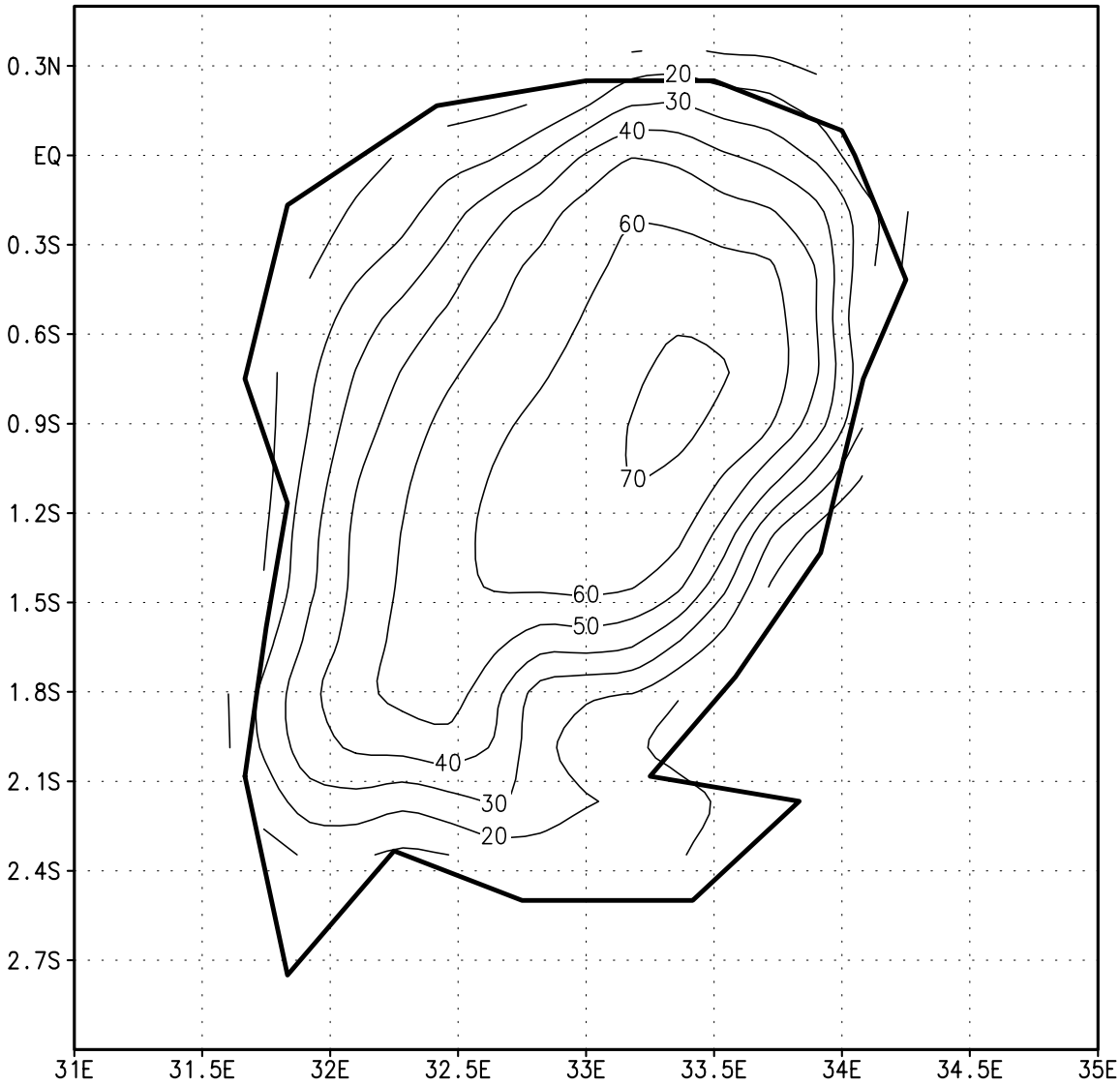

Fig. 2.1. Lake Victoria Bathymetry with horizontal resolution of 20 km (redrawn from Johnson, 1997). Units in meters.

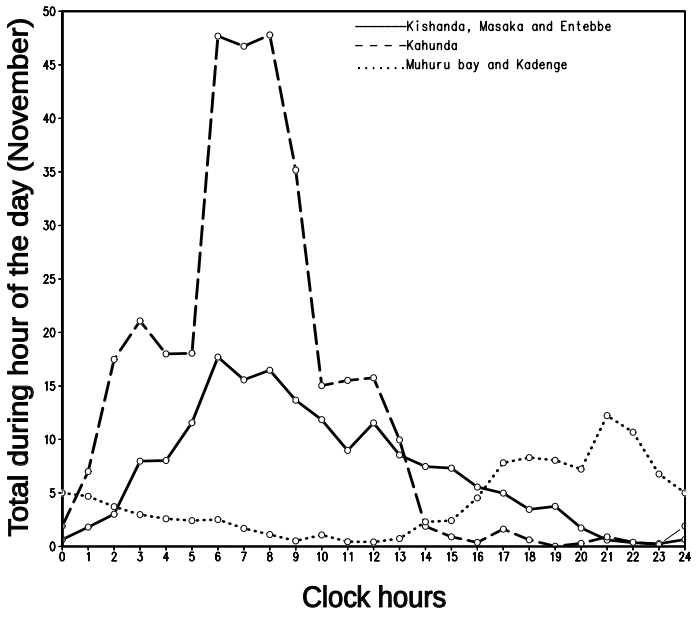

Fig. 2.2. Simulated precipitation distribution and diurnal change over Lake catchment in November 1988.

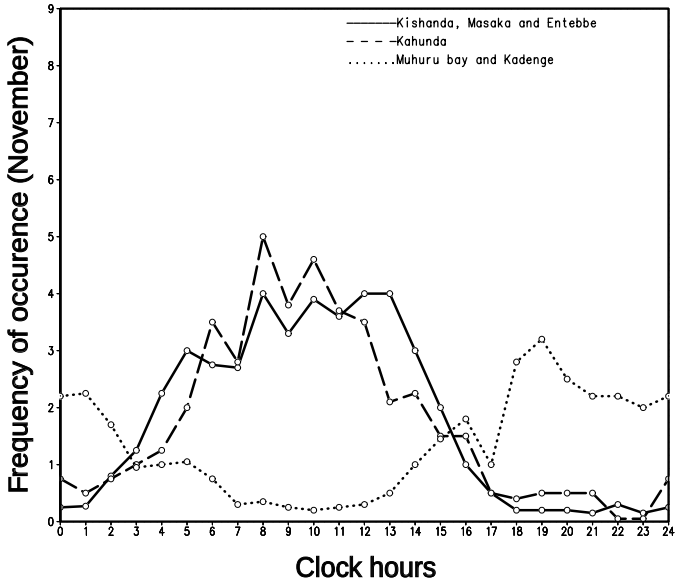

Fig. 2.3. Observed mean precipitation frequency distribution and diurnal change over Lake catchment in November (adapted from Datta, 1981).

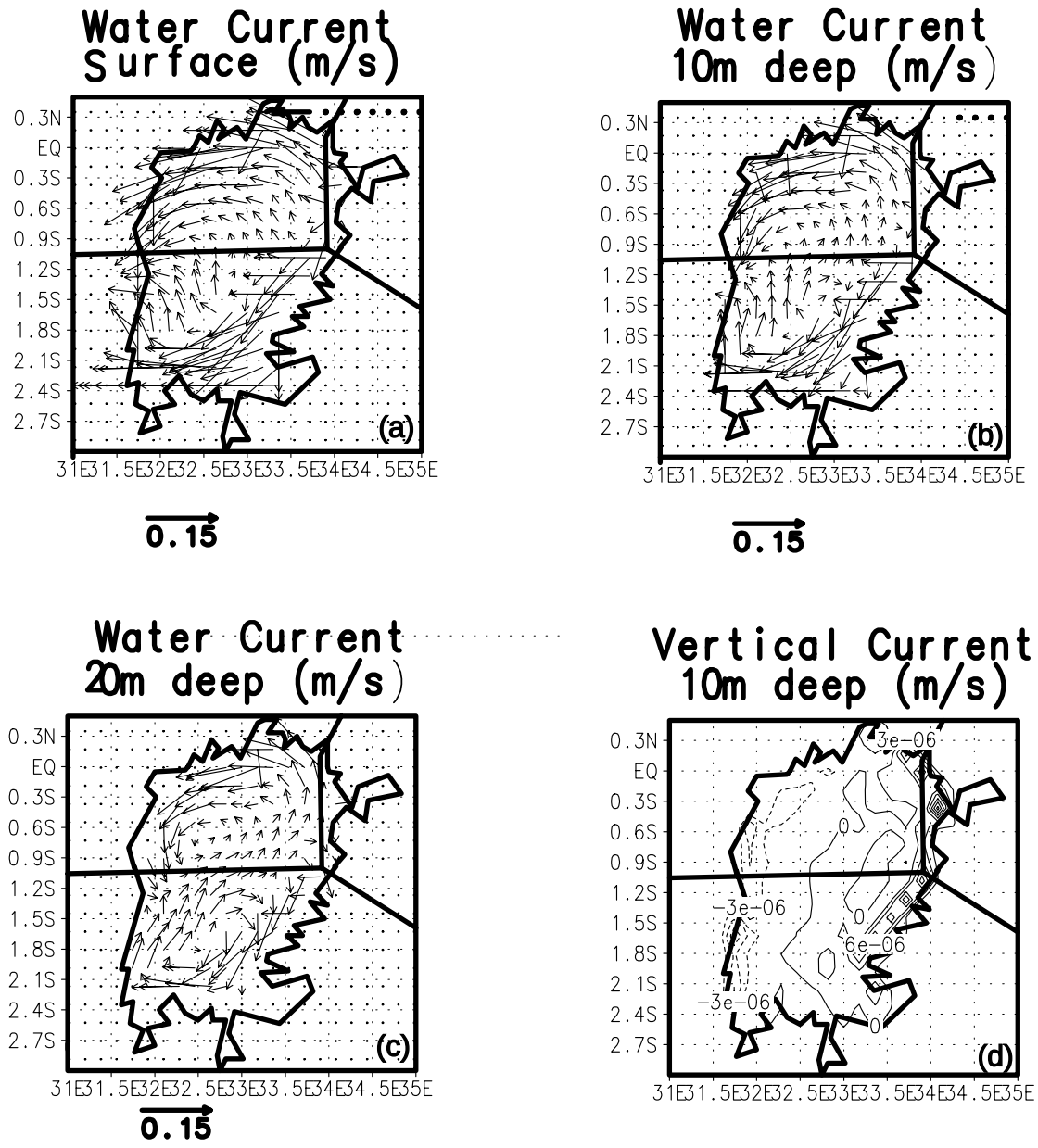

Fig. 2.4. Simulated circulation of Lake Victoria driven by easterly wind. a). surface current. b) current at 10m depth. c). current at 20m depth. d). vertical velocity at 10m depth. Units in m/s.

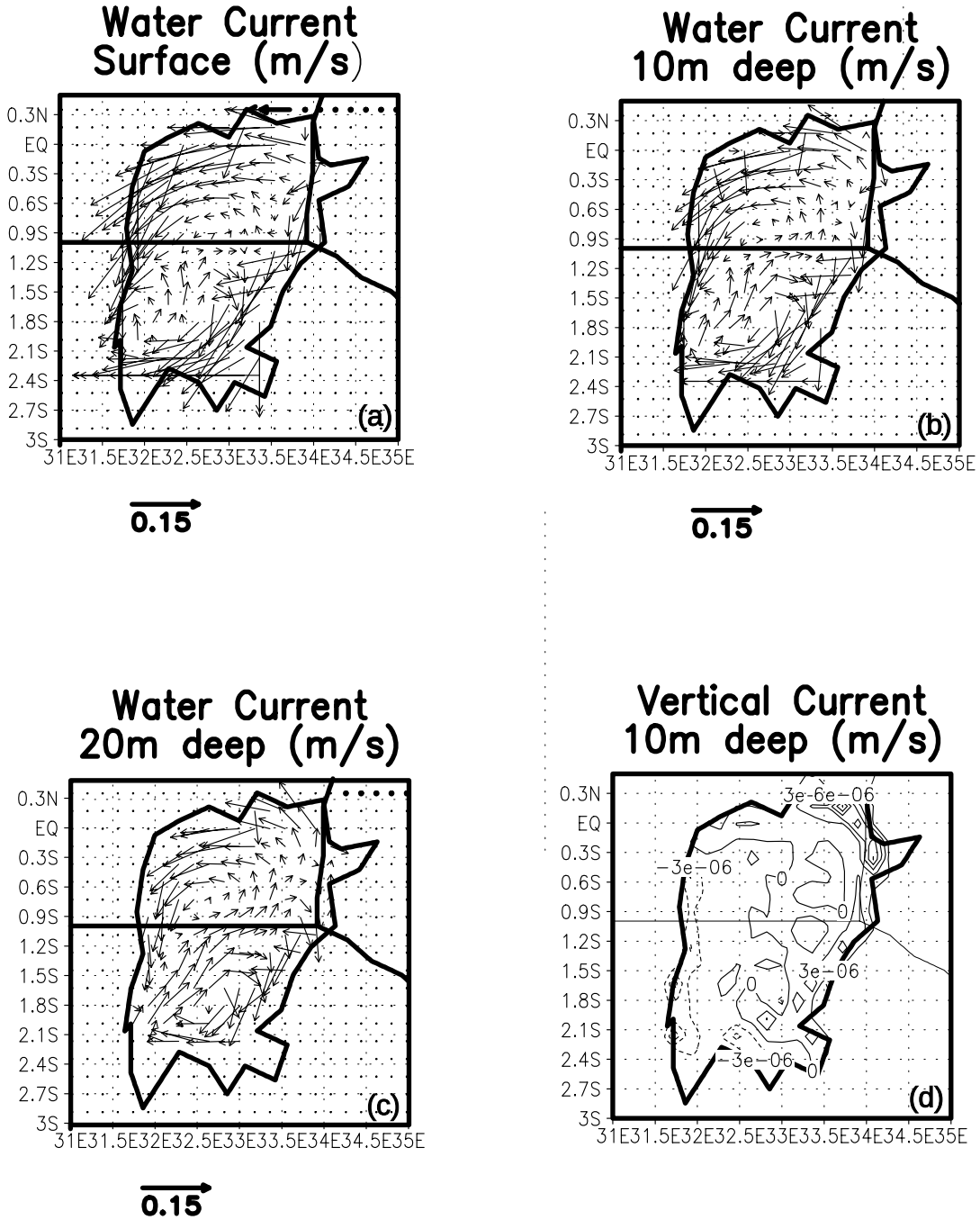

Fig. 2.5. Same as Fig. 2.4 except for northeast wind.

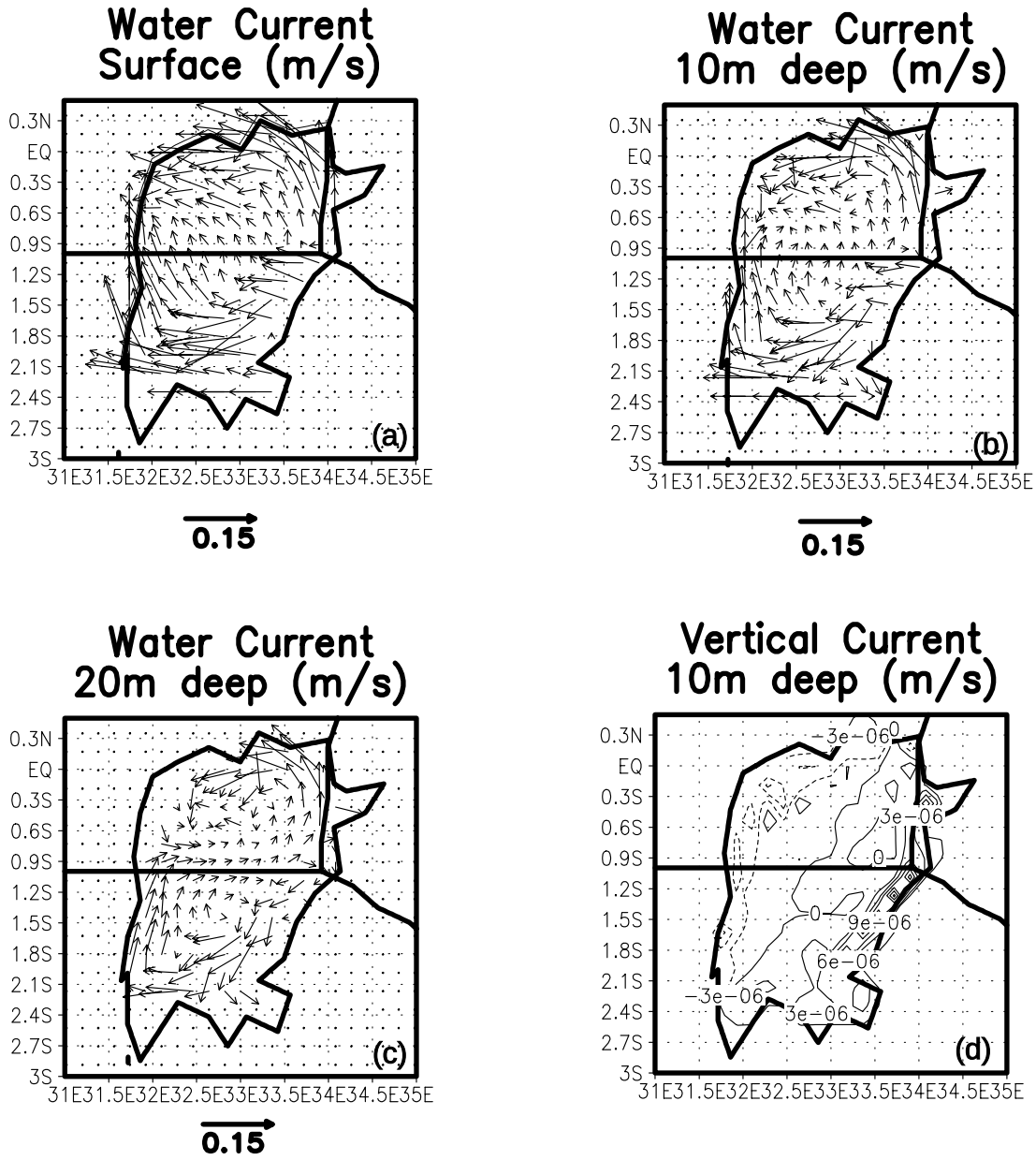

Fig. 2.6. Same as Fig. 2.4 except for southeast wind.

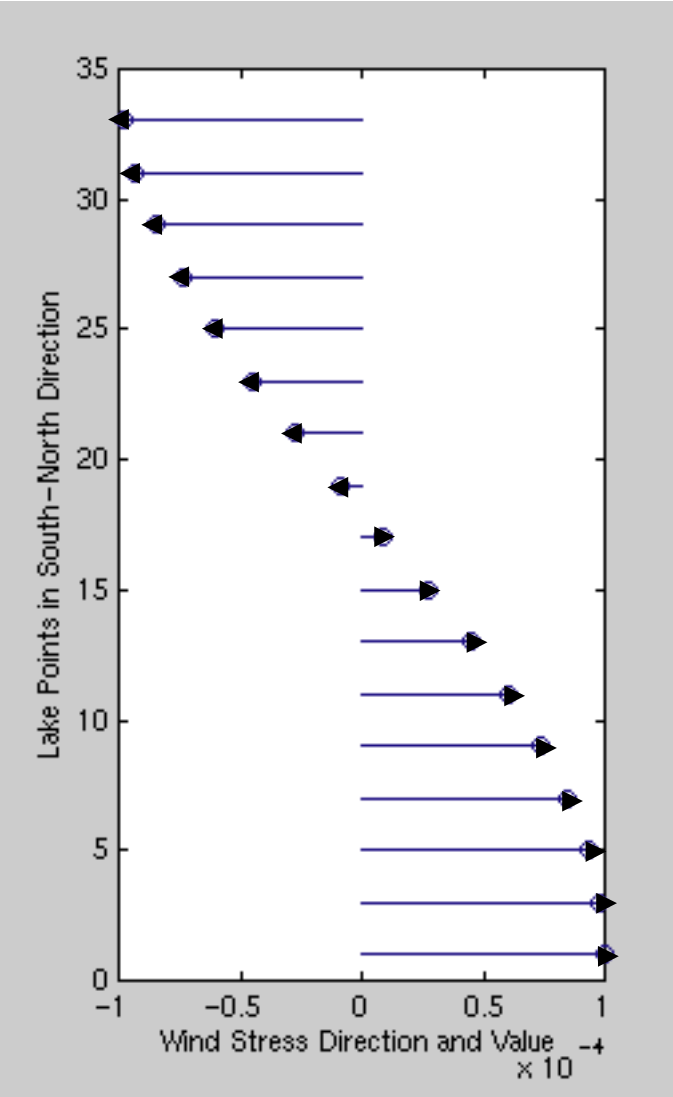

Fig. 2.7. Distribution of wind stress in Exp. 2. Units in m^2s^{-2}.

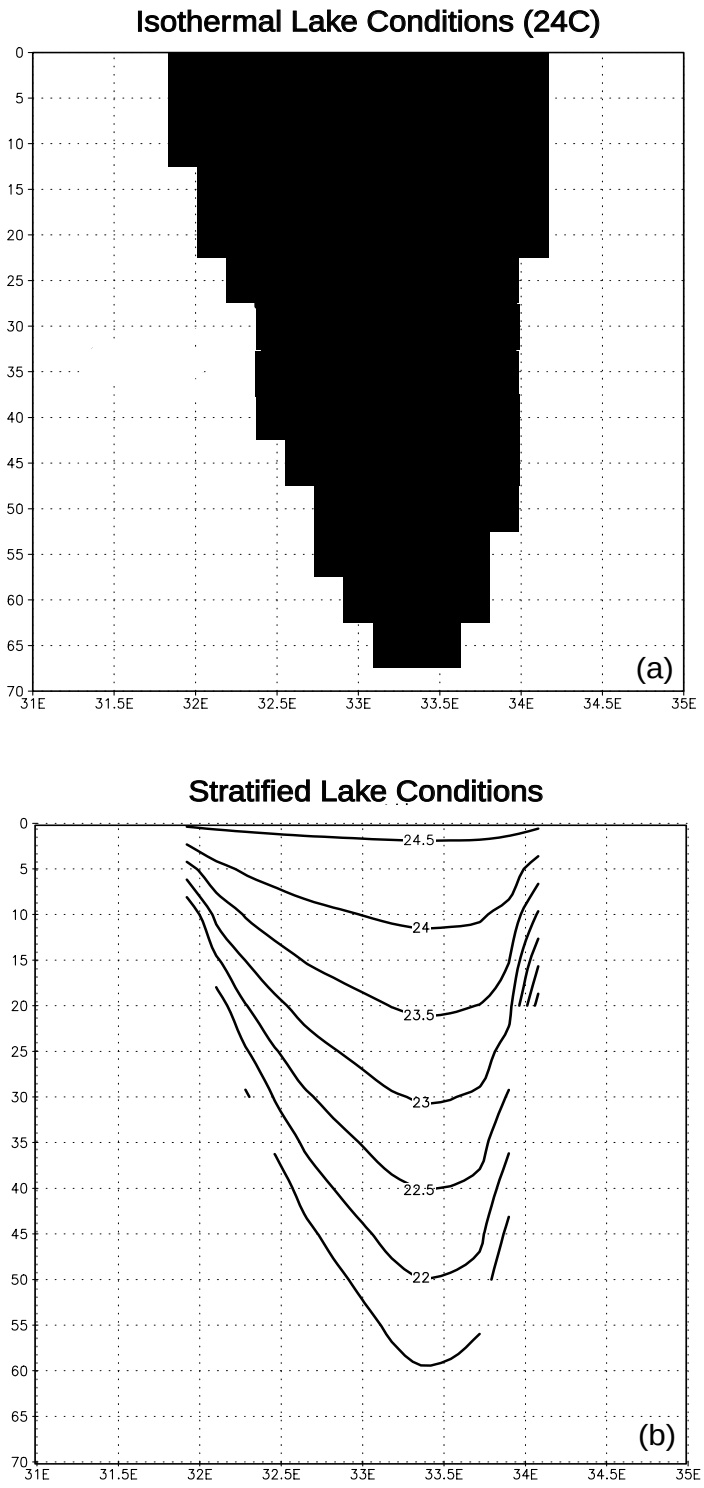

Fig. 2.8. Initial vertical temperature distribution along 0.5°S. a) isothermal conditions. b) non-isothermal conditions. Units in °C

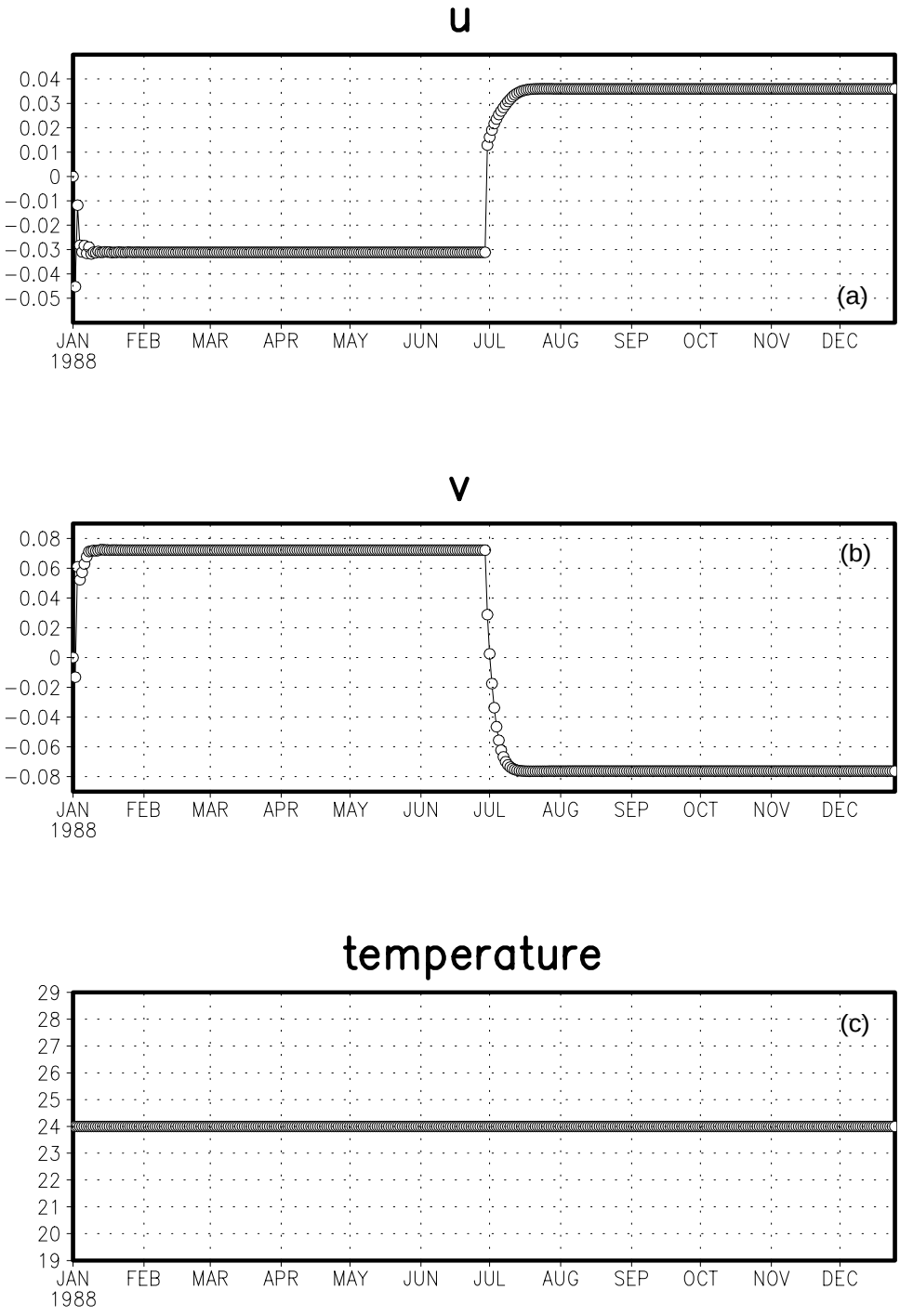

Fig. 2.9. Simulated time series of Lake Victoria driven by reversed wind stress in Exp. 2a under isothermal conditions in Fig. 2.8a: (a) u component of water current at 5m depth at (33.5°E, 0.5°S). Units in m/s. (b). v component of water current at 5m depth at (33.5°E, 0.5°S). Units in m/s. (c). water temperature at 5m depth at (33.5°E, 0.5°S). Units in °C.

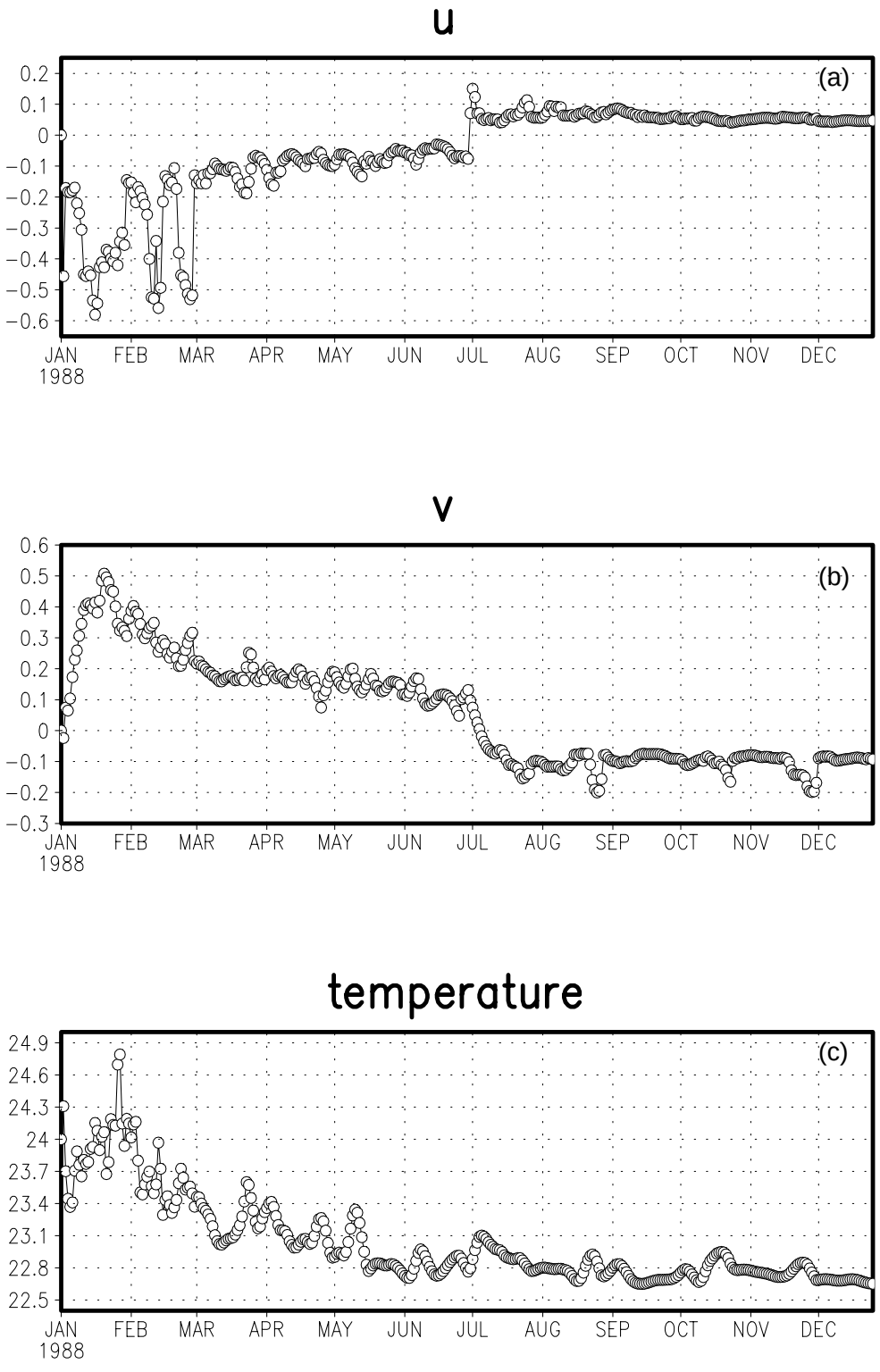

Fig. 2.10. Same as Fig. 2.9 except for the non-isothermal initial condition in Fig. 2.8b

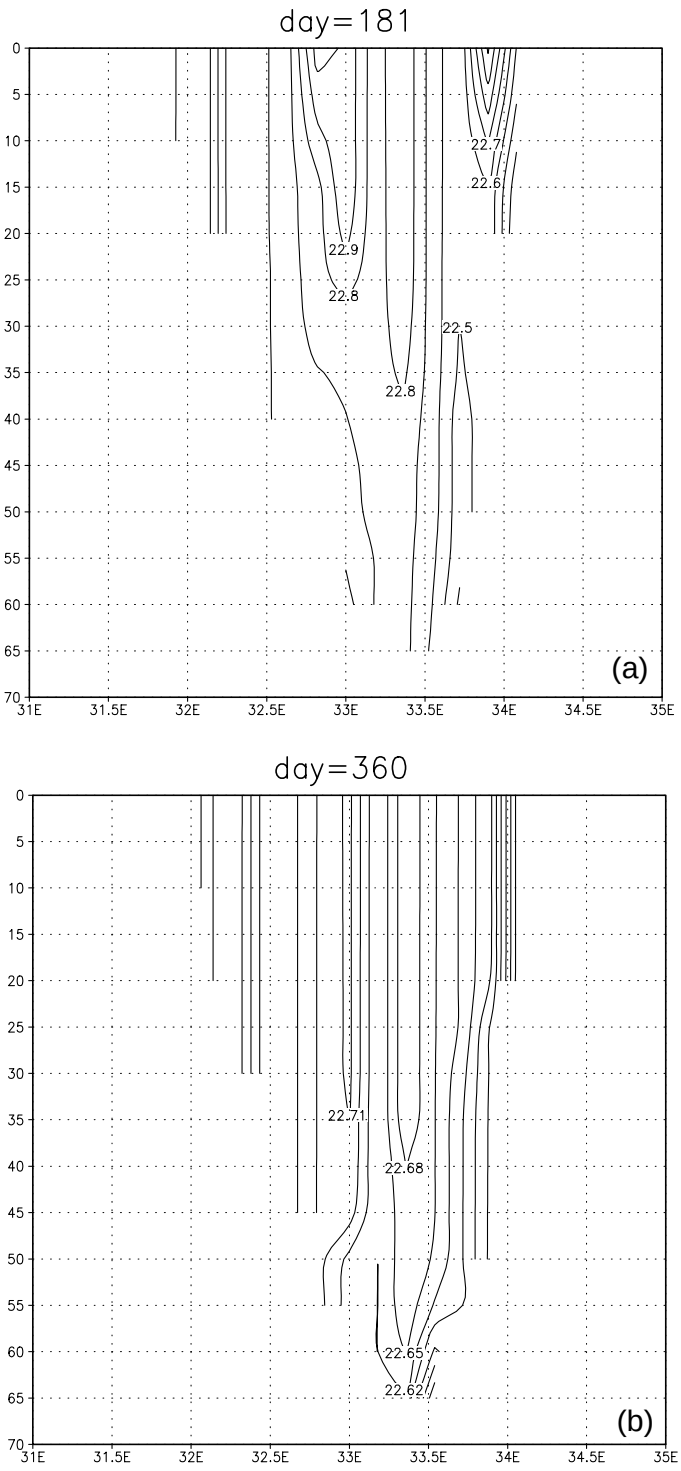

Fig. 2.11. Simulated vertical temperature distribution along 0.5°S in Exp. 2b. a) day 181. b) day 360. Units in °C

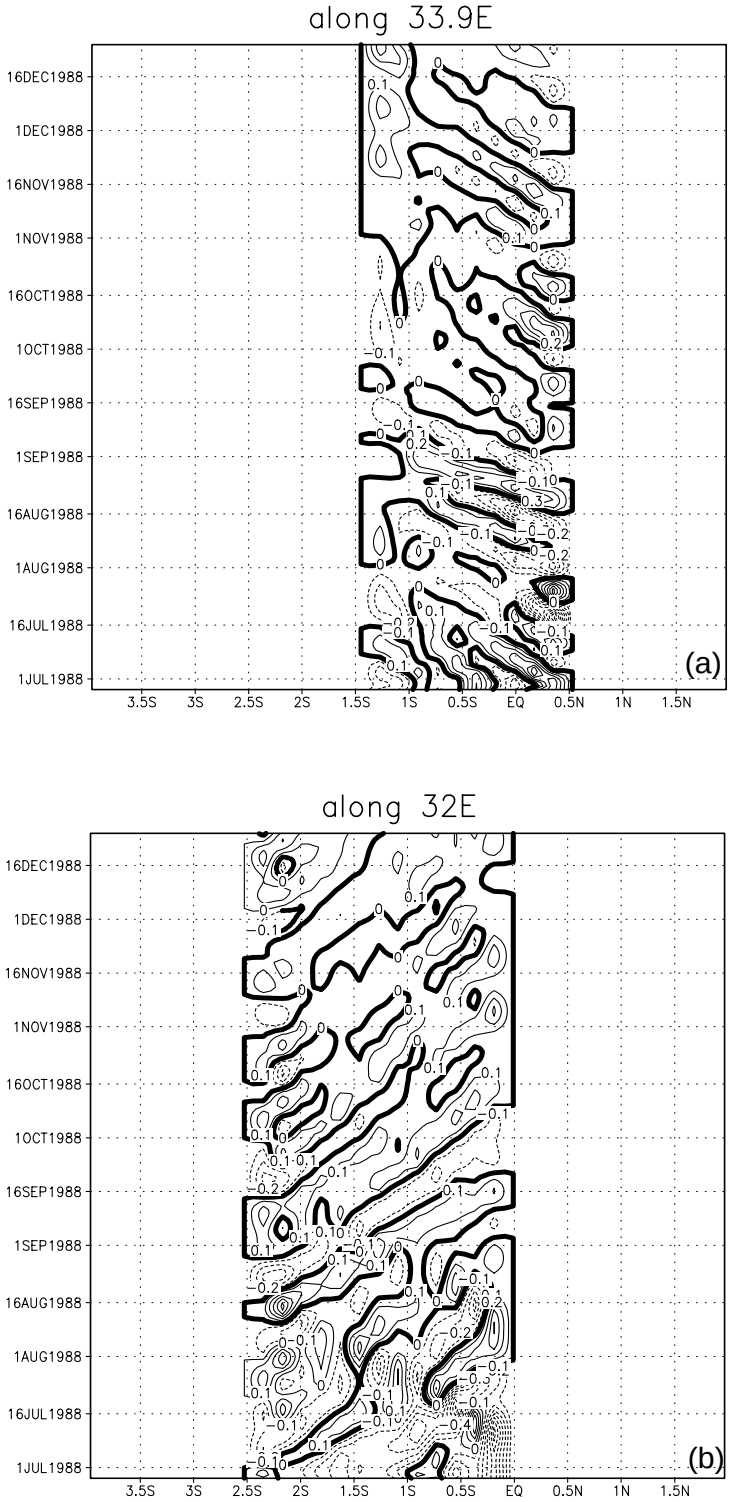

Fig. 2.12. Time-latitude cross section of the simulated lake temperature at 5m depth from day 180 to day 360. a) along 32°E. b) along 33.9°E. Units in °C.

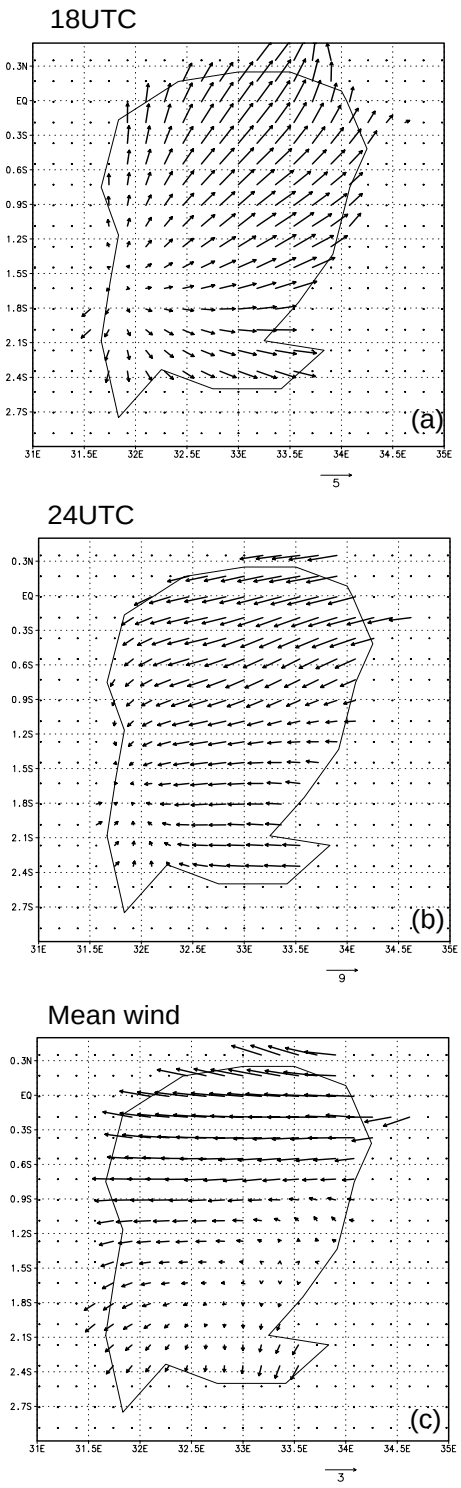

Fig. 2.13. RegCM2 simulated wind at 10m height above Lake Victoria in December 1988. a). at 18UTC. b). at 24UTC. c) monthly mean wind. Units in m/s.

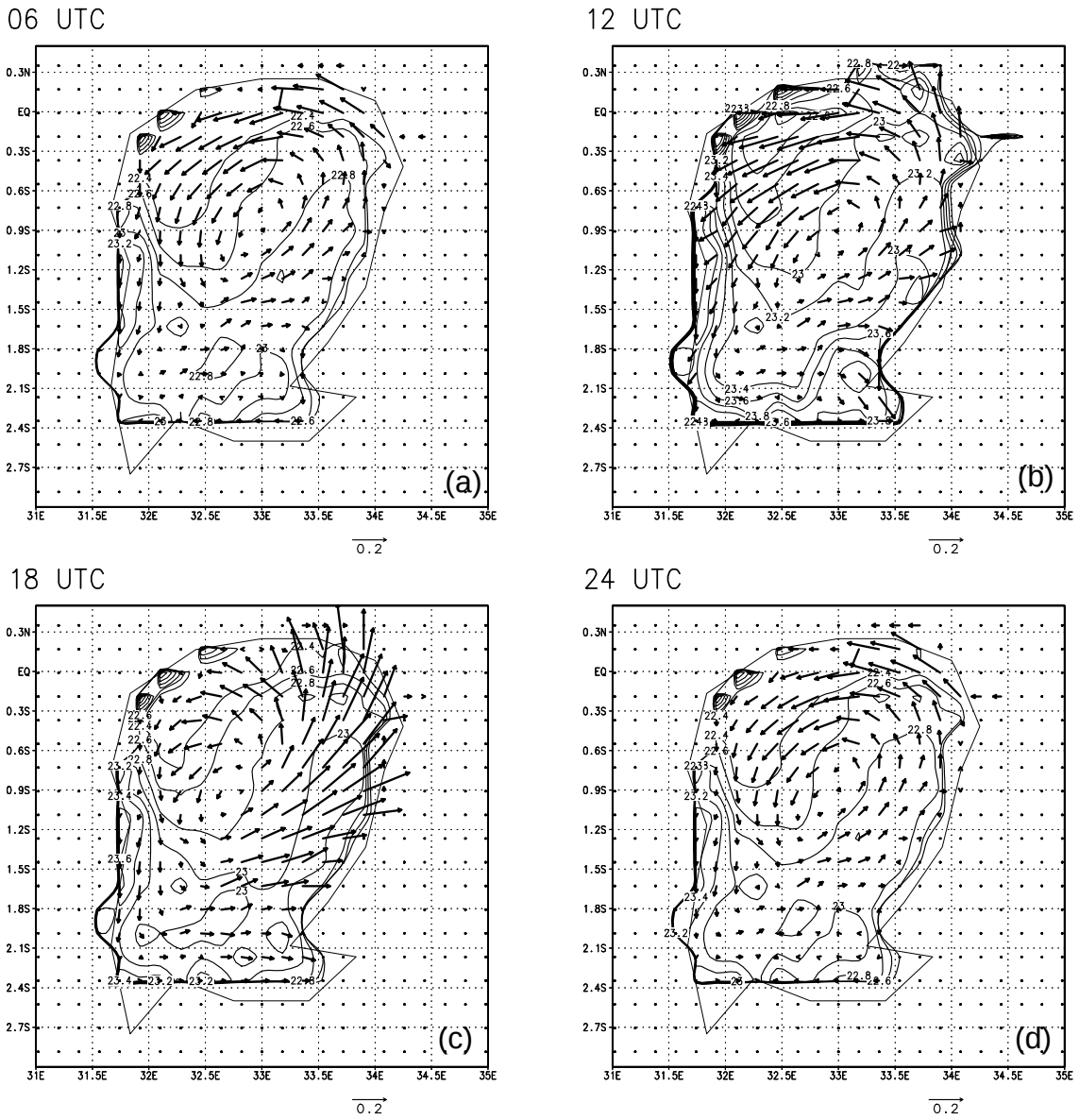

Fig. 2.14. Simulated surface circulation and temperature of Lake Victoria driven by the wind stress and heat flux in December 1988. a). at 06UTC. b). at 12UTC. c). at 18UTC. d). at 24UTC. Units in m/s (current) and °C (temperature).

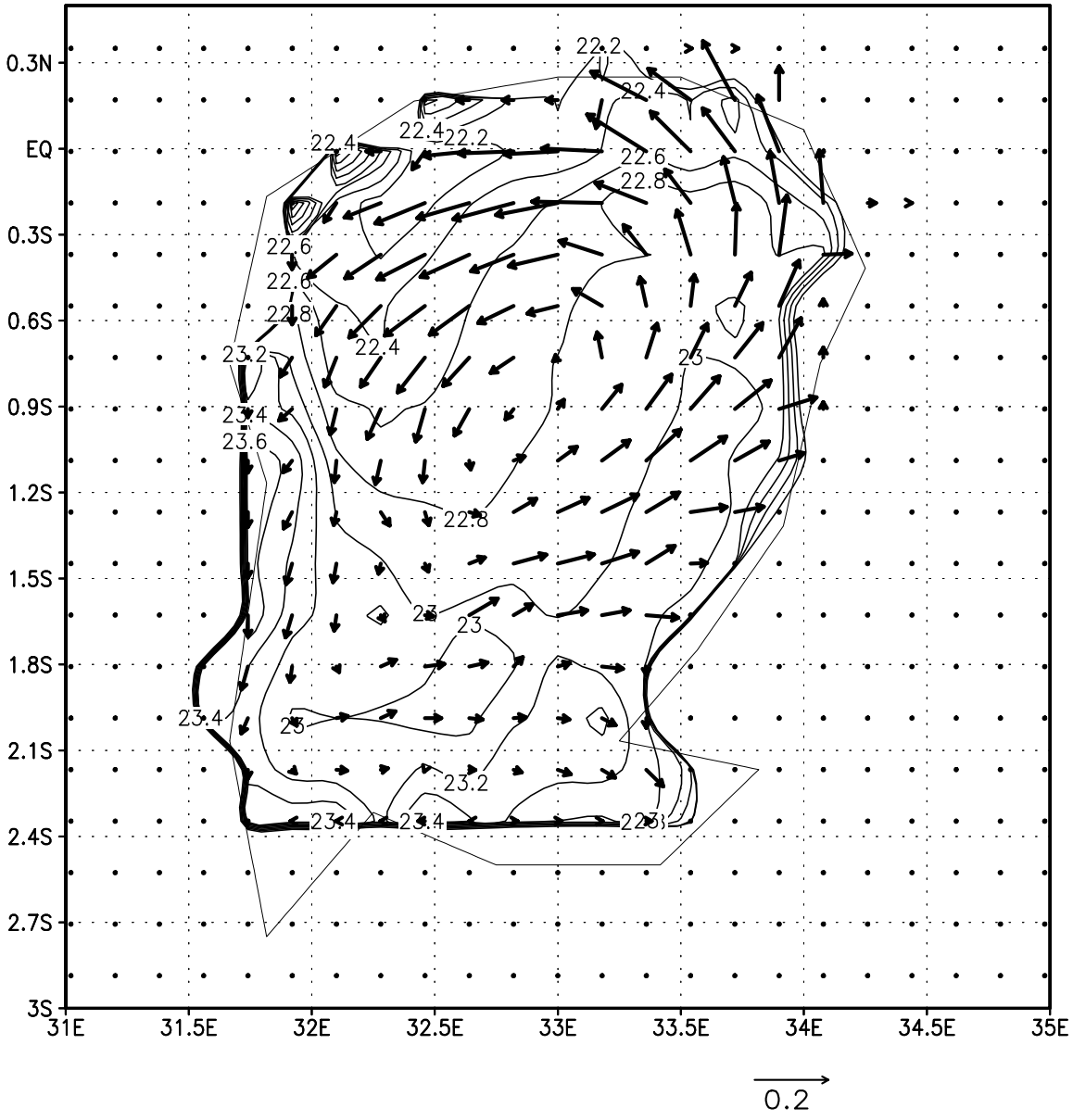

Fig. 2.15. Simulated monthly mean surface circulation and temperature of Lake Victoria driven by the wind stress and heat flux in December 1988. Units in m/s (current) and °C (temperature).

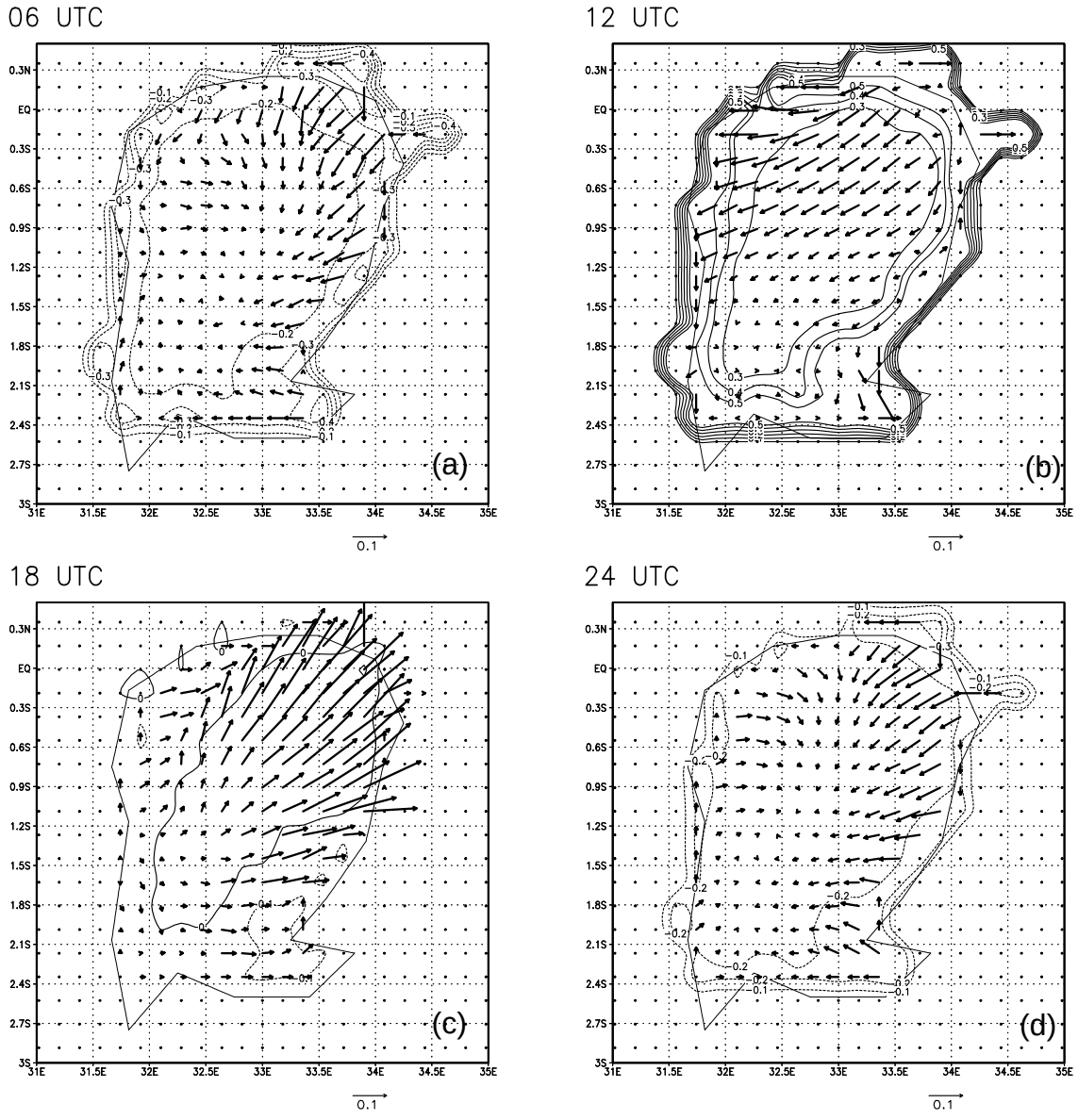

Fig. 2.16. Same as Fig. 2. 14 except for the anomalous field. a). at 06UTC. b). at 12UTC. c). at 18UTC. d). at 24UTC. Units in m/s (current) and °C (temperature).

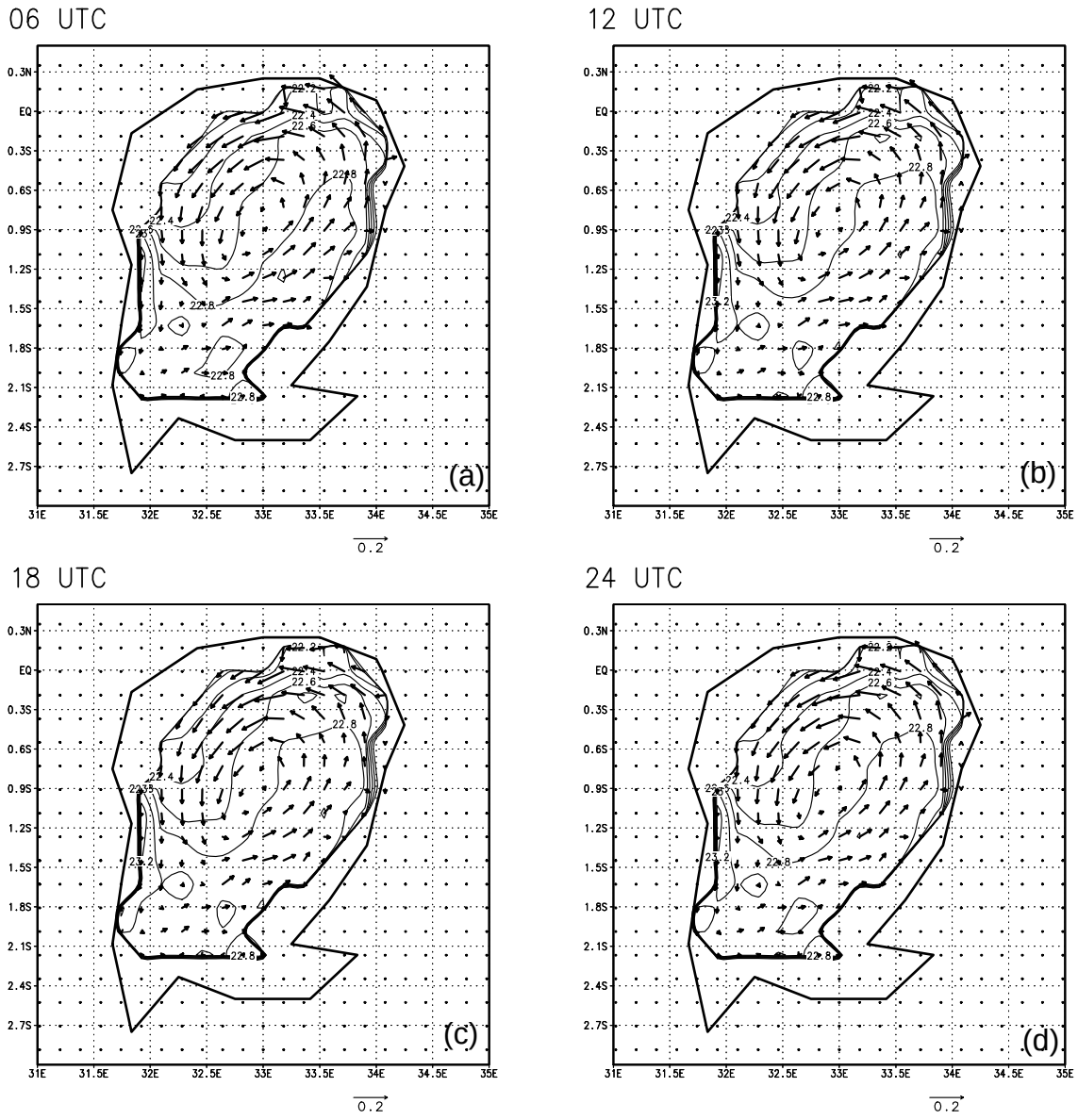

Fig. 2.17. Same as Fig. 2.14 except for field at 20m depth.

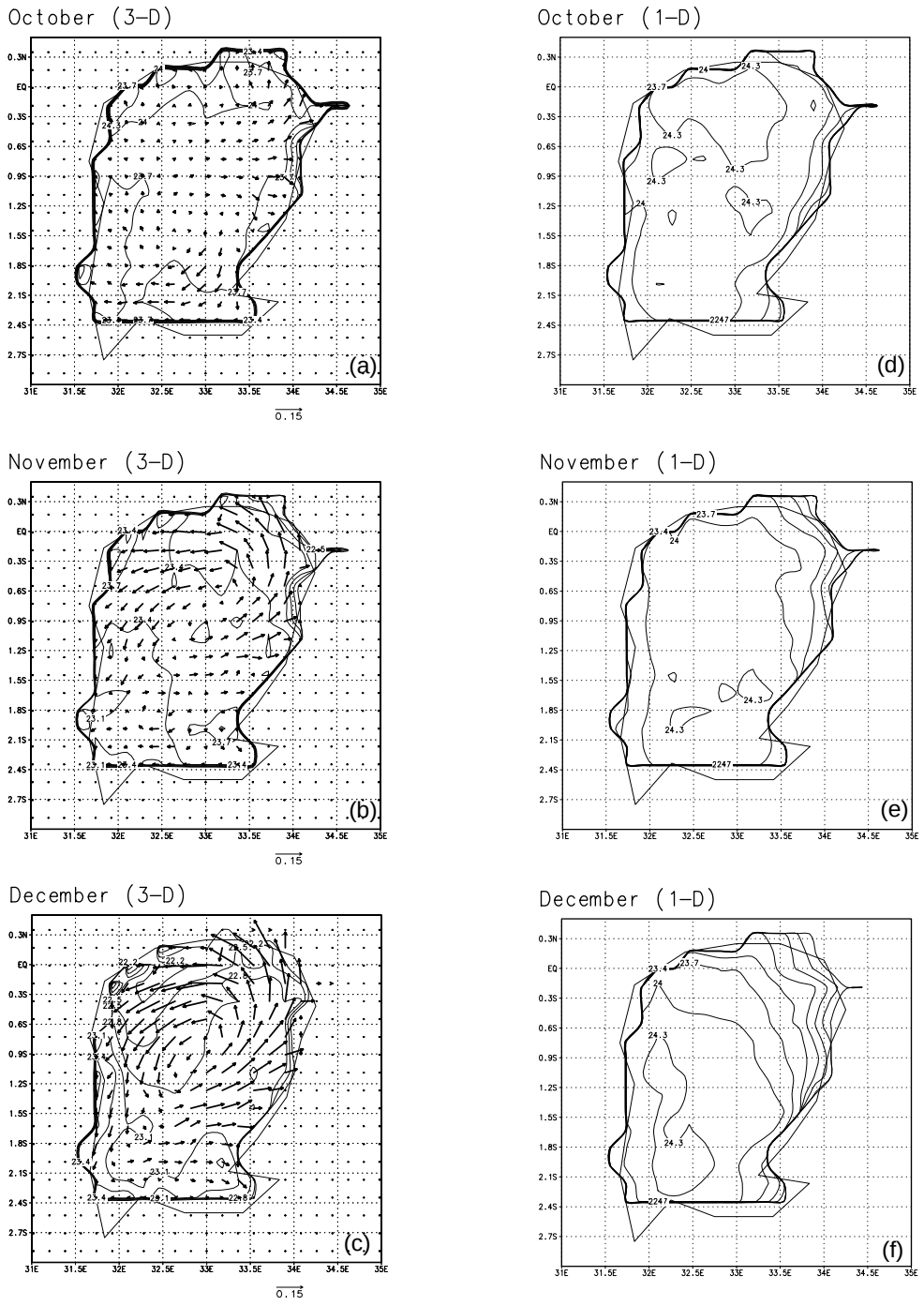

Fig. 2.18. Monthly mean surface water circulation and temperature distribution over Lake Victoria (October-December 1988), simulated by the 3-D and 1-D lake model. a). October, b). November and, c). December, based on the 3-D model; d). October, e). November, and, f). December, based on the 1-D model. Units in m/s (current) and °C (temperature).

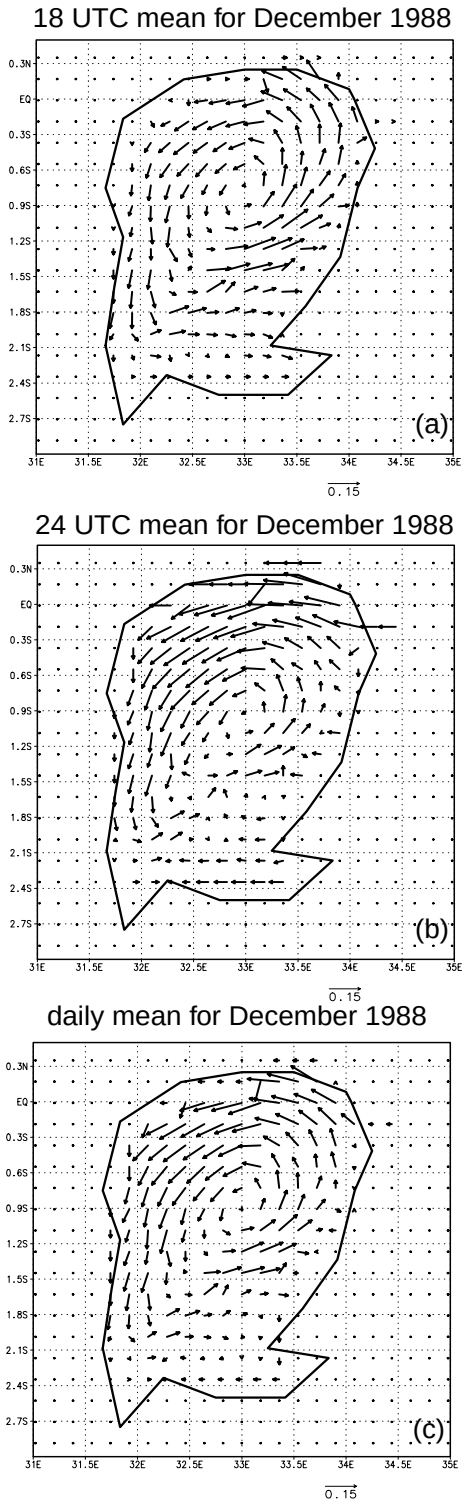

Fig. 2.19. Simulated surface circulation of Lake Victoria driven by surface wind stress. a). at 18UTC. b). at 24UTC. c). mean for one month. Units in m/s.

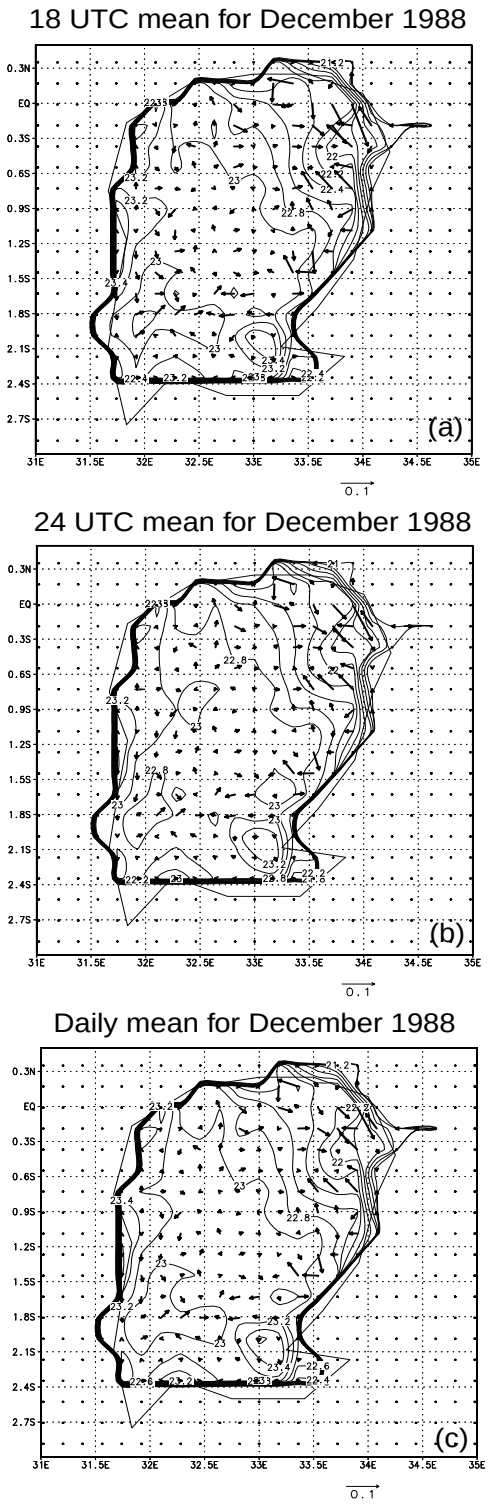

Fig. 2.20. Same as Fig. 2. 19 except driven by heat flux.

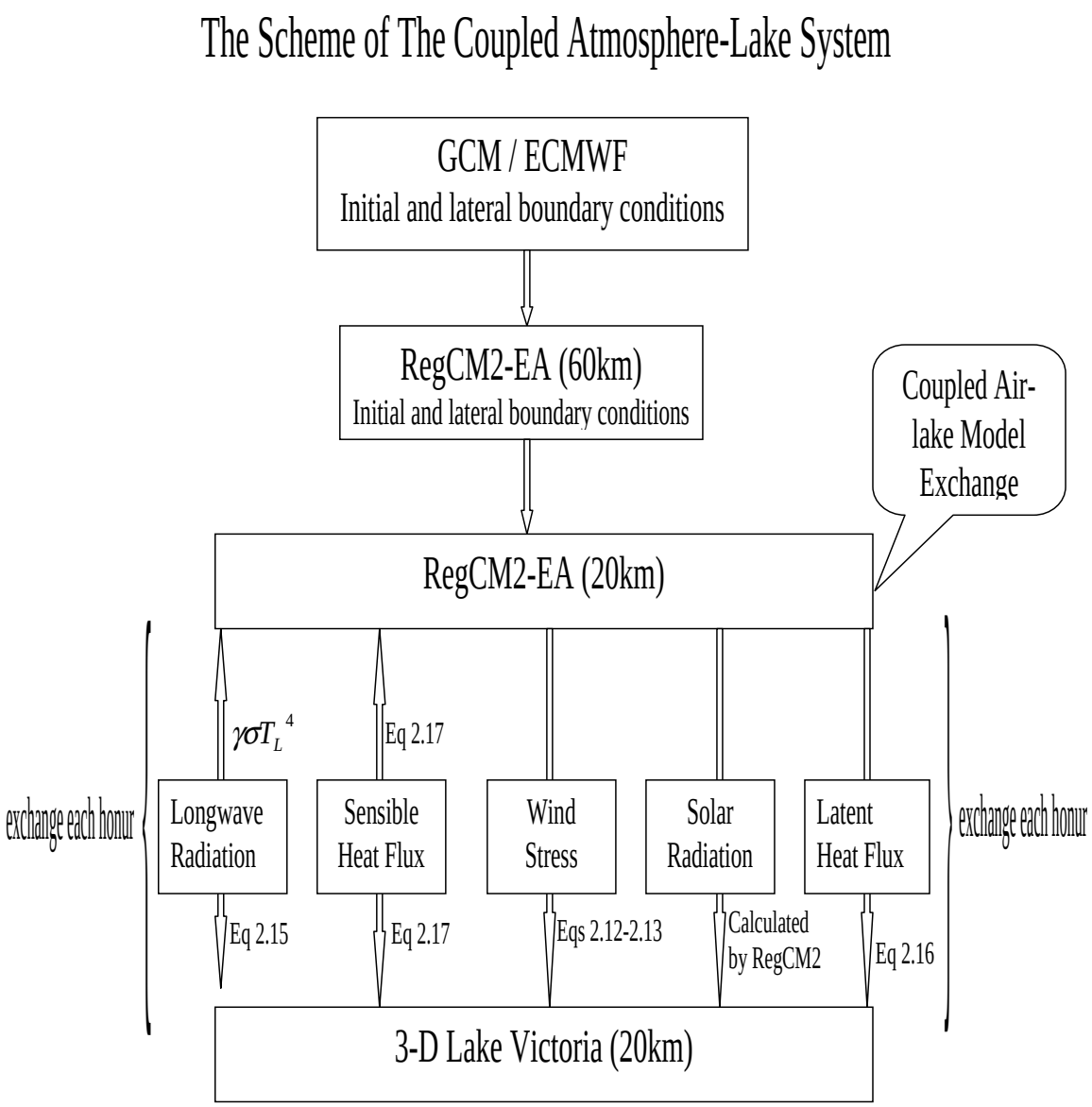

Fig. 2.21. The scheme of the coupled atmosphere-lake system.

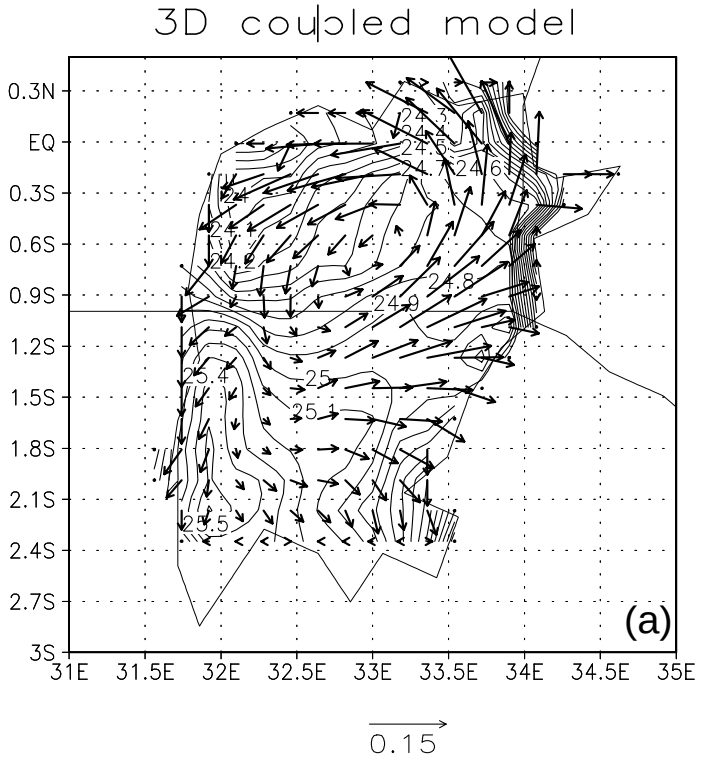

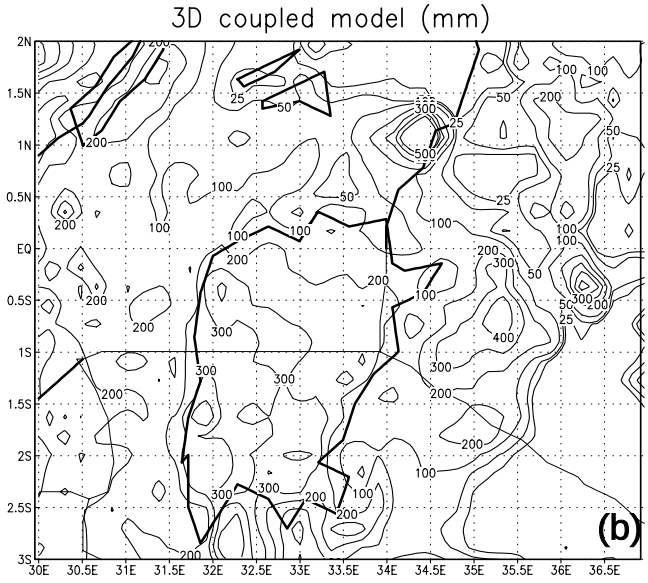

Fig. 2.22. December average: (a) Lake surface circulation and temperature in °C, and (b) rainfall in (mm), simulated by the coupled RegCM2-POM model.

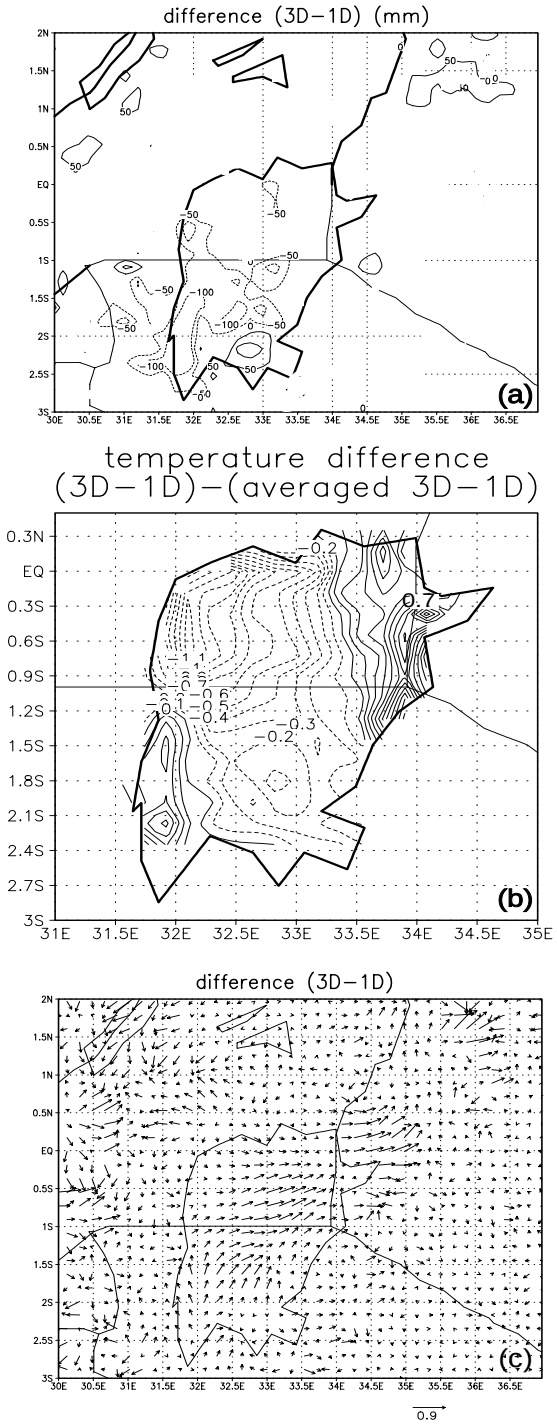

Fig. 2.23. December average difference (RegCM2-POM minus RegCM2-1D): (a). Rainfall (mm), (b) lake surface temperature, and (c) lake surface circulation. In the case of surface temperature the area mean values are removed to highlight the surface gradient and hence the following formula is adopted, $[3D-1D]-ave[3D-1D]$

Chapter 3

An Investigation of the Climate of the Lake Victoria Basin Using a Regional Coupled Atmosphere-Lake Model

3.1 Background

The primary factor responsible for the climatological seasonal variations of rainfall in eastern Africa is the meridional movement of the Inter tropical Convergence Zone (ITCZ) and the influence of the adjacent ocean basins. Lake Victoria is a large reservoir of energy and momentum, perhaps, capable of releasing it in a delayed mode and therefore influencing subsequent seasonal climate through its memory. Furthermore, the land-lake breeze effect (Cocheme, 1960) plays an important role in re-distributing the moisture and energy across the region. For a broad range of environmental problems, it is necessary to characterize and understand the time-dependent three-dimensional dynamical and thermodynamic behavior of the lake's circulation. The climatology of large lakes is particularly interesting dynamically because they have similar forcing as coastal ocean dynamics and mesoscale water circulation regimes (Csanady 1984).

In many previous studies of lake-atmosphere systems, models have been used that do not fully include the circulation of the water. For example, a coupled regional climate-lake model has been used to investigate the water balance of the Aral Sea (Small, et al, 1999). In this study, the lake is represented by a one-dimensional thermodynamic diffusion equation and does not permit transfer of heat or other quantities between adjacent lake points. The climate study of atmosphere-lake interaction over Lake Victoria showed that the hydrodynamics of the lake plays an important role in determining the coupled variability of the lake and the regional climate (Song, et al, 2000). The studies further showed that the traditional modeling approach in which the lake hydrodynamics are neglected and the formulation is entirely based on thermodynamical considerations is not satisfactory for eastern Africa. Such a strategy deprives the coupled regional climate model of the ability to transport heat efficiently within the lake and thereby degrades the simulation of the climate downstream over the rest of the lake and the surrounding regions. Thus, a regional coupled atmosphere-lake model is essential for investigating the coupled variability of the regional climate of eastern Africa.

Over Eastern Africa ENSO plays a dominant role in modulating the regional climate. The ENSO phenomenon is a quasi-global climatic fluctuation related to the strong air-sea interaction. A number of recent studies have analyzed the rainfall over eastern Africa and have uncovered further interesting associations with ENSO. Nicholson and Entekhabi (1987), Ropelewski and Halpert (1987), Ogallo (1987) and Farmer (1988) have all demonstrated a strong link between the rainfall in eastern African and the global

ENSO phenomenon. The interannual climate variability of the eastern African climate is dominated by ENSO. Widespread positive anomalies of precipitation tend to occur during the short rains of the ENSO years, drought conditions during the long rains of the following year and the short rains of the year prior to ENSO. The link appears to be indirect, and the main causal mechanisms appear to be fluctuations in SST of the tropical Atlantic and Indian Oceans that in turn are loosely coupled to ENSO (Nicholson 1996). In the eastern Africa, the strongest effect of ENSO appears to be during the short rainy season (Nicholson 1996). ENSO can explain about 50% of the eastern Africa rainfall variance and the remaining variations are determined by the other factors (Ogallo, 1988). In a recent study, Indeje, et al, 2000, noted that the relatively wet conditions were observed during the months of March-May and October-December during the ENSO years; Dry conditions dominate the period during June-September of the ENSO onset years and the two seasons of the post-ENSO years. However, due to limitation of the observational data over Lake Victoria, relatively less attention has been directed to explore the effects of ENSO on the atmosphere-lake interaction associated with Lake Victoria and its role in modulating the climate variability over eastern Africa. The object of this study is to (a) investigate the variability of the circulation that is associated with the El Nino and non-El Nino years, (b) understand the physical mechanisms responsible for the flooding and drought conditions over eastern Africa during the short rains. Results from this study may provide the background for the short-term climate prediction.

In this study, the regional coupled RegCM2-POM model (Song, et al., 2000) which was

developed at North Carolina State University is adopted to simulate the climate conditions over Lake Victoria basin. The simulations were conducted for the near normal year (1988) and two contrasting years (the wet (1982) and dry (1987)) to investigate the dynamical and thermodynamical mechanisms responsible for determining the corresponding climate anomaly conditions in this case study for eastern Africa during the short rainy season.

The outline of this chapter is as follows. Section 3.2 provides the experiment design. Section 3.3 discusses the model simulation in the near normal year of 1988. Section 3.4 compares the results from the simulated atmospheric and lake portions of the modeling system, respectively, in an El Nino year with those in the non-El Nino year. Conclusions are given in section 3.5.

3.2 Experiment Design

The coupled RegCM2-POM model described in Chapter 2 is used here to study the climate variability over Lake Victoria basin and the physical mechanisms involved. The atmospheric portion of the coupled RegCM2-POM model adopted here includes 15 σ levels with the model top at 50mb. The horizontal grid size is 20km in both the x and y directions. The lake portion employs 9 sigma levels in the vertical, and layer thickness of approximately 8m over the deepest region of the lake and 0.5m over the shallowest locations. The horizontal grid spacing is also 20 km in both the x and y directions which

gives 191 grid points covering the entire lake. The topography of the model domain and the lake bathymetry is shown in Fig.3.1. The surface fluxes across the atmosphere-lake interface are updated every hour in the lake model. The predicted lake surface temperature by the lake model is kept constant within the one-hour interval, and it is used as the lower boundary condition for the atmospheric model.

According to the analysis of the observational data by Indeje (2000), during the period 1980-1990 over eastern Africa, the wettest year over eastern Africa is 1982, and the driest year is 1987. During 1988 the conditions were near normal. The year 1982 is associated with one of the strongest El Nino of this century (Trenberth, 1997). In this case study, model simulations for 1982 and 1987 were conducted using the coupled RegCM2-POM model to investigate the physical mechanisms responsible for the wet and dry condition during those years. The simulation for 1988 is considered as the control experiment. Four-month simulations using the coupled RegCM2-POM model were conducted from September 1 to December 31 for 1982, 1987 and 1988. The model domain is 1660 km by 1480 km centered at (33°E, 1°S), which covers the Lake Victoria catchment (Fig.3.1). The initial and lateral boundary conditions of the atmospheric model were taken from the output of the coarse resolution (60km) RegCM2-NCSU model with the simple formulation of Lake Victoria, run for the three different years. The results of the RegCM2-NCSU with 60 km resolution have been discussed in previous studies (Sun et al, 1999ab, Song et al 2000). The initial lake temperature was set to isothermal

conditions of 24°C and the lake model was integrated from motionless initial conditions. Table 3.1 is a summary of the numerical experiments that were conducted.

Table 3.1 Summary of Numerical Experiments

	Simulation period	Initial conditions for the atmosphere part	Lateral boundary condition for the atmosphere part	Initial temperature structure for the lake part
Experiment for the normal year (Control)	Sept. 1, 1988 to Dec. 31, 1988	Based on the output of the RegCM2 for 1988 by 60km	Based on the output of the RegCM2 for 1988 by 60km	isothermal conditions of 24°C
Experiment for the wet year	Sept. 1, 1982 to Dec. 31, 1982	Same but for 1982	Same but for 1982	Same
Experiment for the dry year	Sept. 1, 1987 to Dec. 31, 1987	Same but for 1987	Same but for 1987	Same

3.3 Simulated results of the control run

As discussed in section 2.4, the climate conditions in 1988 were observed to be representative of a normal year during 1980s. Therefore, the simulation corresponding to 1988 is considered as the control experiment in this investigation. The major features of the simulation results are discussed below.

3.3.1 Atmospheric analysis

The simulated wind field at 850mb for December is shown in Fig.3.2. In the large-scale flow pattern we note an anticyclone located over the Arabian peninsular and the Mascarene high pressure cell is located over the southern Indian Ocean. Influenced by the two high-pressure systems, Northeasterly monsoon which controls the seasonal climate over eastern Africa during the short rains is determined. In the wind field at 850mb (Fig.3.2a), the strong northeasterly flow dominates the eastern part of the domain, the northwestern part of the domain is dominated by northeasterly to easterly flow, and the southwestern region is mainly dominated by northerly flow. The simulated winds over Lake Victoria are relatively weak, especially over the southwestern region of the lake where the monthly averaged wind speed is less than 2m/s (Fig.3.2b). Over the northeastern part of the lake, we find a local maximum in the wind speed with values in excess of 6m/s. Considering the lake area, the eastern bank is a relatively strong wind speed region, while the western bank is a relatively weak wind speed area. This wind patterns is consistent with the results based on 60km resolution RegCM2 that were reported by Sun et al (1999), but the coupled RegCM2-POM model generates more detailed wind structure due to the lake and the complex topography.

Fig.3.3a displays the vertical cross section of the horizontal zonal wind for December along 1°S across Lake Victoria and its catchments. Throughout the entire atmospheric depth there exists uniform easterly flow. Easterly flow stronger than 8m/s is centered at

750mb level (between 35°E and 36°E) and the corresponding northerly wind is greater than 3.5m/s (Fig.3.3b). The strong flow over this part of the atmosphere maybe linked to the northeasterly monsoon. The maximum regarding the easterly winds is located around 500mb and it is in excess of 11m/s nearly throughout the entire model domain, while the meridional wind is relatively weak at 500mb. The simulated strong winds at 500mb maybe related to the mid-tropospheric Africa easterly jet. Inspection of the vertical cross section of horizontal meridional wind for December along 33°E across Lake Victoria and its catchments (Fig.3.3b) indicates that the northerly winds dominate the low and middle troposphere, while southerly winds dominate the upper troposphere. This meridional wind distribution maybe a manifestation of the Hadley circulation over the lake region.

The simulated surface air temperature in December is shown in Fig.3.4a. The air temperature above the entire lake is significantly higher than that over the surrounding regions, and this difference is more than 2.5°C. This pattern of surface air temperature indicates that the lake strongly influences the climate over eastern Africa. Over the lake region, the surface air temperature is relatively high over the southwestern and northeastern sectors of the lake, and low over the northwestern region of the lake. This pattern of the surface air temperature is similar to that in the lake surface temperature (Fig.3.7a). The co-located patterns of the surface air temperature and the lake surface temperature further indicates that there exists strong atmosphere-lake interaction thus reconfirming the importance of realistic representation of the lake in the model to

produce realistic the simulation of the surface lake temperature.

The simulated evaporation is shown in Fig.3.4b. The high evaporation region is located over the northern and eastern lake, especially over the northeastern area of the lake. The low evaporation area is located to the west of the center of the lake. This evaporation pattern is very similar to the wind speed pattern at 850mb (Fig.3.2b). At 850mb, the cold and dry downhill wind from the Kenya mountain is strong, especially over the northeast of the lake (Fig.3.2). We can see that in equation 2.18, the evaporation rate depends on the difference between the specific humidity of the air and the saturation specific humidity of the water surface, and is also determined by the surface air wind speed. The saturation specific humidity of the water surface is a function of surface temperature only. When this strong dry wind crosses the lake surface, high evaporation occurs along the northern and eastern regions, especially over the north and the airflow becomes moist. Furthermore, as this moist airflow changes its direction to slight northeasterly and northerly near the central part of the lake it advects the moisture toward the southwestern region where the heavy precipitation takes place in the model (Fig.3.5a). Although the lake surface temperature is high to the western-central part of the lake (Fig.3.3a), the surface wind is very weak. Consequently, the evaporation is relatively weak there too. Hence, the evaporation patterns are strongly influenced by the wind speed, and the contribution of moisture advection may be a very important factor in explaining the heavy rainfall over the southwestern part of Lake Victoria.

The simulated precipitation in December 1988 is shown in Fig.3.5a. There are three heavy rainfall areas located over the northwestern, southwestern and southeastern regions of the lake. For the lake surface temperature field (Fig.3.7a), the warm water is also located over the southwestern and southeastern regions, and a strong temperature gradient is located over the northwest. This co-located feature characterized by the heavy rainfall and over the warm water or the strong LST gradient area indicates existence of strong interaction between the atmosphere and the lake. The patterns of the lake surface temperature strongly influence the distribution of the precipitation over the lake region. The strong atmosphere-lake interaction is also evident in Fig.3.6, in which the time series for lake surface temperature and daily precipitation averaged over the lake in December 1988 are shown. For most of the rainfall events, the lake surface temperatures are also relatively high. The precipitation is highly related with the lake surface temperature.

Characterization of the rainfall over Lake Victoria and its catchment has attracted much research interest over the years. Spigel and Coulter (1996) found that the monthly rainfall annual range is about 80mm to 225mm, with about 130mm in December. Ochumba (1996) pointed out that the monthly rainfall varies from 10mm to 135mm over the northeastern region of Lake Victoria and the rainfall in December is about 130mm. Ba and Nicholson (1998) investigated the rainfall over the lake and its catchment, and estimated the monthly area-averaged rainfall in 1988 to be in the range of 48mm to 185mm and with about 137mm in December 1988.

Table 3.2 Comparison of observed and simulated rainfall using the RegCM2-POM model for December 1988.

	RegCM2-POM	Observed	Difference (simulation-observed)	Percentage (difference/observed)
Region based on Bugenyi et al (1996)	143.5 mm	130 mm	13.5 mm	10.38%
Entire lake basin	140.0 mm	135 mm	5.1 mm	3.77%

Table 3.2 shows comparison of the model simulations and the observations. Spigel and Coulter (1996) averaged the rainfall over the stations of Entebbe, Kisumu, Mwanza and Bukoba along the perimeter of Lake Victoria and produced an estimate of 130mm for December. The corresponding monthly precipitation simulation based on the RegCM2 model averaged over the same four stations is 143.5mm for December 1988. This is 13.5mm (10.38%) more than the observed average. Ba and Nicholson (1998) estimated 135mm for December 1988 over their study area (5°N-10°S, 25°-40°E) which covers much of Lake Victoria basin. We computed the simulated rainfall averaged over the model domain (Fig.3.5a), which is smaller than their study region. For December 1988 we obtained 140.1mm for RegCM2-POM. The corresponding rainfall bias is +3.77% (RegCM2-POM). We note that the observational stations are not located over the lake. The regions considered in the comparison of the model performance and the estimates given by in Ba and Nicholson (1998) are slightly different. Furthermore, the time period

used by Spigel and Coulter (1996) is different from the one adopted in our study. Despite these differences, the balance of evidence indicates that the performance of RegCM2-POM is very encouraging as a vehicle for investigating climate variability over eastern Africa in general, and the climate over the basin of Lake Victoria, in particular.

Fig.3.5b is the difference (P-E) between precipitation and evaporation. The negative P-E means that the precipitation is less than the evaporation, and the positive P-E indicates that the precipitation is greater than the evaporation. The P-E value is strongly negative over the western, central and southern sections of the lake, especially over the southwestern part of the lake where maximum precipitation occurs. This P-E pattern suggests that moisture convergence play an important role in determining the precipitation pattern over the lake basin. Over the eastern and northern areas where downhill wind prevails, the evaporation is more than the rainfall. The averaged P-E over the entire lake is –13.4 mm. This implies that the total evaporation during December 1988 is more than the rainfall over Lake Victoria, which is also evident in the climate conditions computed by Yin and Nicholson (1997). The net result is that the lake loses water to its surrounding regions. This unbalanced hydrological cycle may contribute to the recent lake level decrease (Yin et al, 1997). However, under the conditions of December 1988, Lake Victoria not only sustains itself, but also provides water vapor to its surround regions. Therefore, Lake Victoria plays an important role in determining the hydrological conditions over eastern Africa.

3.3.2 Lake surface analysis

The simulated lake surface water temperature and surface water circulation during month-4 (i.e. December 1988) are shown in Fig.3.7a. The simulation results are characterized by a horizontal spiral pattern in the water current field which transports warm water to the northern section and cold water to the southern section. A distinct warm pool of water is located over the southwestern part of the lake. The net result is a warm tongue in the northeastern part and a cold tongue over the northwestern part of the lake.

Over the years, several studies have provided assorted observational data of the temperature of the lake at different locations and for different years. Spigel and Coulter (1996) discussed the surface temperature of Lake Victoria in December for the period 1960-1961 and for 1990-1991, about 32 km south of the source of River Nile, at Jinja in Uganda. Ochumba (1996) described observed monthly mean surface temperature at numerous locations over the northeastern part of the lake for 1992. Spigel and Coulter (1996) discussed the surface temperature during the course of the year based on Talling's data (Talling, 1968). However, the locations of observational stations used to obtain these data are offshore. Yin and Nicholson (1997) have argued that Talling's surface temperatures probably best represented the temperature during the period of 1956-78 and used it to calculate the water balance of Lake Victoria using their hydrological model. Since more suitable observational data is not readily available, Talling's surface temperature is also used in this study to assess the performance of the coupled RegCM2-

POM model.

Table 3.3 Model simulated lake surface water temperatures averaged over the entire lake in December 1988 and Talling's observational data.

	RegCM2-POM	obs (Talling, 1976)	model-obs	Percentage (difference/obs.)
Mean LST	24.4°C	25.2°C	-0.8°C	-3.17%

Table 3.3 summarizes the comparison of the lake surface temperature based on Talling's observed data and the RegCM2-POM model. The lake maximum surface temperature simulated by the coupled RegCM2-POM is 25.5°C and it is located over the southwest sector of the lake, which is also the shallowest region of the lake. The averaged simulated lake surface temperature over the entire lake is 24.4C which is 0.8°C (3.17%) cooler than Talling's observed temperature. We note that the observational data might be based on only a few stations, while the lake surface temperature considered in the comparison of the model performance is averaged for the entire lake. Furthermore, the time period used by Talling is different from the one adopted in our study. Therefore, we may conclude that the coupled RegCM2-POM model performs well to reproduce the lake conditions. However, this comparison with observations must be considered as preliminary until more compatible observational data becomes available to confirm the analysis. Despite these differences, the balance of evidence firmly indicates that the performance of

RegCM2-POM is superior to the RegCM2-1D model for reproducing and investigating the climate variability of Eastern Africa in general, and the climate over the basin of Lake Victoria, in particular.

Fig.3.7b shows the simulated monthly mean vertical velocity over the water surface in December 1988. The positive value corresponds to upwelling and the negative value to downwelling at the surface, respectively. The downwelling regions are located over the southern, central-western, central-eastern, and central-northern lake, which are co-located with the warm pool and the warm tongue in Fig. 3.6a. The upwelling areas are located over the northern, northwestern and the areas along the east boundary, which is also co-located with the cold of water. These co-located patterns between upwelling/downwelling and cold/warm areas indicate that the surface warm water is transported into the deep part of the lake by the downwelling current and the deep cool water is raised by the upwelling current. Along the east and north shore, the strong easterly and northeasterly wind regimes (Fig.3.2) drive the surface water off shore and thus induce the upwelling there. The anti-clockwise lake circulation transports the water to the southern lake where the surface current is very weak, and the water piles there and thus induces downwelling over the southern region of the lake. Therefore the coupled RegCM2-POM model reproduces a reasonable three-dimensional temperature and circulation patterns even though adequate observational data is not readily available to validate these simulation results definitively.

3.3.3 Diurnal variation

Simulation of the realistic diurnal cycle is an important attribute of credible climate models. In particular, this is important in the vicinity of large water bodies to ensure that the simulation of the lake/land breeze is realistic. Analyses of satellite observational data shows that the maximum convection occurs over Lake Victoria during the morning, and over the surrounding land region during the late afternoon and evening (Ba et al., 1998). Based on rain gauge data Datta (1981) showed that the diurnal cycle is characterized by morning to midday maximum in rainfall frequency over the western shore, afternoon maximum over the eastern shore, and an early morning maximum over the center of the lake in the vicinity of the western island of Nabuyongo and nearby locations. The seasonal changes in the large-scale flow pattern associated with the movement of the ITCZ are further modified on the mesoscale by the land-lake breeze effect (Cocheme, 1960). The results show that the model remarkably reproduces the observed asymmetries in the diurnal cycle around Lake Victoria and correctly simulates a diurnal peak in rainfall around 6-9 am in the morning for the western shoreline of Lake Victoria. The peak for the eastern shoreline occurs between 8:00pm and mid-night. For the model to produce these results many processes have to be correctly modeled.

The simulated monthly mean wind vectors at 850mb for 06UTC (09 local standard time (LST)), 12UTC (15 LST), 18UTC (21 LST) and 24UTC (3 LST) December 1988 are shown respectively in Fig.3.8 a-d. The land and lake breeze changes are strongly evident.

The lake breeze dominates the lake catchment during the afternoon (12UTC) and early evening (18UTC) when the easterly component reaches its maximum over the western shore and the westerly component reaches its maximum over the eastern coast. The strong divergence dominates over the lake and convergence over the surrounding land during this period of the day. Strong land breeze circulation occurs late at night (24UTC) and early in the morning (06UTC) when the convergence dominates over the lake. This simulated lake-land breeze is consistent with the observational analysis produced by Datta (1981).

Corresponding to the lake-land breeze analysis, the simulated precipitation for 0-06UTC, 06-12UTC, 12-18UTC, 18-24UTC December, 1988, over the lake catchment are displayed in Fig.3.9 a-d. The maximum rainfall is located over the western part of the lake, and the minimum rainfall is located over the northeastern part of the lake. Over the western part of the lake, most of the precipitation occurs during early morning (0-06UTC), little during late part of the night (18-24UTC) and late morning (06-12UTC), and no precipitation during the afternoon (12-18UTC). Over the central part of the lake, the precipitation takes place from night (18UTC) to morning (06UTC), and no precipitation during the daytime (06-18UTC). Over the eastern part of the lake, the maximum precipitation occurs around midnight (18-24UTC), and a sharp decrease in rainfall is evident after midnight with little or no rainfall during daytime (06-18UTC). Therefore, the precipitation mainly occurs around the mid-night and early morning when the land breeze dominates over the lake. Little or no rainfall occurs during daytime and

early evening when the lake breeze dominates over the lake. These results show that the diurnal variations in the precipitation are therefore highly related to the lake-land breeze.

Fig.3.10a shows the time cross section of streamline at 10m height for December along 1°S across Lake Victoria. Divergence and convergence activities are clearly indicated by the streamline pattern. Divergent flow forms over the eastern coast around 09UTC and then shifts westward. This wind divergence passes through 33°E around 10:30 UTC, which is also confirmed in Fig.3.10b in the time cross section of streamline along 33°E, and arrives along the western coast around 15UTC. The wind convergence originates from the east coast at about 18:30 UTC and also moves westward. The signal crosses 33°E at about 21UTC, which is also evident in Fig.3.10b, and arrives along the western cost around 21:30UTC. It therefore, takes about 6 hours for the divergent air to travel across the lake, while about 3 hours for the convergent air to travel the same distance. Since the basic flow is the northeasterly at 1°S (Fig.3.2a), the lake breeze counteracts the easterly component during the daytime (Fig.3.8b) and the land breeze intensifies the easterly component (Fig.3.8d). This westward movement of divergent and convergent zone may be mainly attributed to Sun's insolation, but it is apparent that the interaction between the basic flow and the lake-land breeze also influences this pattern of movement. In Fig.3.10b, the divergent zone is stationary, however the convergent zone travels southward between the northern coast and the southern coast from 18:30UTC to 21:30UTC. Similar to the divergent zone along 1°S in Fig.3.10a, the convergent zone

along 33°E is also affected by the interaction between the northeasterly flow and the lake-land breeze. We find that the basic flow is northeasterly along 33°E (Fig.3.2a), and the lake breeze counteracts the northerly component during the daytime (Fig.3.8b). Consequently, the land breeze intensifies the northerly component (Fig.3.8d).

Fig.3.11a shows the monthly mean diurnal variations for surface temperature in December 1988 along 33°E. The surface water responds strongly to the variations of the surface atmospheric forcing, especially near the shore over the southern region of the lake where the surface temperature is higher than over the northern sector. The surface temperature reaches its maximum value of 25.8°C at 12UTC and drops to a minimum of 24.6°C around 03UTC near the shore of the southern part of the lake. The diurnal change in surface temperature is about 1.2°C. Fig.3.11b displays the departures from the monthly mean. The results are obtained by abstracting the entire monthly mean surface temperature from the monthly mean diurnal surface temperature. From 05UTC, the lake absorbs energy from the Sun and its temperature begins to rise. During the 7 hours of the Solar heating, the lake surface attains its maximum departure of +0.9°C at about 12UTC, and then begins to decline thereafter. Around 04UTC, the lake surface attains its minimum temperature which corresponds to about –0.3°C departure from daily mean. In contrast, the variation in the water temperature at the center of Lake Victoria is relatively insignificant.

To further explore temperature diurnal changes with depth simulated using the coupled lake model, the simulated lake temperatures variation with depth around (32.7°E, 1°S) is displayed in Fig.3.12. Since most of the temperature changes occur within the upper portion of the lake above the thermocline, only the top 45m are shown in the figure to indicate more detail of the diurnal changes. From midnight to early morning, the mixed layer is isothermal and this isothermal layer deepens as the lake cools and the thermocline erodes. During the early morning, the lake becomes isothermal at 35m depth at a temperature of about 24.6°C. During the late morning, the water near the surface warms rapidly, the lake stratifies, and the mixed layer deepens. The surface lake water reaches maximum daily temperature of 25.5°C at 12UTC. Therefore, the mixed layer varies diurnally.

In the monthly mean diurnal variation of the lake surface circulation (figures omitted), similar to the diurnal changes in the "stand-alone" 3-D lake model (Song et al, 2000), although the surface winds reverse direction during the course of the day in association with the land/lake breeze, and also dominate the total wind field, the water circulation maintains the same anti-clockwise circulation (Fig.3.7a) throughout the day. However, the diurnal variation occurs at the strength of the surface currents. This observation re-enforces the conclusion based on the "stand-alone" lake model results that the circulation of the lake is primarily controlled by the prevailing wind pattern rather than the component associated with the land/lake breeze.

3.4 Simulation of a wet and dry event using the coupled RegCM2-POM model

1982-1983 El Nino is the strongest air-sea interaction global climate anomaly signal during the decade of the 1980s. The climate response over the eastern Africa is also the strongest and the climate conditions over eastern Africa in 1982 is the wettest year in 1980s (Indeje, 2000). In contrast, the climate condition over eastern Africa in 1987, which is a post year of ENSO, is the driest year during the 1980s.

3.4.1 Comparison of the simulated circulation

The simulated wind flow patterns at 850mb for December during the wet El Nino year (1982) is shown in Fig.3.13a, and the corresponding anomaly pattern (wet year minus the control year) is displayed in Fig.3.13b. The wind flow is relatively stronger over the lake catchment, especially the northerly component. The averaged wind speed over the lake catchment is 2.7m/s in 1982 compared to 2.2m/s in 1988. The northeasterlies decelerate over the eastern lake and forms a convergent area there. In the wind anomaly patterns (Fig.3.13b), the relatively strong northwesterlies anomaly dominate over the northwestern part of the model domain, the strong northerly anomalies prevail over the lake. Westerly anomalies dominate over the eastern part of the domain. According to the study over a larger domain (Indeje 2000), over eastern Africa in 1982, the easterly originates from the Indian Ocean while the westerlies are from the moist Congo forest/Atlantic Ocean. The westerly anomaly flow over our domain indicates that the moisture advection from the

Congo forest/Atlantic Ocean might be important for the wet anomaly conditions over eastern Africa, while the Indian Ocean perhaps does not seem to have played a critical role in 1982.

The simulated wind flow patterns for the dry year (1987) and the corresponding anomaly pattern (dry year minus the control year) at 850mb level are displayed in Fig.3.14a and Fig.3.14b. The easterly wind speed over the lake is on average or weaker comparing to that in 1988. The averaged wind speed over the lake catchment is 1.8m/s in 1987 compared to 2.2m/s in 1988. The northeasterlies decelerate over the eastern lake and which results in a convergent zone there. In the wind anomaly patterns, we note a divergence anomaly pattern located over the lake over south of the Equator where the heavy rainfall occurs under the normal conditions, while the convergent flow dominates over the central-northern part of the lake associated with relatively light rainfall under normal conditions (Fig.3.5a). According to a study based on a larger model domain over eastern Africa in 1987(Indeje 2000), the southeasterly and northeasterly flows exhibit a longer continental track and a relatively short maritime track. The corresponding divergent circulation over the lake and the drier moisture conditions might be an important mechanism for supporting the dry anomaly over eastern Africa in 1987.

The latitude-height cross sections for the meridional wind speed averaged between longitudes 32°E and 33.5°E for the wet minus control and dry minus control are shown in Fig.3.14. In the wet year (Fig.3.15a), the southerly wind anomaly extends from surface to

above 500mb level with overlying northerly wind anomaly centered at 200mb level. This negative wind shear may benefit the Hadley circulation over the lake and strengthen the convection. In the dry year (Fig.3.14b), the southerly wind anomaly is observed throughout the entire troposphere. This pattern might be conducive for the stable troposphere and weakened Hadley circulation.

The corresponding latitude-height cross sections of vertical wind speed averaged between longitudes 32°E and 33.5°E for the wet year and dry year are displayed in Fig.3.16. The relatively stronger upward movement is located over the lake basin during the wet year while the relatively weaker upward movement takes place during the dry year. These vertical movement patterns are further conducive for the heavy rainfall during the wet year and light rainfall during the dry year.

These results indicate that the convergence and associated convection and vertical motion are enhanced over the lake basin during the wet year, and strongly suppressed during the dry year. During 1982, the moisture advection from the Congo forest/Atlantic Ocean might have been an important mechanism for the wet anomaly conditions over eastern Africa, while the Indian Ocean perhaps did not play a critical role.

3.4.2 Comparison of the rainfall distribution

The simulated precipitation over eastern Africa in December 1982 and its difference from

the precipitation in December 1988 are shown in Fig.3.17a and Fig.3.17b, respectively. In December 1982, very wet conditions prevailed over the entire lake and most of the model domain, such as Kenya Highland and the coastal areas of the Indian Ocean. Ogallo (1988) investigated the relationships between seasonal rainfall over eastern Africa and the global sea surface temperature (SST) anomalies based on the period 1923-1984, and found that rainfall was greater than the long-term mean over the Lake Victoria catchment during El Nino years. Similar positive precipitation anomalies in December 1982 are evident here. The averaged monthly rainfall over the lake is about 345.8mm, which is 112.2mm more than that of 1988. Different from the normal conditions (Fig.3.5a) in which the maximum rainfall occurs at the western lake, the maximum precipitation in 1982 is located over the central-eastern part of the lake. The maximum anomalous rainfall also occurs over the central-eastern lake where the strongest anomalous convergence takes place (Fig.3.13b).

The simulated precipitation over eastern Africa in December 1987 and its departure from the precipitation in December 1988 are displayed in Fig.3.18. The climate conditions are relatively dry over most of the model domain, including the whole lake. The averaged monthly rainfall over Lake Victoria is about 144.9mm, which is 88.75mm less than that in the control run and 200.9mm less than that in 1982. Over the lake, the maximum negative rainfall anomaly occurs at the southern lake where the strongest anomalous divergence takes place (Fig.3.14b). Indeje et al (2000) investigated the relationships between seasonal rainfall over eastern Africa and the ENSO based on the period 1961-

1990, and found significantly dry conditions over the eastern highlands of Kenya and the Lake Victoria basin in the one year post-ENSO. These simulated precipitation anomalies are consistent with their results.

The simulated surface air temperature anomaly pattern for 1982 December (the wet year minus the control) and for 1987 December (the dry year minus the control) are displayed in Fig.3.19. The heavy cloud cover in 1982 blocks the Sun's radiation and causes the surface air temperature to decrease over most of the domain (Fig.3.19a), while the relatively light cloud cover permits more shortwave radiation to penetrate and raises the air temperature near the surface over most of the model domain (Fig.3.19b). The net results is that the surface air temperature averaged over the lake in 1982 is 22.9°C, which is 0.3°C cooler than that in 1988, and in 1987 it is 25.3°C, which is 0.9°C warmer than that in 1988. The other features are that the surface air temperature anomalies over the lake are relatively weaker than those over the surrounding regions in both the wet year and dry year. It might be the large heat capacity of the lake body blocking the strong variation.

Fig.3.20 shows the simulated evaporation departures for 1982 December (the wet year minus the control) and 1987 December (the dry year minus the control). In 1982 (Fig.3.20a), the area of positive evaporation anomalies is located over the western part of the lake where strong wind speeds are located (Fig.3.13a) and the anomalous divergence occurs (Fig.3.13b). The negative evaporation anomalies occur over the northeastern and

eastern lake where the convergence occurs. The monthly averaged evaporation in December 1982 over the entire lake is about 235.5mm, which is 10.8mm less than that in 1988. This anomalous evaporation suggests that evaporation be strongly influenced by horizontal circulation. In 1982, horizontal wind convergence transports the moist air from the surrounding area and suppresses evaporation locally over the convergent zone. On the other hand wind divergence transports the moist air outward and enhances the evaporation locally in the divergent zone. In 1987 (Fig.3.20b), the evaporation over the whole lake is less than that in the control run. The monthly averaged evaporation in December 1987 over the entire lake is about 227.5mm, which is 18.88mm less than that in 1988. Since the surface air temperature in 1987 over the lake is warmer than that in the control run (Fig.3.19b), the reduced evaporation over the lake may be attributed to the weaker wind circulation in 1987 (Fig.3.14).

Fig.3.21 shows the difference between the precipitation and the evaporation (P-E) for December 1982 and 1987. In 1982, except for two small areas over northeastern and northwestern sections of the lake, P-E is positive over the entire lake, especially over the central-eastern regions of the lake where the maximum precipitation occur (Fig.3.17a). Over Lake Victoria, the monthly averaged P-E is 110.3mm, which constitutes 32.4 percent of the precipitation. Over the whole domain, the monthly averaged P-E is 54.4mm. The lake and its catchment can not provide enough water vapor to support the rainfall, especially over the lake. This result suggests that one third of the precipitation in December 1982 comes from the external sources. Moreover, the large positive P-E

region is co-located with the strongly convergent anomalous area in Fig.3.14b. Therefore, the increased precipitation is mainly due to water vapor convergence through advection. These results confirm the relationship in which the eastern Africa rainfall fluctuations are clearly linked with large-scale features of the general atmospheric circulation (Nicholson 1996). The strong anomalous westerly flow over Lake Victoria (Fig.3.14b) and its basin in 1982 may be an indication that the Indian Ocean perhaps did not play a critical role in the strong precipitation anomaly, and the precipitation fluctuations over Lake Victoria might have been more directly influenced by SST fluctuations over the Atlantic Ocean.

In 1987 (Fig.3.21b), except for some individual small areas, the precipitation is less than the evaporation over the entire domain, especially over the lake. Over Lake Victoria, the monthly averaged P-E is –82.57mm, and the extra evaporation accounts for 56.99 percent of the precipitation. Over the entire model domain, the monthly averaged P-E is –36.31mm. The lake basin not only provides adequate water vapor to support the local rainfall, but also is a net source for the region outside. At 850mb, the anomalous wind divergence is enhanced over the lake (Fig.3.15b), which results in water vapor divergence away from the lake. This water vapor divergence anomaly pattern could have contributed to the dry climate condition in 1987.

Observed precipitation data over Lake Victoria was not readily available for this study. However, previous investigations indicate that there is a strong correlation between the

lake level and monthly precipitation over the Lake Victoria catchment (Morth 1967). If the runoff is disregarded, changes in the lake level are driven by P-E; when P-E is positive, the lake level increases, when P-E is negative, lake level decreases. Birkett (1997) analyzed the evolution of the lake level during 1992 and 1993. The slight decrease of the lake level occurred during October, November and December, 1992. Since both 1987 and 1992 are a post-ENSO years associated with dry seasonal climate condition, the lake level in December 1987 also should decrease and P-E should be negative. This indirectly suggests that the simulated negative P-E patterns for 1987 are realistic.

Table 3.4 Summary of the precipitation and the evaporation over Lake Victoria.

	Precipitation (mm)	Evaporation (mm)	Difference (P-E)
1982	345.8	235.5	110.3
1987	145.0	227.5	-82.5

In Table 3.4, the P-E is 110.3mm during the wet year and –82.5mm during the dry year over the lake. These different P-E value between the wet year and dry years indicate that Lake Victoria plays an important role in moderating the climate variation over eastern Africa. It stores water during the wet years, and releases it during dry years. Thus, the lake alleviates the strength of the extreme drought and flood events.

3.4.3 Comparison of the lake variations

Examining the pattern of the monthly averaged lake surface water temperature and current for December 1982 (Fig.3.22a) we find that the LST ranges from 24.5°C to 25.5°C. Except over the southwestern lake, the lake surface is warmer than that in 1988 (Fig.3.22b). The monthly averaged LST over the entire lake is 24.82°C, which is 0.38°C higher than that in 1988. The maximum LST area is located over the middle-eastern part of the lake during the wet year, rather tan located over the southwestern lake during the normal year. An anti-clockwise circulation dominates over the entire lake surface (Fig.3.22a), thus in this respect, similar to the results in the control experiment. Influenced by the strong anomalous northerly flow over the lake (Fig.3.13b), strong anomalous southward currents occupy the lake south of 0.6°S latitude (Fig.3.22b). The monthly averaged lake surface current velocity over the entire lake is 0.068 m/s in 1982 compared to 0.056 m/s in the control run. This stronger water current enhances the warm and cold water mixing, and induces stronger vertical motion for transporting heat. The net results is that the horizontal variation is weaker than that of 1988, especially over the western lake where the heavy precipitation happens in the control run (Fig.3.5a). This LST pattern further induces mesoscale flows converging over the central-eastern part of the lake and diverging over the southwestern region, which is almost a reversal to that conditions during 1988. This mesoscale circulation further modifies the large scale circulation and influences the precipitation pattern. Therefore, the relatively light rainfall

over the western region of the lake and the relatively heavy rainfall over the central-eastern part of the lake in 1982 (Fig.3.17a) may be attributed to the variations in the LSTs.

The monthly averaged lake surface water temperature and currents for December 1987 are displayed in Fig.3.23. The LST ranges from 24.6°C to 26.1°C (Fig.3.23a). The warm anomaly pool of water spreads over the entire lake (Fig.3.23b). The monthly averaged LST over the entire lake is 25.3°C, which is 0.9°C higher than that in the control experiment. The maximum difference is 1.2°C and it is located over the northwestern part of the lake. An anti-clockwise circulation dominates the entire lake surface, which is similar to the control experiment, but the circulation is weaker than that in the control experiment. The horizontal LST gradient is much stronger over the northwestern region where the induced mesoscale circulation is also relatively strong and the precipitation is relatively heavy there (Fig.3.18a). Observed lake surface temperature for the period of simulation are not readily available, however, the lake surface temperature produced by the coupled model system in general approximately approaches the observed value of 25°C for December 1992 that is also the post year of ENSO in Kenya stations (Ochumba, 1996).

The summary of the lake surface temperature, surface air temperature and the evaporation over Lake Victoria are displayed in Table 3.5. Temperature differentials between lake

and atmosphere affect air moisture. In Equation 2.18, the evaporation rate is governed by the difference between the specific humidity of the air and the saturation specific humidity of the water surface, the latter being a function of surface temperature only. The wind speed also affects the evaporation rate.

Table 3.5 Summary of the results on the lake surface temperature, surface air temperature and the evaporation.

	Lake surface temperature (°C)	Surface air temperature (°C)	Wind speed at 850mb (m/s)	Evaporation (mm)
1982	24.8	22.9	2.7	235.5
1987	25.3	24.0	1.8	227.5
1988	24.4	23.2	2.2	246.2

In December 1982, although the higher evaporation is expected due to the higher temperature differential 1.8°C (24.8°C-22.9°C) between lake and surface air than that in 1988 (24.4-23.2=1.2°C), the higher air moisture convergence forced by large scale circulation suppresses the evaporation. Moreover, the weaker LST gradient is not conductive for the mesoscale circulation development which further suppresses the evaporation. Thus negative evaporation anomalies occur in December 1982. In December 1987, the temperature differential (1.3°C) between lake surface and lake masses does not deviate too much from 1988 (1.2°C), but the surface wind speed (1.8

m/s) is weaker than that in 1988(2.2 m/s). The negative evaporation anomalies are mainly attributed to the weaker wind. On the other hand, the negative anomalous in the evaporation are the main contributor to the warmer lake surface temperature anomalies during both 1982 and 1987.

3.5 Conclusions

In this study, we have used the coupled RegCM2-POM model to simulate the climate conditions over the Lake Victoria basin. The simulations have been conducted for a normal year (1988), two contrasting years (El Nino (1982) and non El Nino (1987)) to investigate the dynamical and thermodynamical mechanisms responsible for the occurrences of wet and dry conditions over eastern Africa during the short rainy season. The model captures the interannual variations in the atmosphere-lake interaction system.

We find that the variation of the large-scale circulation is a very important factor in determining the climate anomaly conditions. The results for the simulated circulation indicate that convergent anomalous wind conditions are located over the lake during the wet year, and divergent anomalous wind conditions are simulated during the dry year. The vertical motion is substantially strengthened during wet year and weakened during the dry year. This strong/weak vertical motion associated with the convergent/divergent horizontal circulation intensifies/suppresses moisture convergence and thus influences

precipitation over Lake Victoria during the wet/dry years.

The strong atmosphere-lake interaction was confirmed over eastern Africa. The simulated air temperature above the lake is 2.5°C warmer than that in the surrounding regions. In both the surface air temperature and water temperature, the relatively warmer areas are located over the southwestern and central-eastern regions of the lake, and the cooler region is located over the northwestern lake sector. This co-located distribution for the surface air temperature and the lake surface temperature indicates that it is very crucial for represent the lake thermodynamics and hydrodynamics for realistic model reproduction of the regional climate.

The precipitation mainly occurs during midnight and early morning when the land breeze dominates the lake. Little or no rainfall occurs during daytime and early evening when the lake breeze dominates over the lake. The divergent/convergent flow originates from the eastern lake during day/night time, and moves southwestward. The interaction between the lake-land breeze and the prevailing northeasterly flow provides the mechanism for the diurnal rainfall geographical asymmetries across the lake and the divergence/convergence movement.

Lake Victoria plays a very important role in moderating the climate variation and supporting the hydrological cycle over eastern Africa. The positive/negative P-E distribution indicates that the lake stores water moisture during a wet year, and releases

the moisture during the dry year. Thus the lake alleviates the strength of potential extreme drought and flood events. The negative P-E during the wet year also indicates that the moisture convergence plays an important role in determining the heavy precipitation. The westerly anomaly wind regime during 1982 further suggests that the moisture advection from the Congo tropical rain forest and Atlantic Ocean, might be an important factor in explaining the wet anomaly conditions over eastern Africa, while the Indian Ocean perhaps did not play a critical role during 1982.

The lake circulation variation plays an important role in modulating the LST structure over Lake Victoria and thus influences the regional coupled climatic conditions. The simulated lake circulation is characterized by a horizontal spiral pattern that transports warm water toward the northern section and cold water toward the southern section. The net result is a warm tongue over the northeastern part and a cold tongue over the northwestern part of the lake. The lake is warmer during both wet and dry year, but the water current is stronger during the wet year and weaker during the dry year as a result of the strong/weak momentum forcing. The enhanced/weakened lake circulation mixes the warm and cold water and results in weak/strong horizontal LST gradient during wet/dry years. The weakened/intensified horizontal LST induces weak/strong mesoscale circulation and further impacts the regional climate conditions. The warmer LST during both wet and dry years may be attributed to the lower evaporation rate in both wet and dry years. Hence, the LST patterns are mainly determined by the heat flux, and modified

by lake water flow variations.

The patterns of precipitation are strongly influenced not only by the large scale circulation, but also modified by the mesoscale circulation induced by the LST gradient. During the wet year, although the averaged LST over the lake is warmer, the LST gradient over the western region of the lake is weakened, the LST over the southwestern region is cooled and the maximum LST area moves to the central-eastern part of the lake away from the southwestern lake. The rainfall is relatively light over the western region and heavy over the central-eastern region responding to the variation in the LST. During the dry year, the LST horizontal gradient is enhanced over the western part of the lake, especially over the northwestern sector. Thus the mesoscale circulation over the lake basin is enhanced there, and the relatively heavy precipitation still occurs at the western lake.

We infer from our results that the hydrodynamics of the lake plays an important role in determining the coupled variability of the lake circulation and the lake basin-wide climatic conditions. This observation is based on the use of the coupled 3-dimensional lake model and it is obscured in the results based on the coupled 1-dimensional lake model due to the shortcomings in the formulation in the latter. It is therefore apparent that neglecting the lake's hydrodynamics and basing the lake model entirely on thermodynamical considerations deprives the coupled regional climate model of the ability to transport heat efficiently within the lake and thereby degrades the simulation of

the climate downstream over the rest of the lake and the surrounding regions.

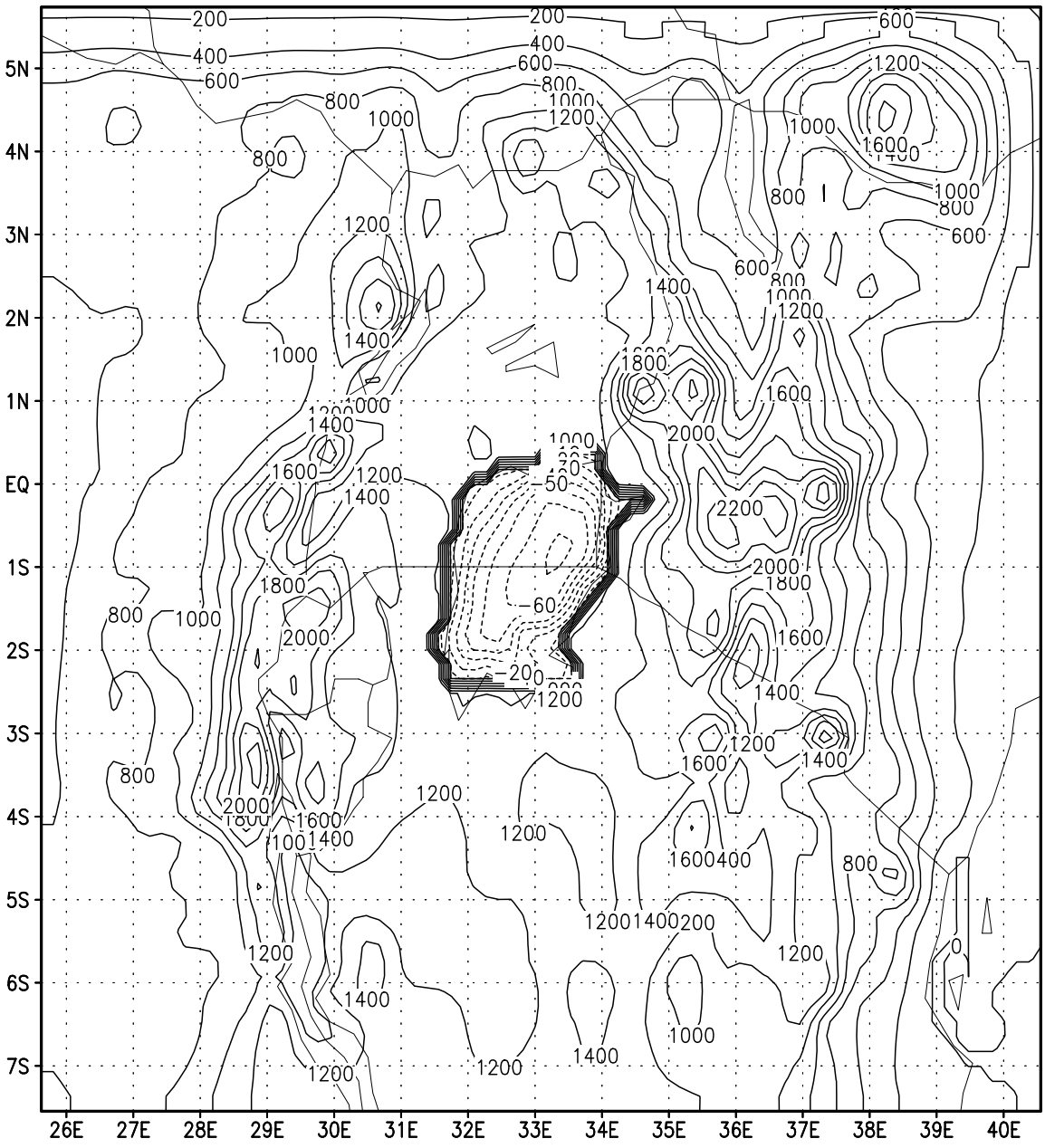

Fig. 3.1. Model domain topography with horizontal resolution of 20 km (combined from NCAR dataset, and Johnson's Bathymetry data). unit: m.

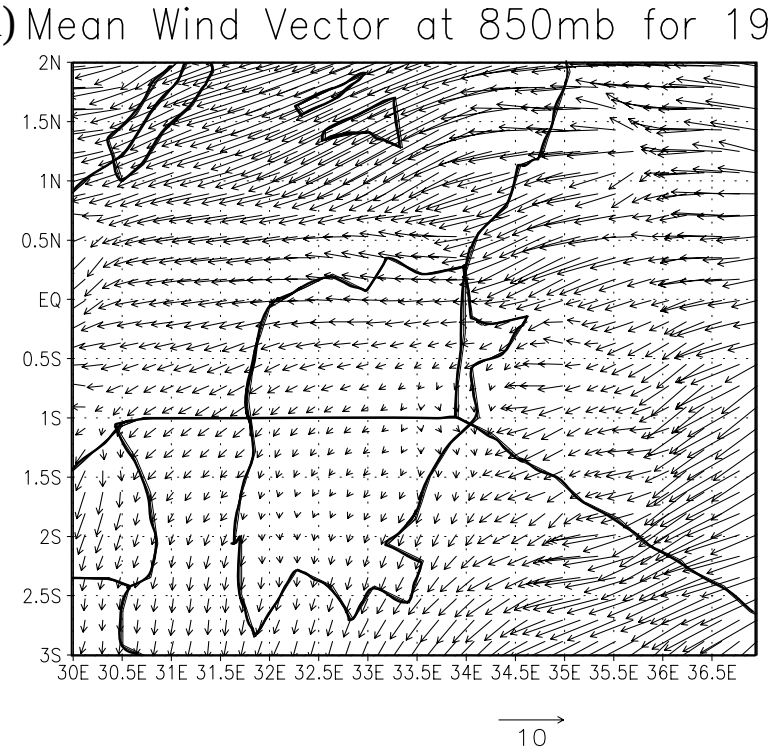

Fig. 3.2. Simulated wind vector and wind speed at 850mb in December 1988. a). wind vector. b). wind speed. Unit: m/s.

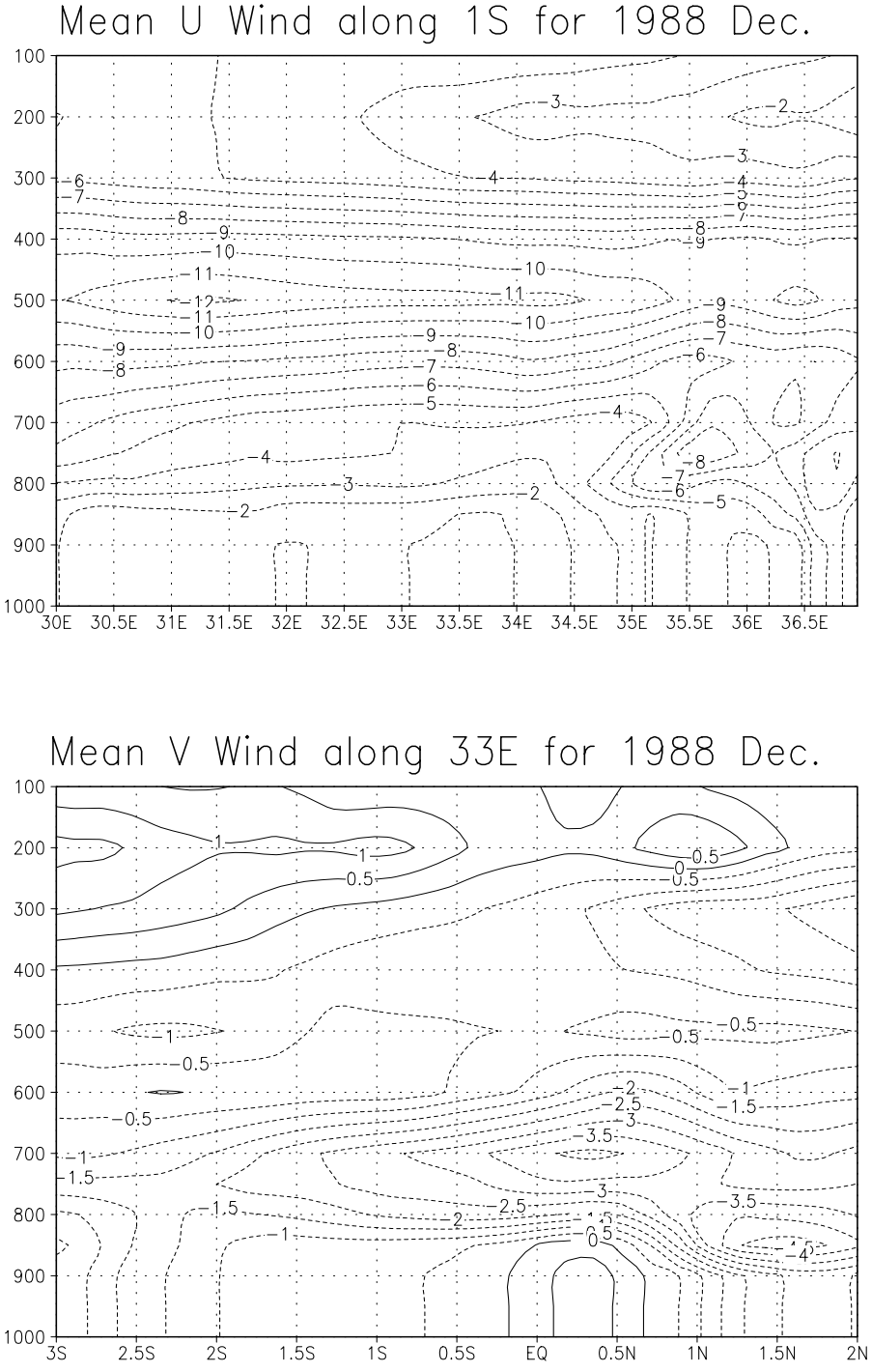

Fig. 3.3. Simulated wind variation with height in December 1988. a). vertical cross section of horizontal zonal wind along 1°S. b). vertical cross section of horizontal meridional wind along 33°E. unit: m/s.

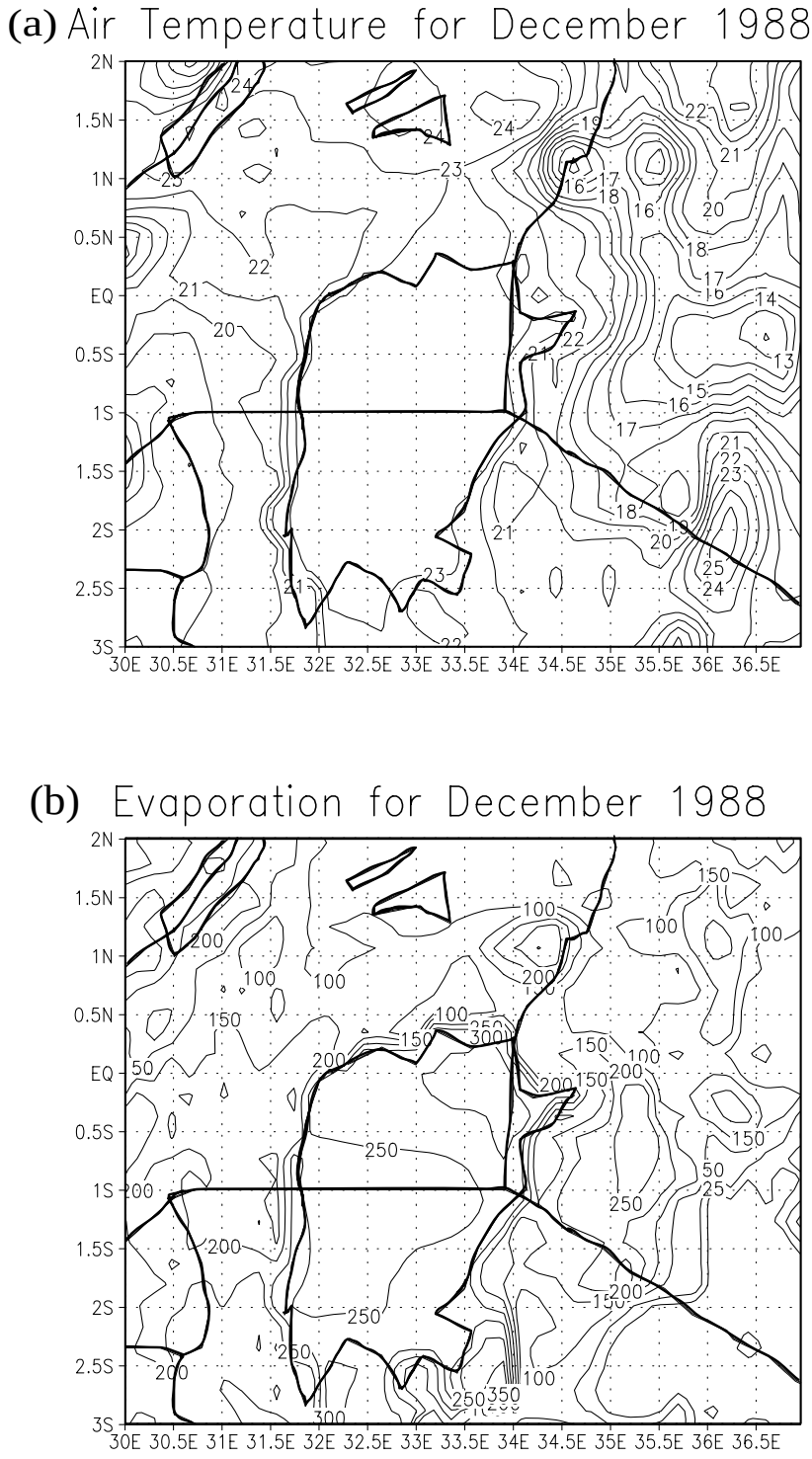

Fig. 3.4. a). Simulated surface air temperature in December 1988. unit: °C. b). Simulated evaporation in December 1988. unit: mm.

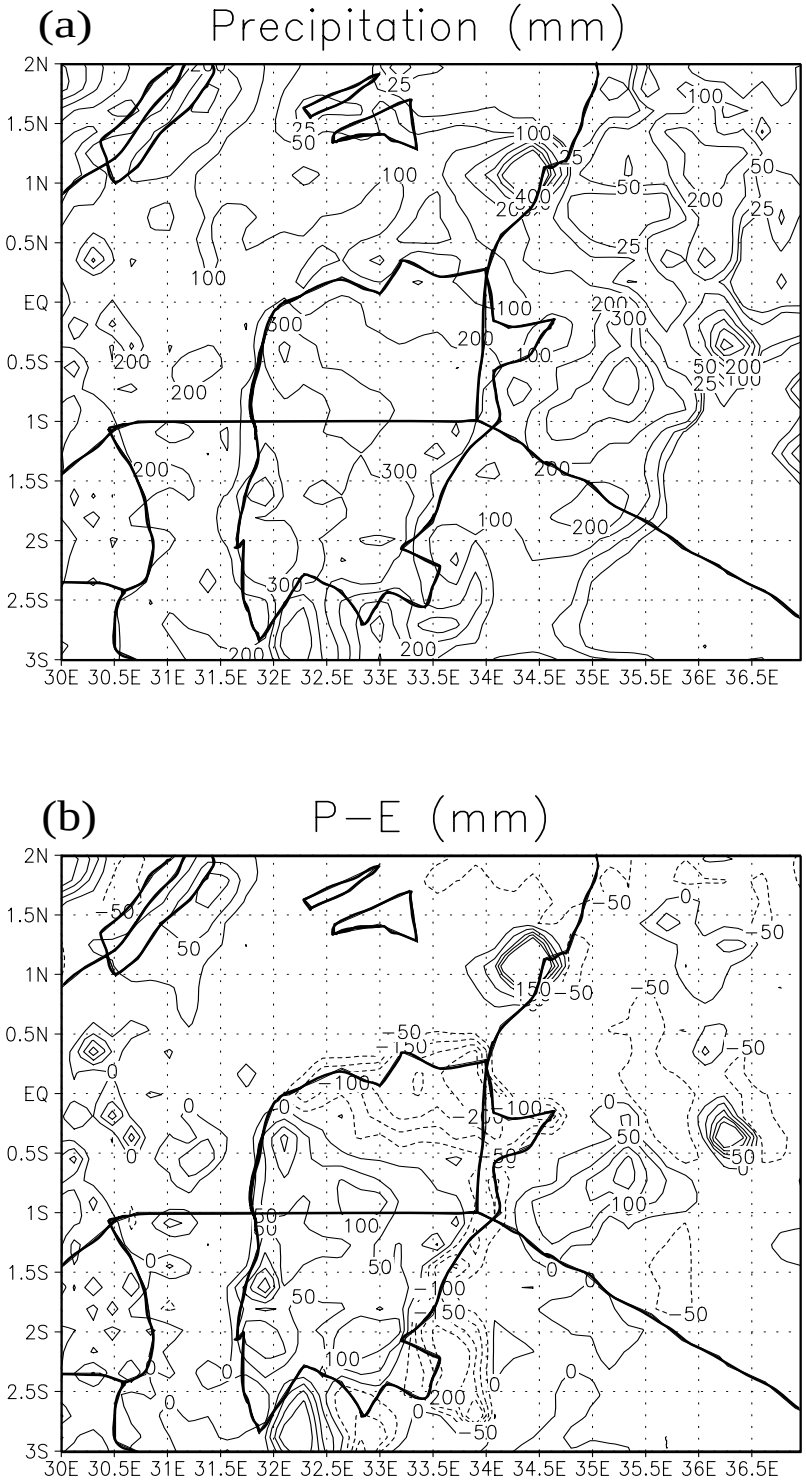

Fig.3.5. a). Simulated precipitation in December 1988. b). Simulated P-E (precipitation minus evaporation) in December 1988. unit: mm.

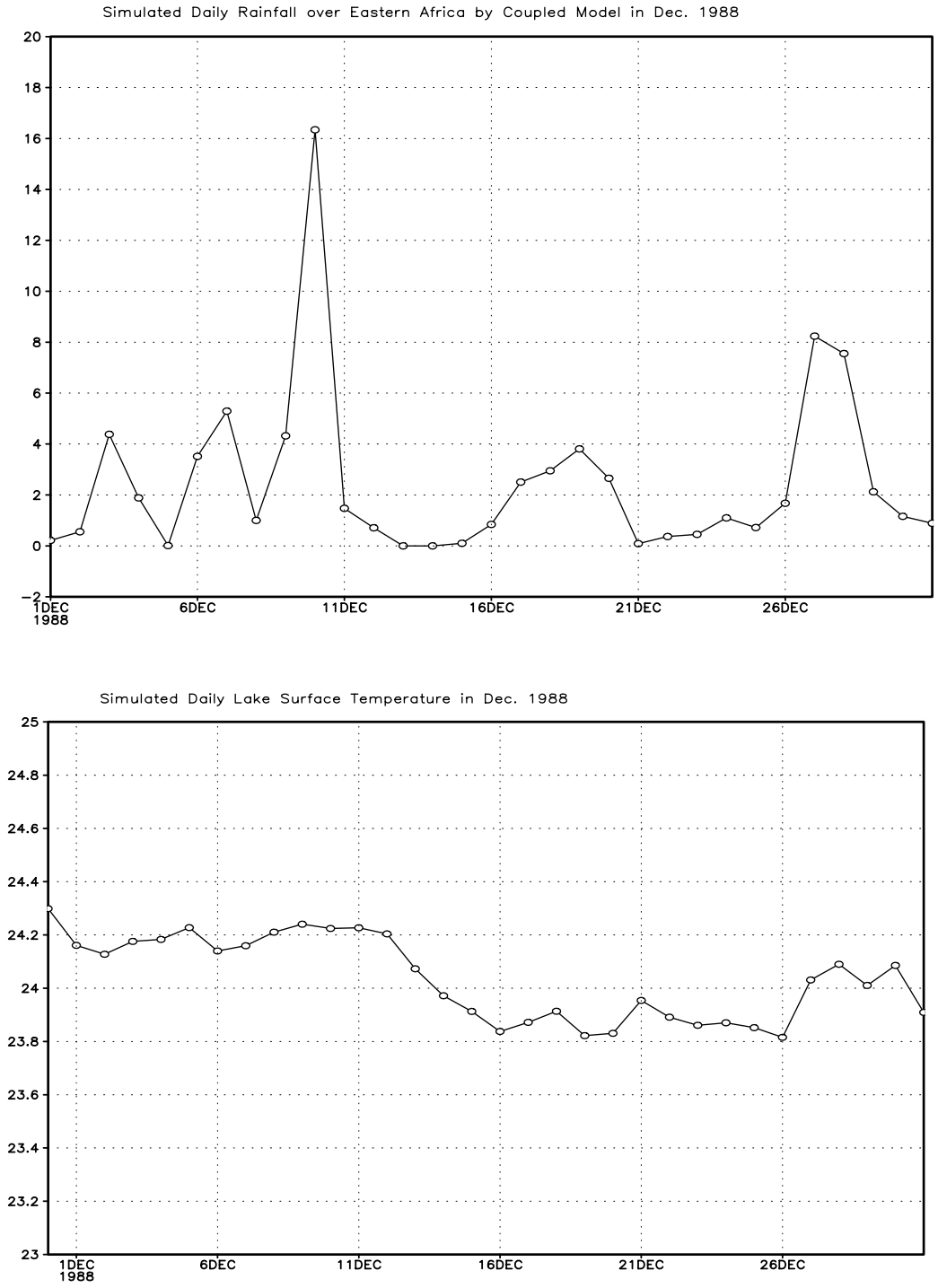

Fig. 3.6. Simulated time series averaged over Lake Victoria in December 1988. a) daily precipitation. unit: mm. b) daily mean lake surface temperature. unit: °C.

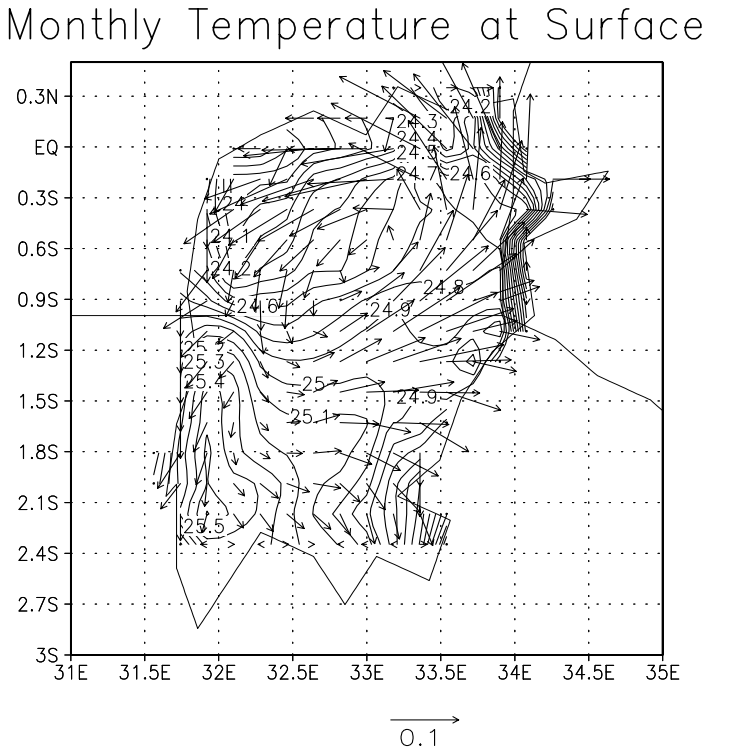

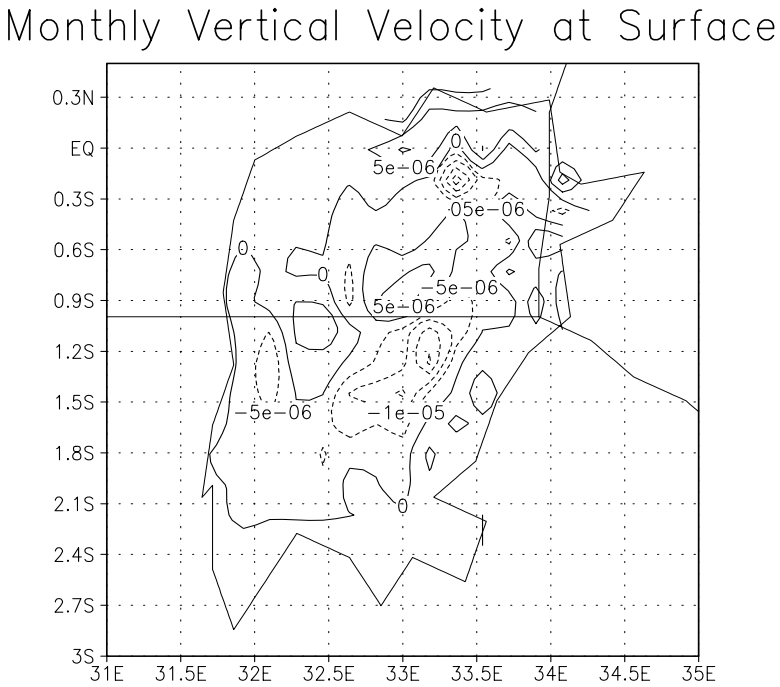

Fig. 3.7. Simulated surface lake parameters of Lake Victoria in December 1988. a). temperature (°C) and current (m/s). b). vertical speed (m/s).

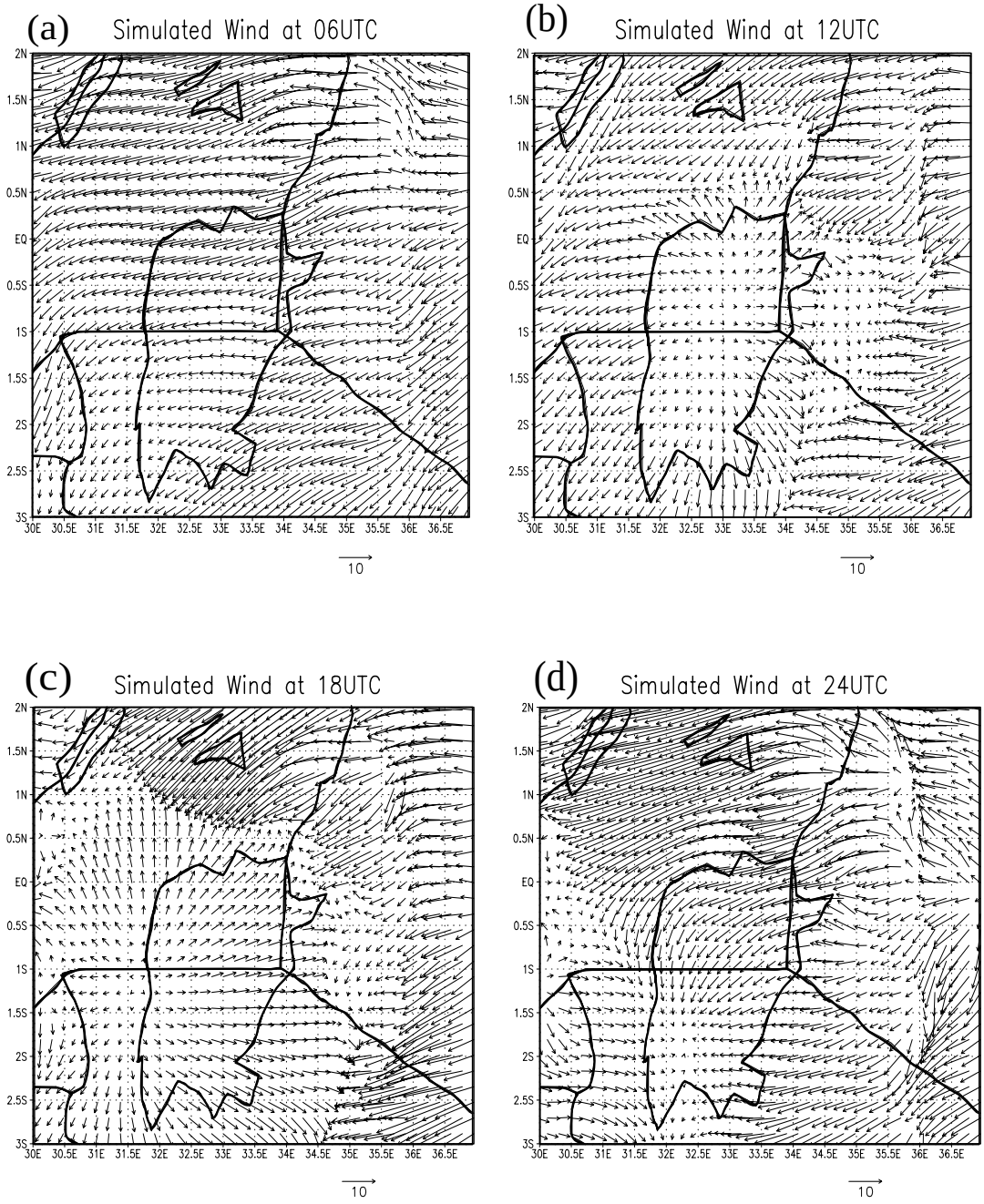

Fig. 3.8. Simulated wind at 850mb in December 1988. a). at 06UTC. b). at 12UTC. c). at 18UTC. d). at 24UTC. unit: m/s.

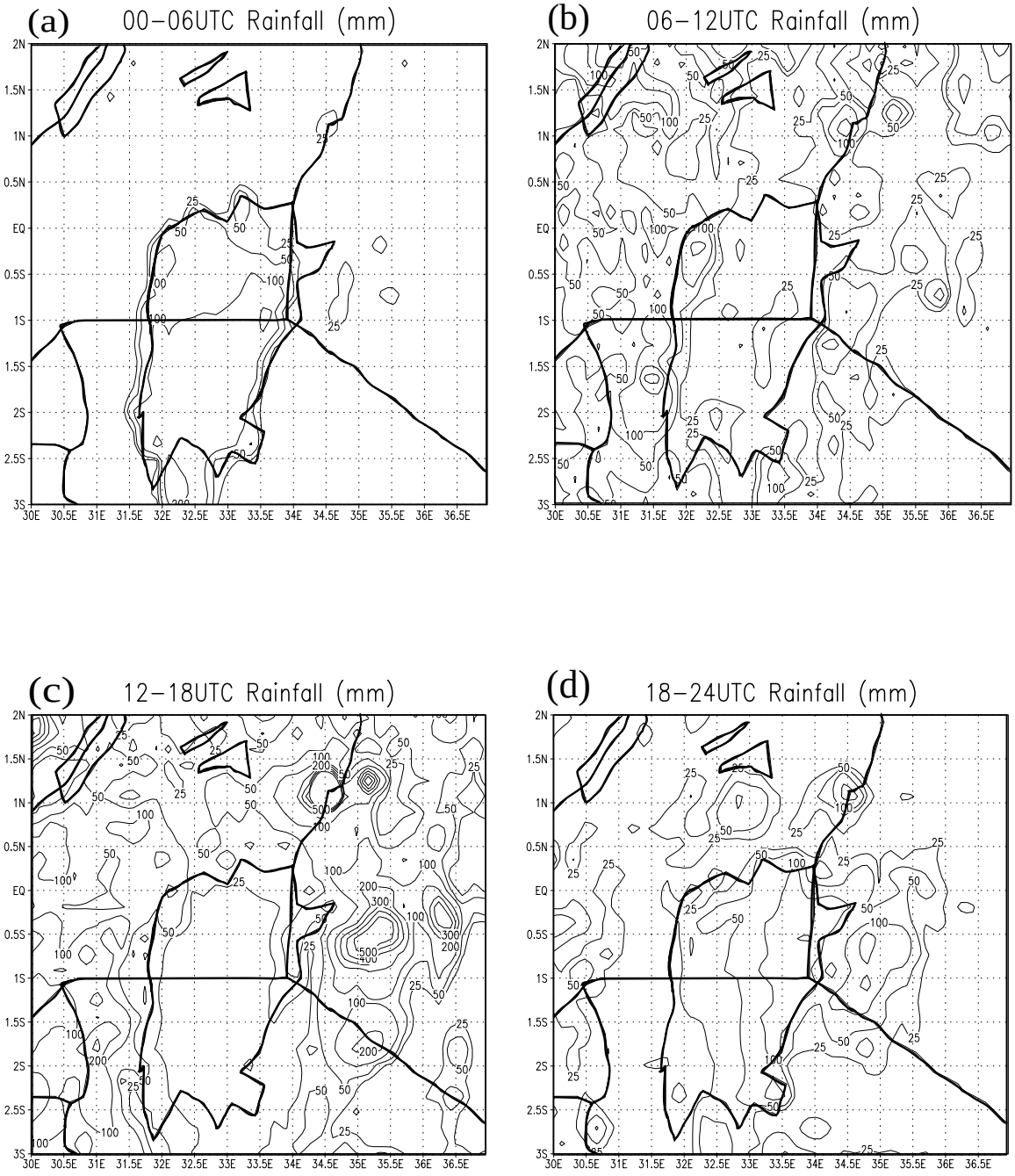

Fig. 3.9. Simulated precipitation in December 1988. a).during 0-06UTC. b). during 06-12UTC. c). during 12-18UTC. d). during 18-24UTC. unit: mm.

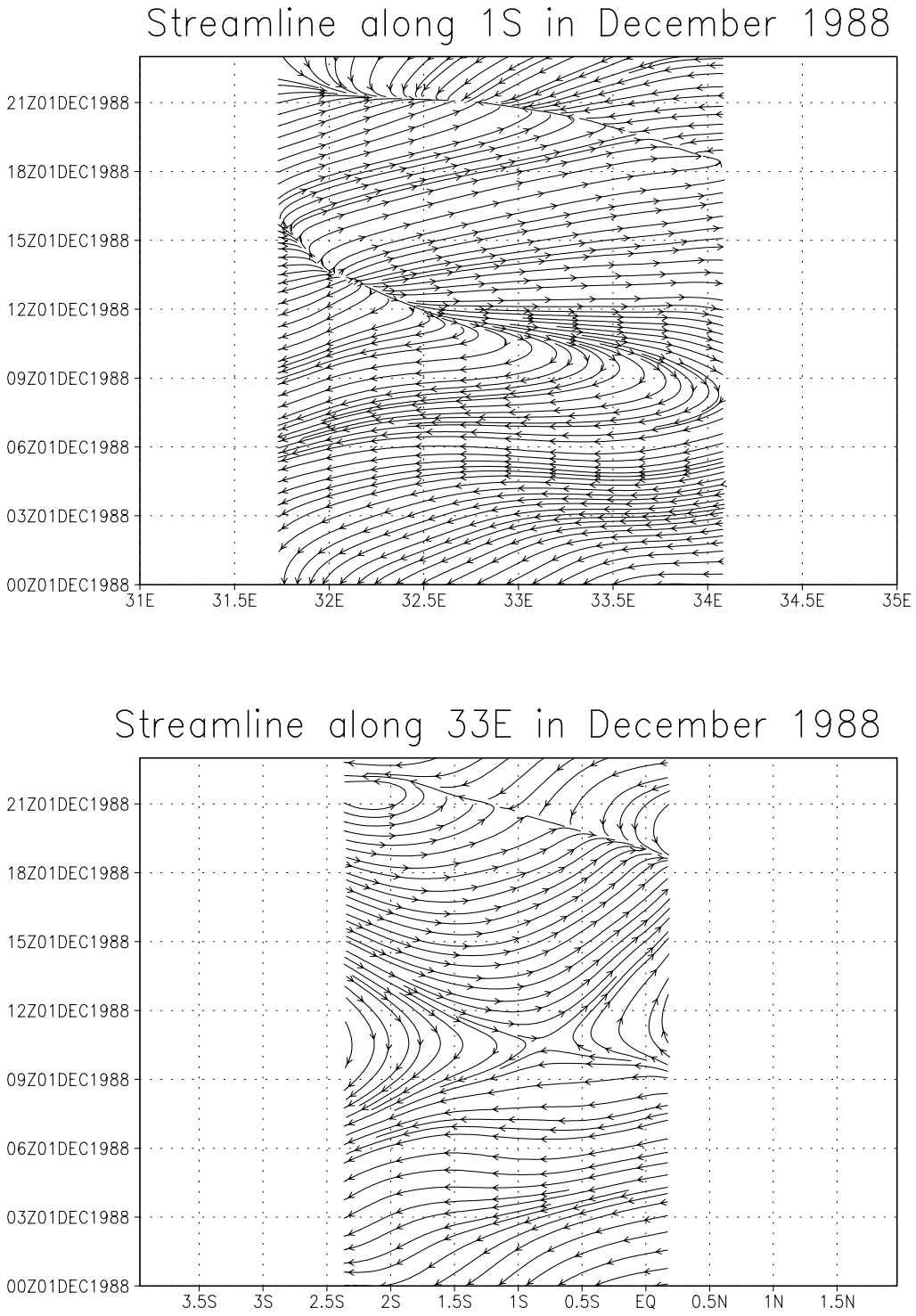

Fig. 3.10. Diurnal time cross section of simulated streamline at 10m height for December 1988. a). along 1°S. b). along 33°E. unit: /s.

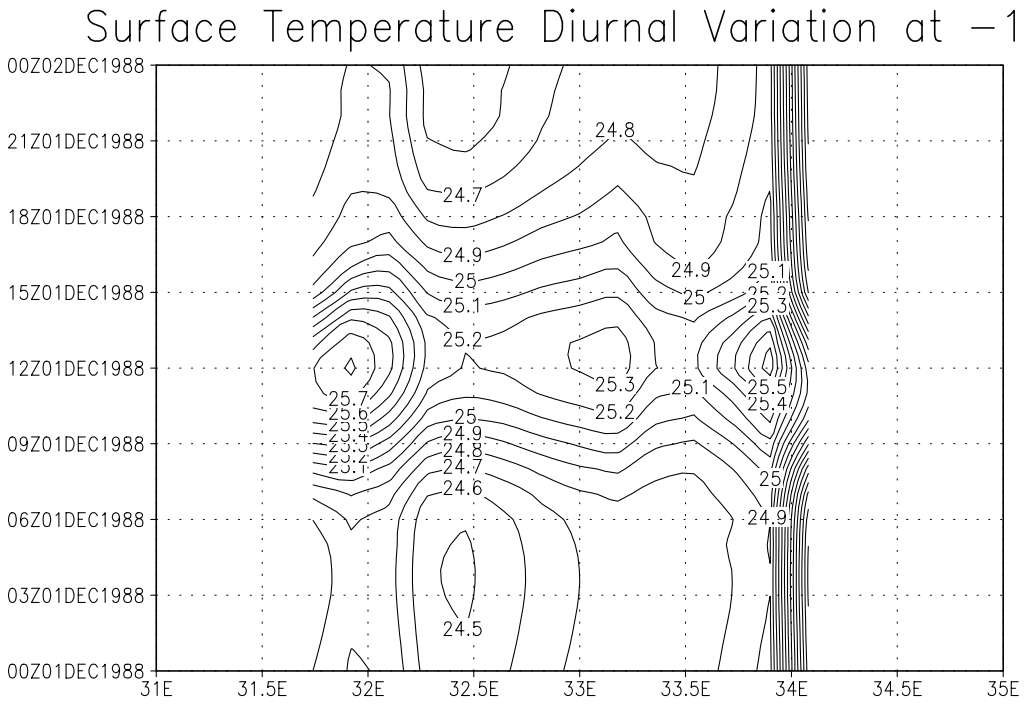

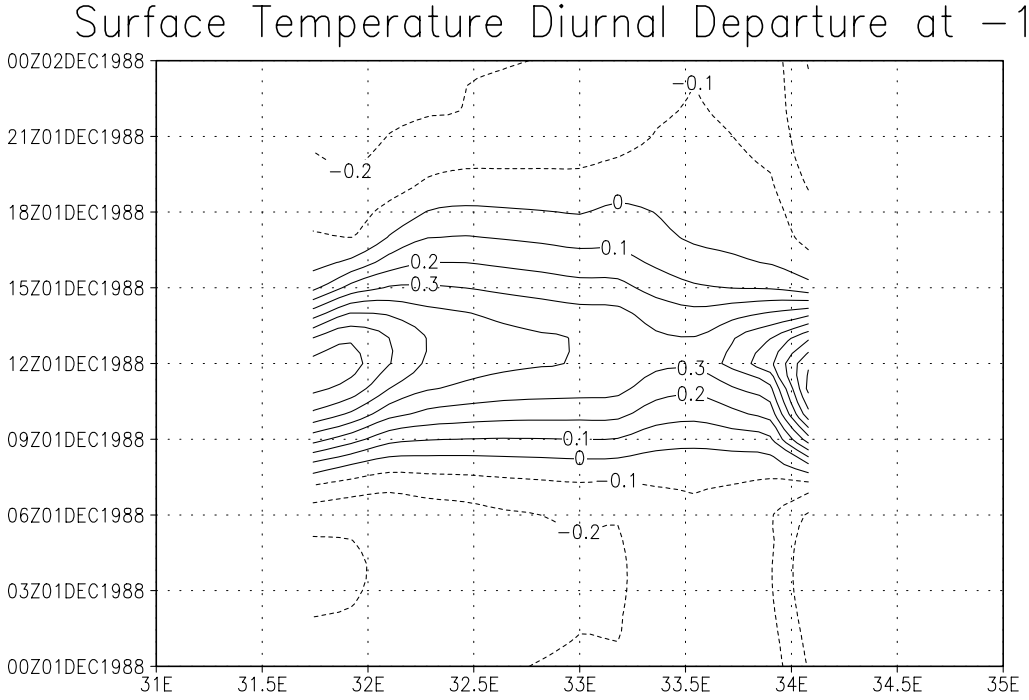

Fig. 3.11. Diurnal time cross section of simulated lake surface temperature for December 1988. a). along 1°S. b). anomaly along 1°S. unit: °C.

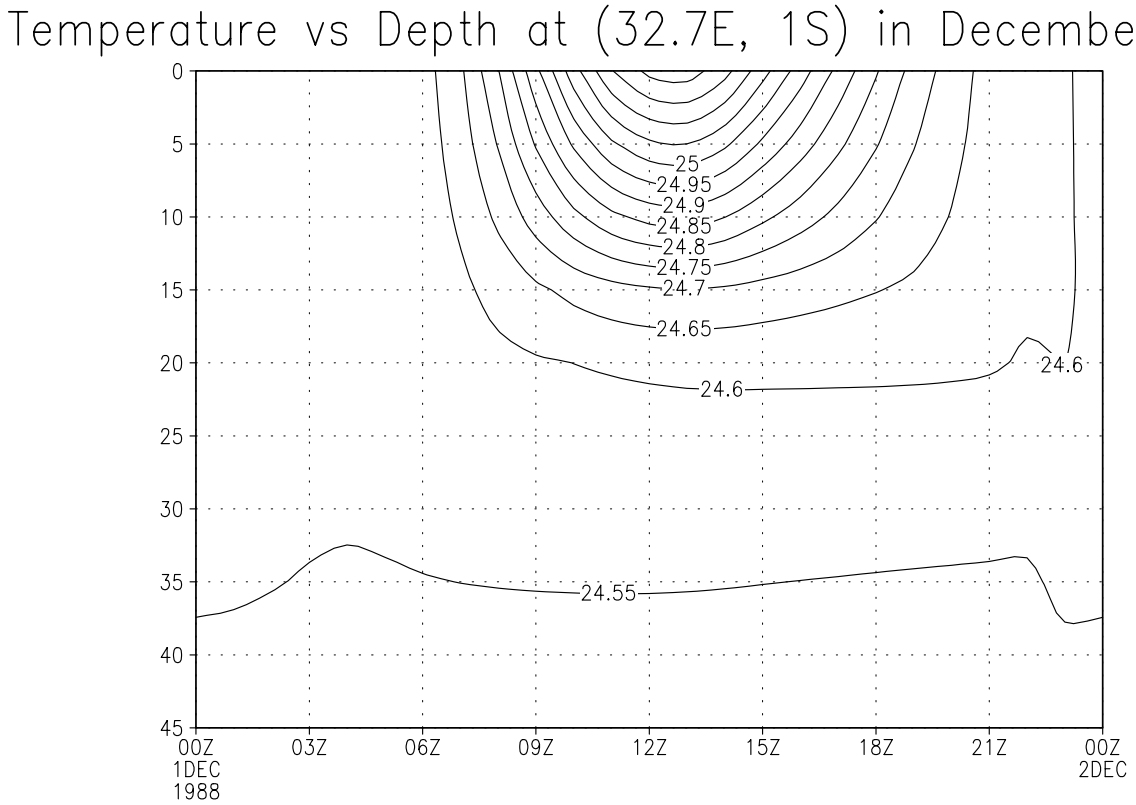

Fig 12. Diurnal time-depth cross section of the simulated lake temperature at (32.7°E,1°S) for December 1988. unit: °C.

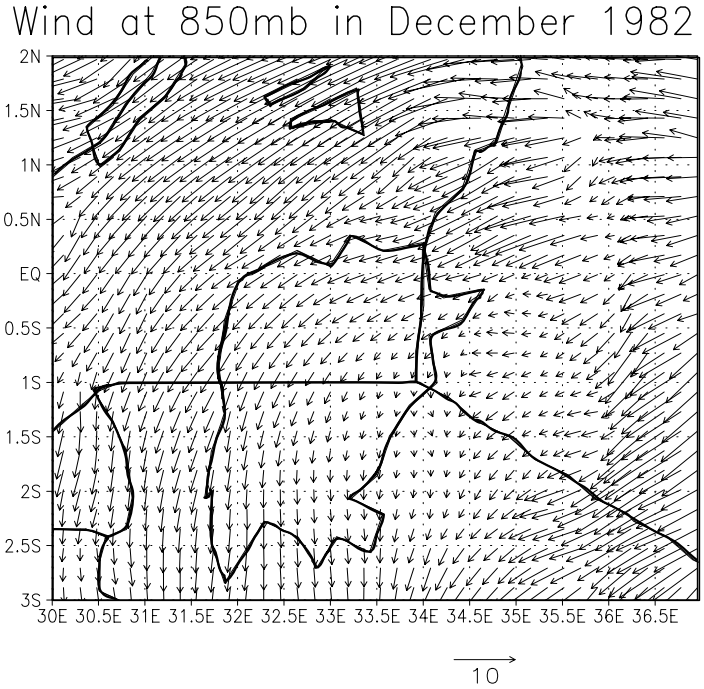

Fig. 3.13. a). Simulated circulation at 850mb for December 1982. b). simulated anomaly wind (1982 minus 1988) at 850mb. unit: m/s.

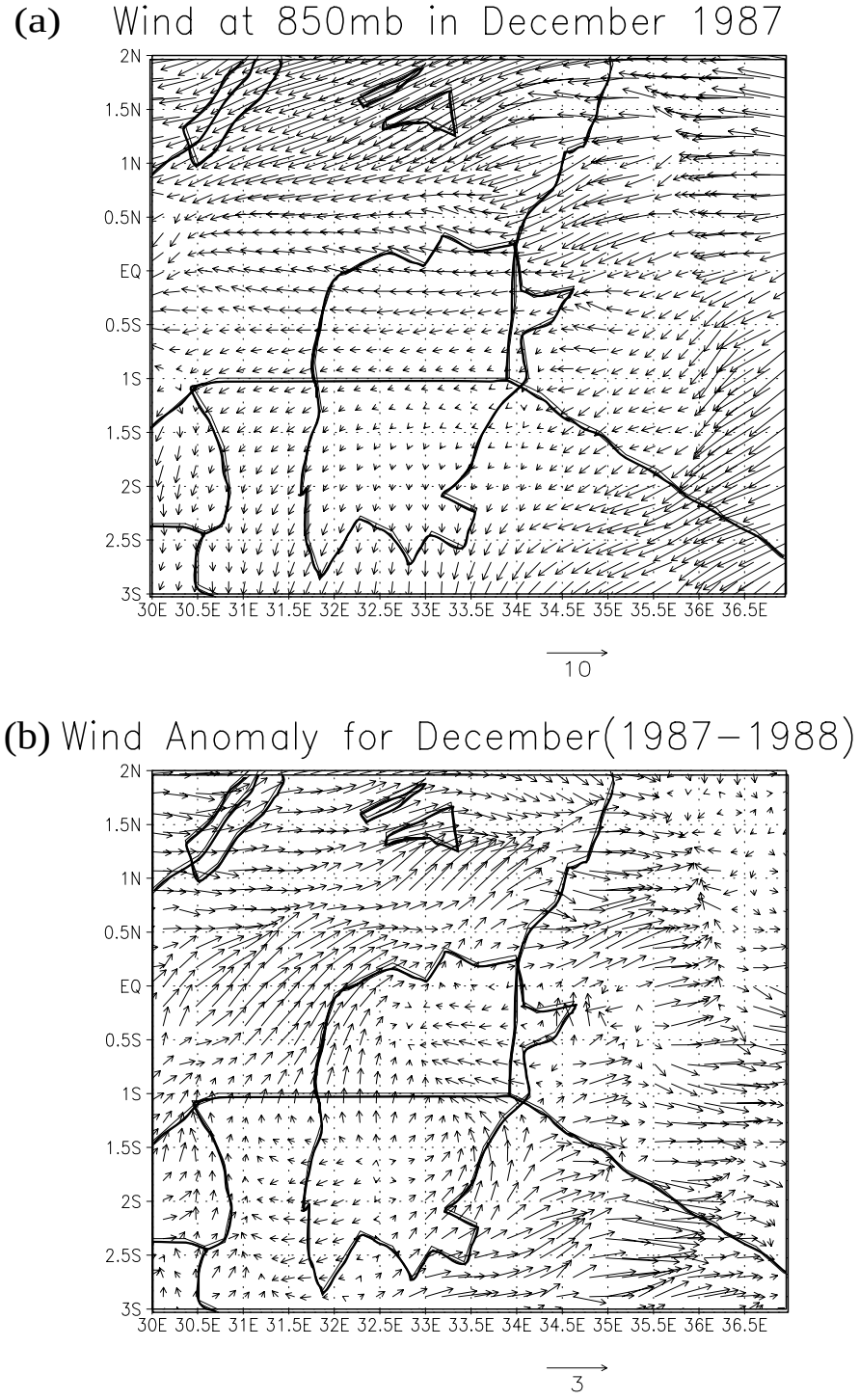

Fig. 3.14. Simulated circulation at 850mb for December 1987. b). simulated anomaly wind (1987 minus 1988) at 850mb. unit: m/s.

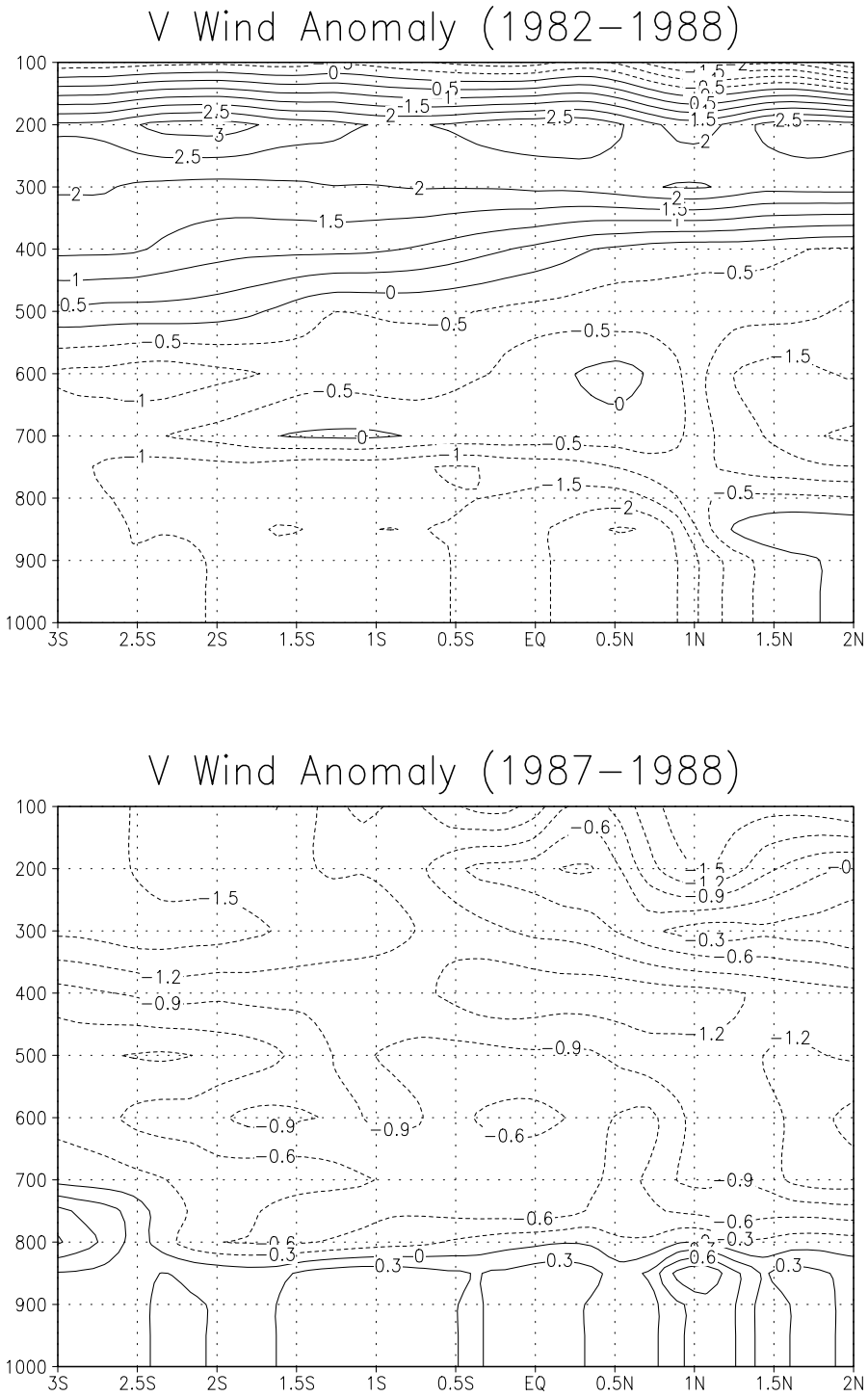

Fig. 3.15. Height cross section with simulated meridional wind anomaly averaged between longitudes 32°E and 33.5°E for December. a) 1982 minus 1988. b). 1987 minus 1988. unit: m/s.

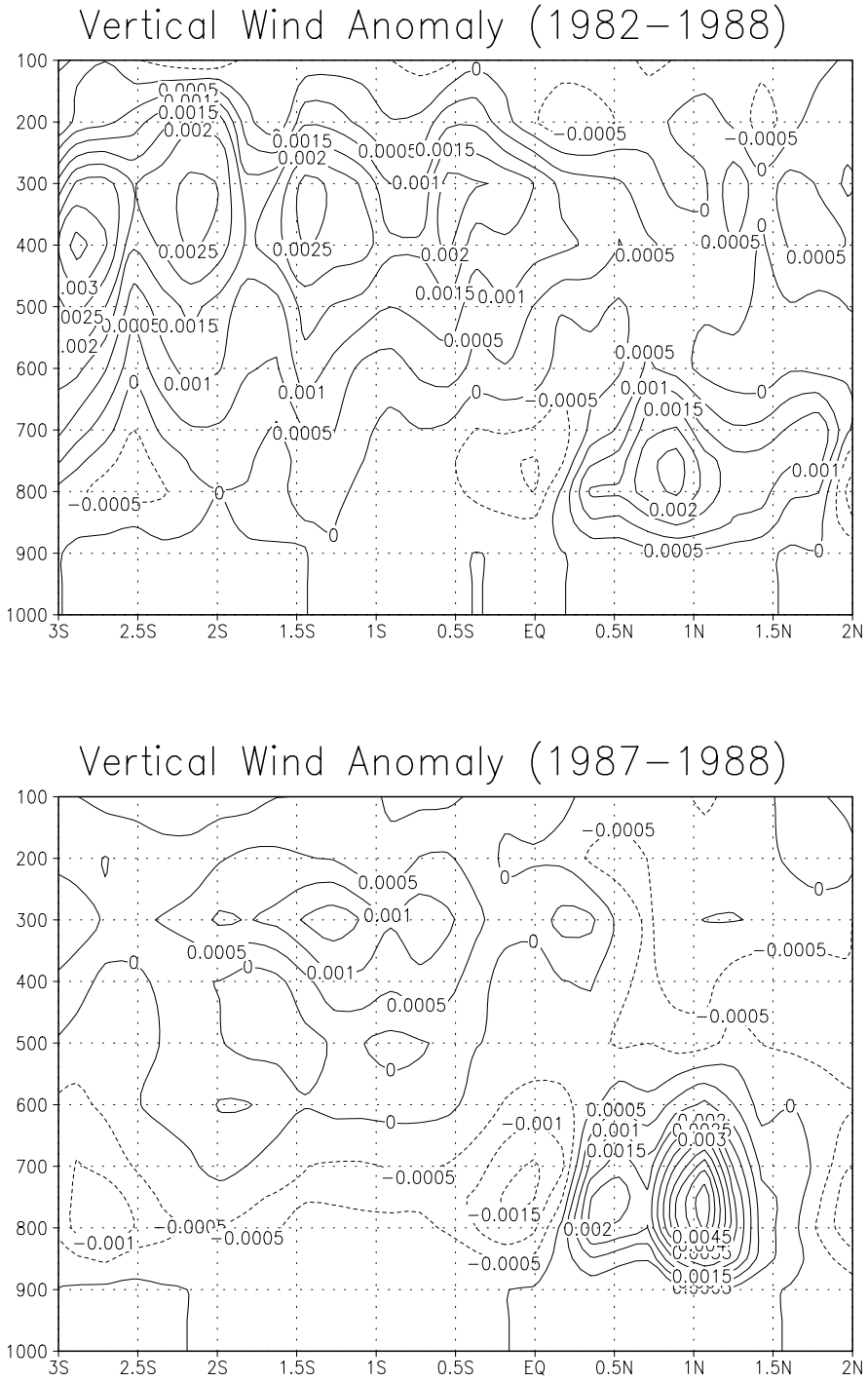

Fig. 3.16. Height cross section with simulated anomalous vertical wind speed averaged between longitudes 32°E and 33.5°E for December. a) 1982 minus 1988. b). 1987 minus 1988. unit: m/s.

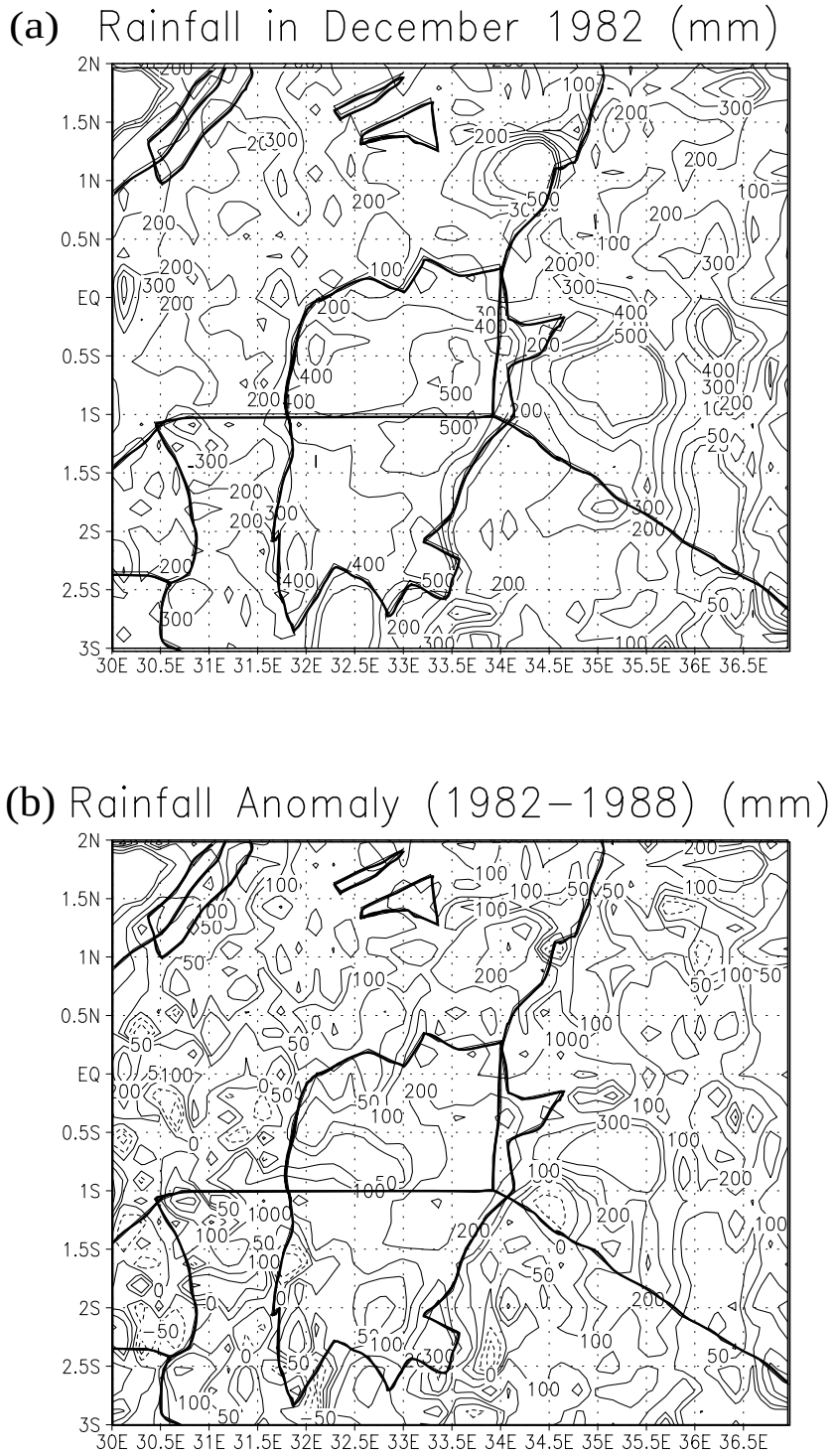

Fig. 3.17. a). Simulated precipitation for December 1982. b). simulated anomaly precipitation (1982 minus 1988). unit: mm.

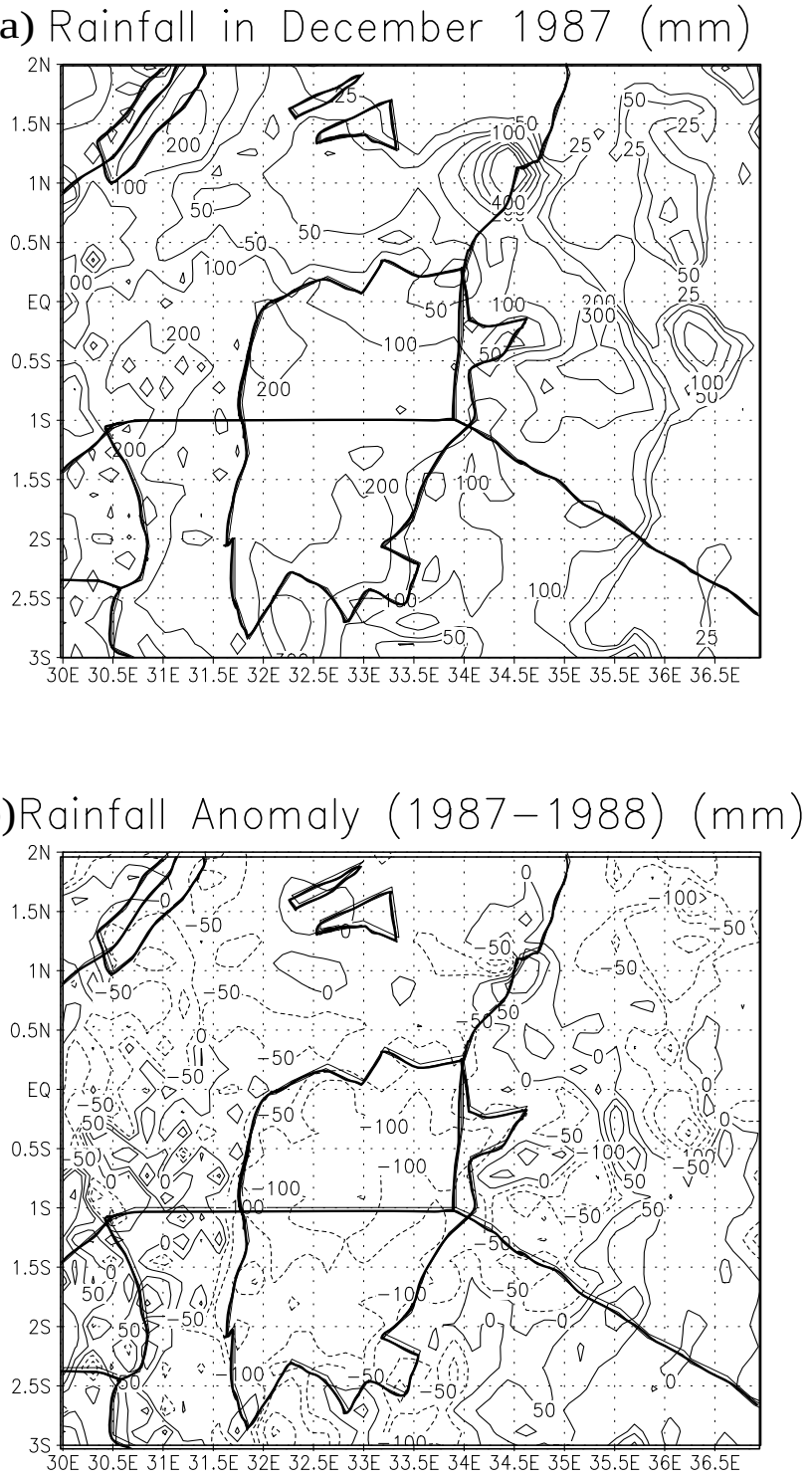

Fig. 3.18. a). Simulated precipitation for December 1987. b). simulated anomaly precipitation (1987 minus 1988). unit: mm.

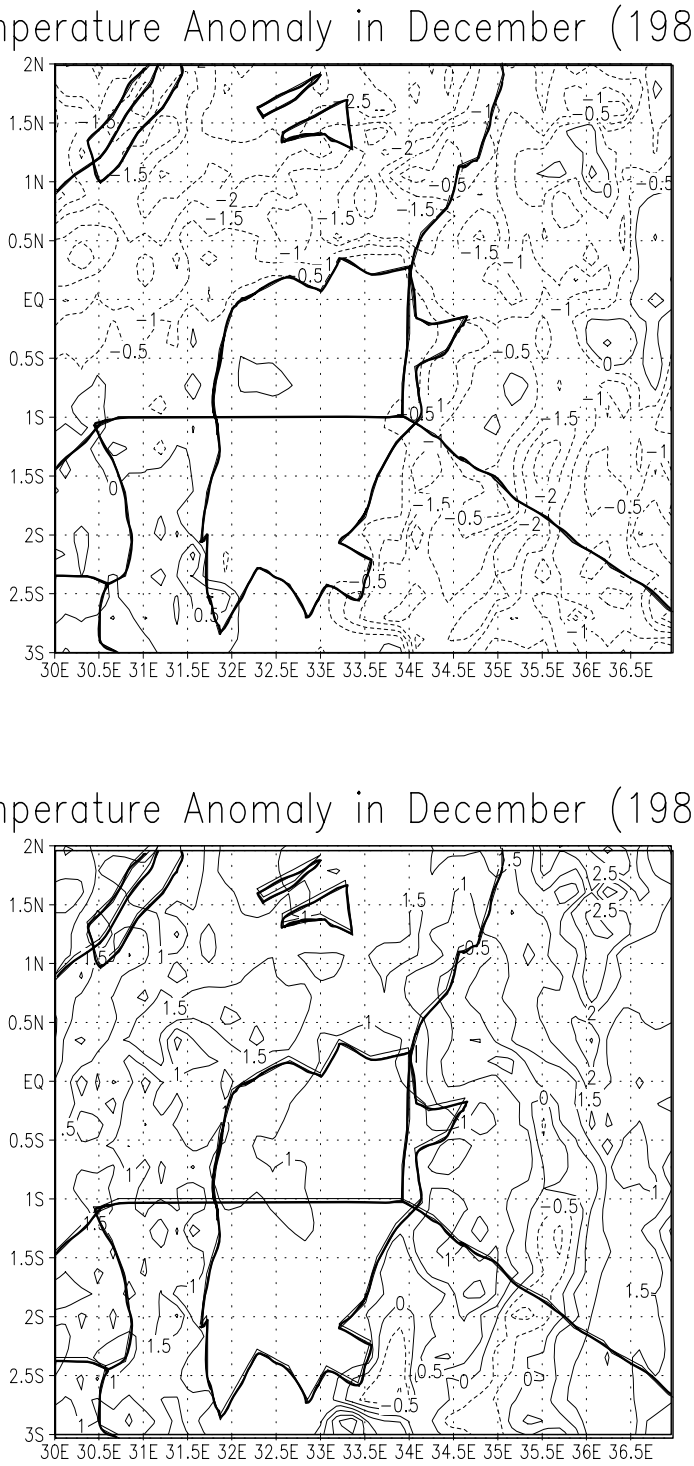

Fig. 3.19. Simulated anomalous surface air temperature for December. a) 1982 minus 1988. b). 1987 minus 1988. unit: mm.

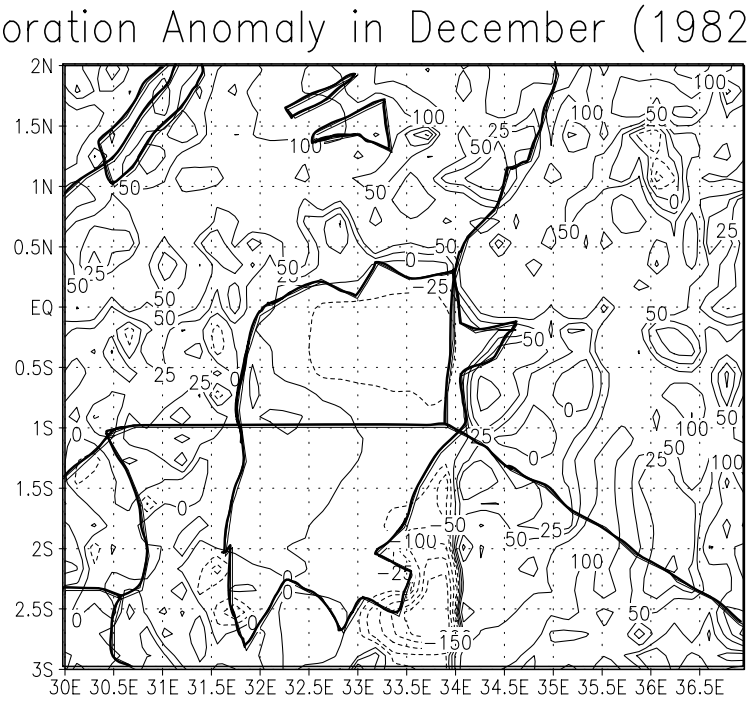

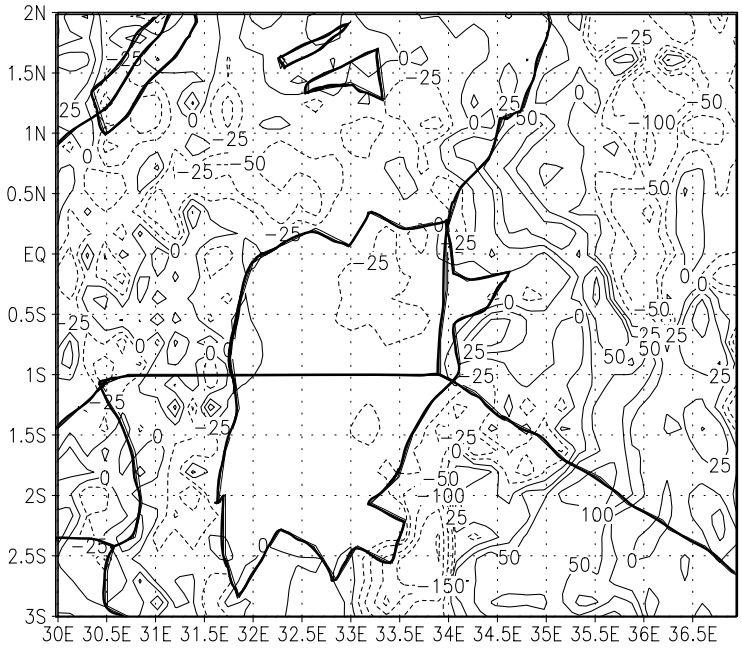

Fig.20. Simulated anomalous evaporation for December. a) 1982 minus 1988. b). 1987 minus 1988. unit: mm.

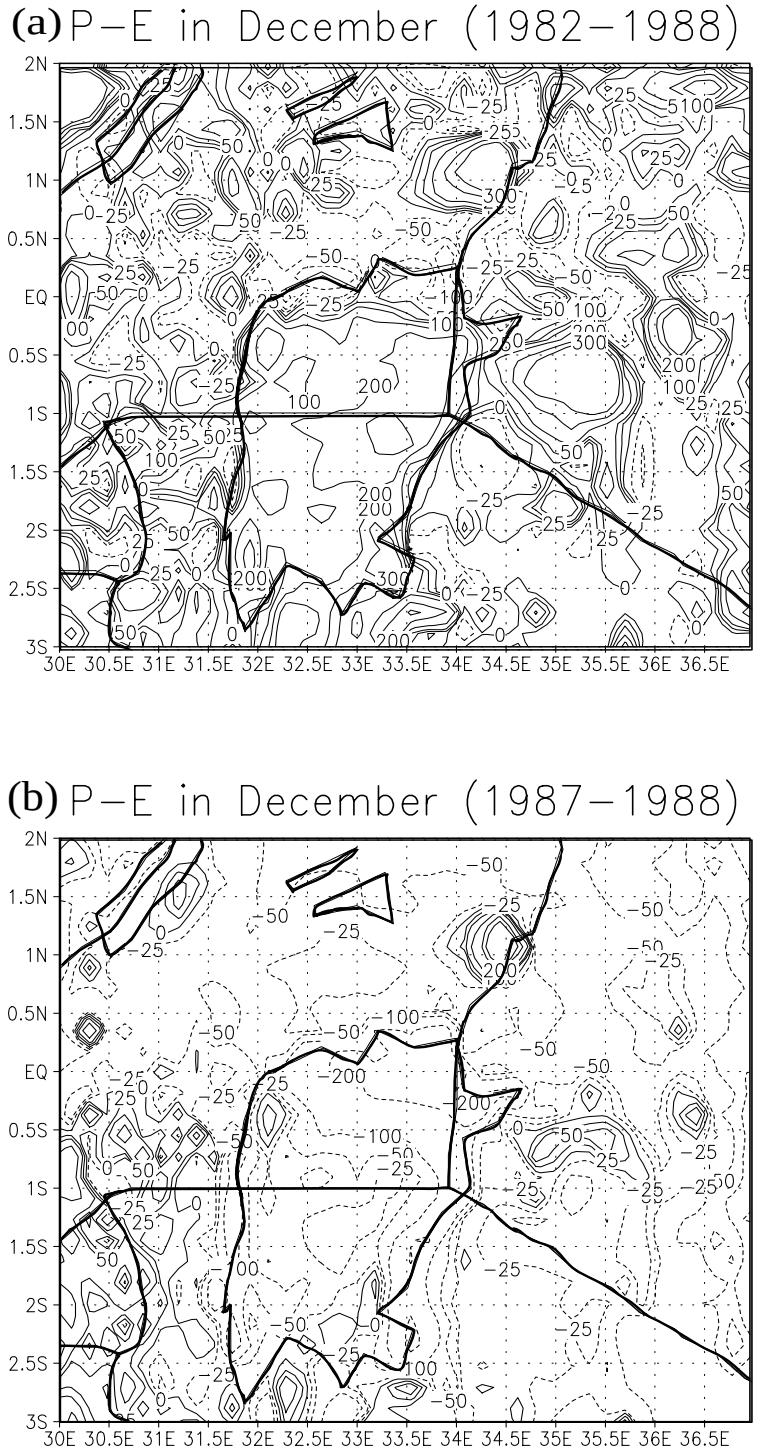

Fig. 3.21. Simulated P-E for December. a) 1982 b). 1987. unit: mm.

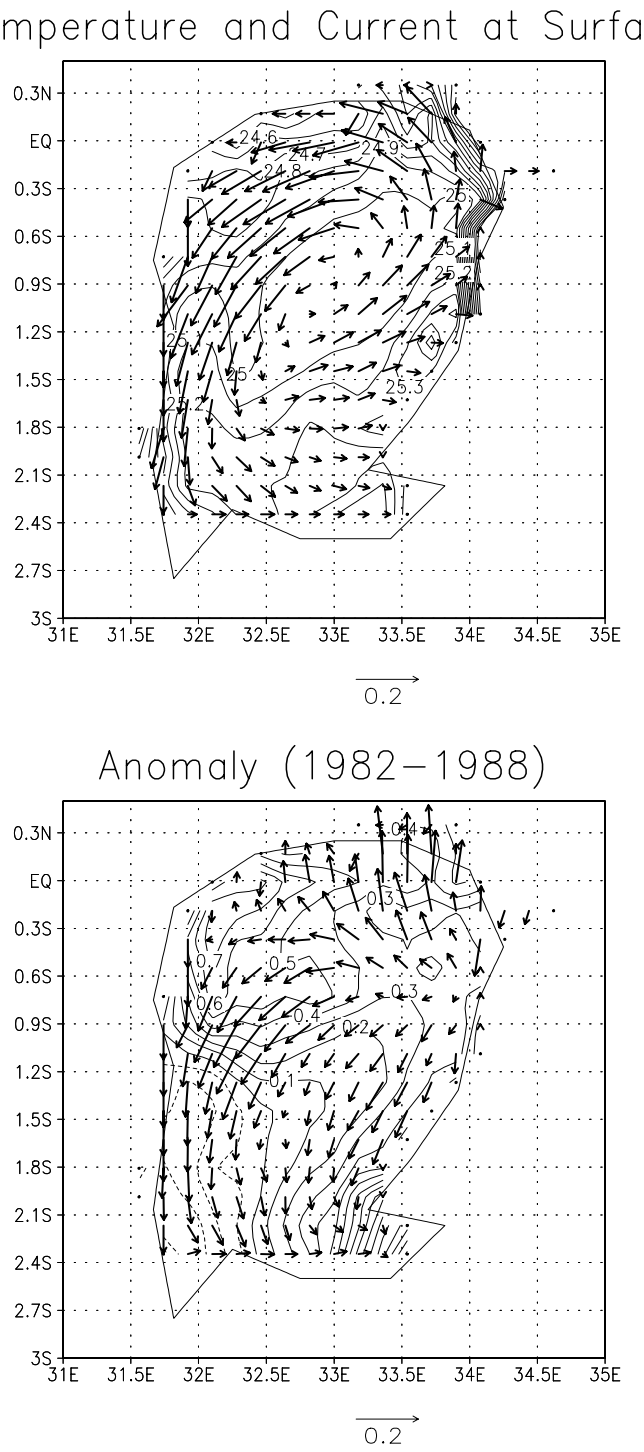

Fig. 3.22. Simulated surface parameters of Lake Victoria for December 1982. a). temperature (°C) and current (m/s). b). anomaly (1982 minus 1988) temperature (°C) and current (m/s).

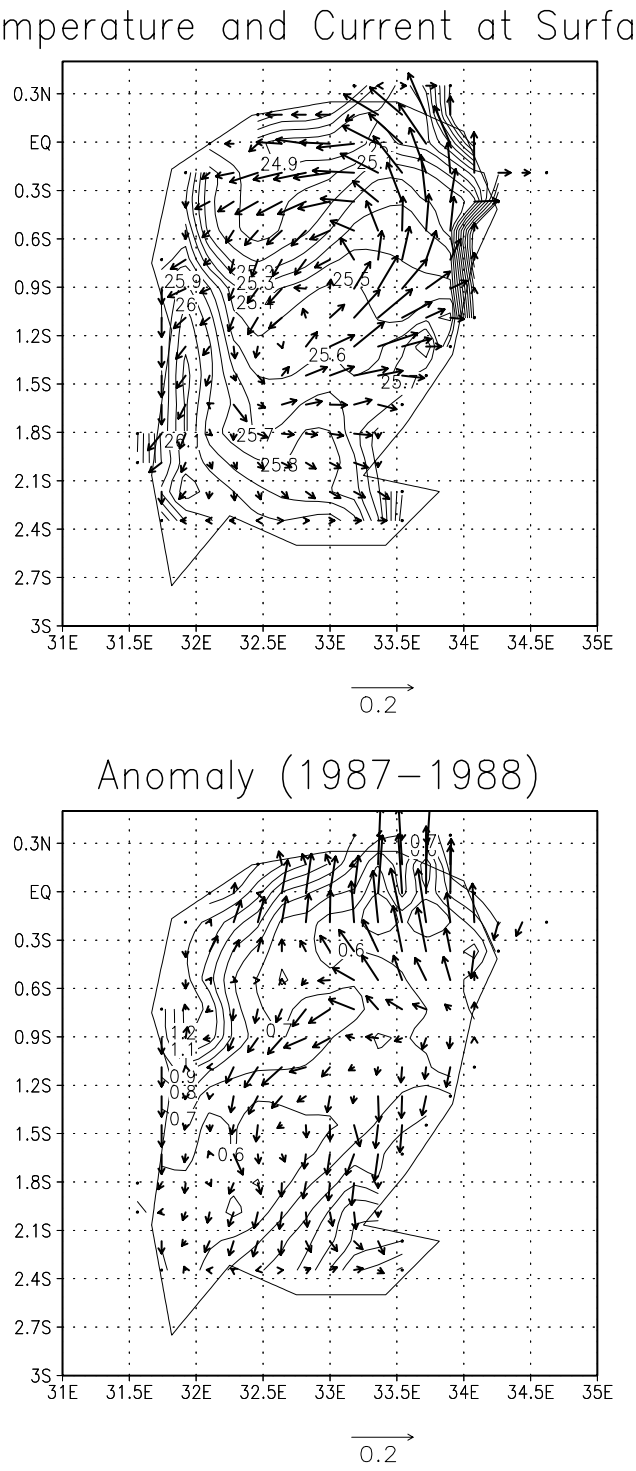

Fig. 3.23. Simulated surface parameters of Lake Victoria for December 1987. a). temperature (°C) and current (m/s). b). anomaly (1987 minus 1988) temperature (°C) and current (m/s).

Chapter 4

A GCM Study of Climate Change Induced by Deforestation in Africa

4.1 Background

Out of nearly 100 countries in the world affected by deforestation and desertification about half of them are in Africa which is more than 80% of the African countries (Brown et al 1990 and 1995, and references therein). Although it is generally accepted that the overall rate of the clearing of the tropical forests is about 0.6% per year, great variation exists between different regions of the continent of Africa. Ground surveys of tropical forests are now being augmented by airborne sampling methods, such as the use of low-altitude photography, satellite systems, and side looking radar (Brown et al 1990). Remotely sensed data have a great deal of promise to offer, but there are many technical problems yet to be resolved. For instance, some state-of-the-art satellite images can distinguish only broad classification of vegetation, others provide greater resolution but a smaller scale, so that the cost of obtaining and interpreting meaningful coverage can be prohibitive (Tucker et al 1984, Malingreau et al 1989). Some space or airborne systems

can be degraded by the frequent cloudiness of the tropics and the smoke from the fires used to clear the forests. Moreover, because deforestation is such a highly charged political issue, even the most impeccable data are subject to considerable differences in interpretation (Matthew 1983, Allen and Barnes 1985). Nevertheless, it is recognized that the present rates of clearing will probably deplete the forest resource within the next 20 to 30 years. As denser road networks are constructed in the presently relatively inaccessible regions such as the interior of the Congo tropical rain forest, accelerated deforestation should be expected.

Since the pioneering study of (Charney et al., 1977) a large volume of modeling & observational studies have investigated the hypothesis which states that the increase in surface albedo, the reduction in evapotranspiration and surface roughness (Sud and Smith 1985, Sud et al. 1988, Nobre et al. 1991, and Williams 1990) associated with the degradation of vegetation could have a positive feedback on future rainfall. The hypothesis postulates that through these biogeophysical feedbacks, an incipient drought can become self-promoting (Williams 1990), It is has been predicted that this mechanism may be partly responsible for the expansion of the sub-Saharan desert boarder region, thus helping to turn it into a true desert. It is estimated that complete removal of the Amazon rain forest would have substantial influence on the regional surface temperature and hydrology (Henderson-Sellers and Gornitz, 1984; Dickinson and Henderson-Sellers 1988; Shukla et al 1990, and Nobre et al 1991). Shukla et al. (1990) showed that the turning into agriculture of the Amazonian tropical forest could result in the suppression of

precipitation larger than the corresponding regional reduction in evapotranspiration, implying that the dynamical convergence of moisture from the surrounding regions also would decrease as a result of deforestation. From this and other studies we hypothesize that the ongoing deforestation over the west and central African countries could significantly affect the regional moisture balance and lead to irreversible regional climatic changes. More recently Zhang et al (1996ab), investigated the deforestation problem by replacing all the world's tropical rain forests with grassland. Their results clarified the important role deforestation could have on global climate in the future. Recent work (Eltahir and Gong, 1996, Zheng and Eltahir, 1998) has shown that the West African monsoon system can be controlled by the meridional gradient of entropy in the boundary layer, a flat (steep) meridional gradient being associated with a weak (strong) monsoon circulation. In particular, numerical experiments (Zheng and Eltahir, 1998) showed that deforestation in the Guinea Coast region could have a greater impact on monsoon circulation strength than desertification in the Sahel area, by reducing this meridional gradient.

The primary goal in the present investigation is to focus on the role of deforestation on the African climate. The primary research vehicle in our investigation is the standard version of the NCAR CCM3 global climate model (GCM) with horizontal resolution of triangular spectral truncation T42 (approximately 2.8 x 2.8 degrees). Two separate ten-year simulations. For each of the ten-year simulations, the global climatological SST field was prescribed. The purpose of the ten year simulations is to provide a sufficiently large

ensemble whose average minimizes model noise errors. In the control simulation normal vegetation is prescribed. The design of the anomaly experiment is similar to the control run except that the tropical rain forest regions in Africa are replaced by savanna grassland vegetation. We employ higher GCM resolution than in most previous studies in order to resolve the continental response to deforestation. We stratify the annual cycle into the seasons, which characterize the main rainy seasons corresponding to the primary climatic zones of Africa.

Downscaling of the climatic effects of deforestation can be performed by taking the CCM3 GCM output and using it to generate lateral boundary conditions for the RegCM2-POM model. However, that will be the subject of a separate investigation in the future.

4.2 Model description

The primary vehicle in this investigation is the standard NCAR CCM3 spectral GCM. The details about the model may be found in several documents (Acker et al 1996, Bath et al 1992, Bonan et al 1996, Bryan et al 1996, Hack et al 1993, Kiehl 1996). Here, we only give a brief outline of the model attributes. CCM3 has a triangular spectral horizontal grid with truncation T42 (approximately 2.8 x 2.8-degree transform grid). In the vertical direction the model's atmosphere is stratified into 18 levels with a rigid lid at 2.917 mb. CCM3 also has the following numerical attributes: a semi-implicit, leap frog time integration scheme; use of the spectral transform method for treating the dry

dynamics; application of a bi-harmonic horizontal diffusion operator; a shape-preserving semi-Lagrangian transport scheme (Williamson and Rasch, 1993) for advecting water vapor, as well as an arbitrary number of other scalar fields (e.g., cloud water variables, chemical constituents, etc.). The physics includes use of a delta-Eddington approximation to calculate solar absorption; use of a Voigt line shape for infrared radiative cooling in the stratosphere; inclusion of a diurnal cycle; the incorporation of a finite heat capacity soil/sea ice model; parameterization and treatment of cloud optical properties (Kiehl et al., 1994); non-local treatment of boundary-layer processes; and use of a simple mass flux representation of moist convection.

CCM3 has state-of-the-art treatment of the fluxes between the land surface and the atmosphere, which is important for the present investigation focussing on deforestation induced climate change. The model is coupled to the land surface model (LSM version 1; Bonan et al 1996) which is a one-dimensional model of energy, momentum, water, and CO2 exchange between the atmosphere and land. Surface types were derived from Olson et al's (1983) 0.5 X 0.5 data. Soil colors were taken from the BATS T42 data set for use with the CCM (Dickinson et al. 1993). Sand, silt, and clay data were derived from Webb et al.'s (1993) 1.0 x 1.0 data set. Inland water data were derived from Cogley's (1991) 1.0 x 1.0 data for perennial freshwater lakes and swamps/marshes

The formulation of LSM accounts for the ecological differences among vegetation types, hydraulic and thermal differences among soil types, and allows for multiple surface types

including lakes and wetlands within a grid cell. Vegetation effects are included by allowing for twelve plant types that differ in leaf and stem areas, root profile, height, leaf dimension, optical properties, stomatal physiology, roughness length, displacement height, and biomass. These 12 plant types are combined to form 28 different vegetated surfaces, each comprised of multiple plant types and bare ground so that, for example, a mixed broad leaf deciduous and needle leaf evergreen forest consists of patches of broadleaf deciduous trees, needle leaf evergreen trees, and bare ground. Lakes and wetland, if present, form additional patches. Soil effects are included by allowing thermal properties (heat capacity, thermal conductivity) and hydraulic properties (porosity, saturated hydraulic conductivity, saturated metric potential, slope of retention curve) to vary as functions of percent sand and percent clay. Soils also differ in color, which affects soil albedos. Consequently, each grid cell in the domain of interest is assigned a surface type, a fraction covered by lakes, a fraction covered by wetlands, a soil texture (percent sand, percent silt, percent clay), and a soil color. In coupling to the atmospheric model, the land surface model provides to the atmospheric model, at every time step, surface albedo (direct beam and diffusion for visible and near-infrared wavebands), upward longwave radiation, sensible heat flux, latent heat flux, water vapor flux, and surface stresses. The atmospheric model provides to the land model, at every time step, incident solar radiation (direct beam and diffuse for visible and near-infrared wavebands), incident longwave radiation, convective and large-scale precipitation, and lowest model level temperature, wind, specific humidity, pressure, and height.

Two model simulations are performed to study the sensitivity of the African continent seasonal and annual climate response to the replacement of the tropical rain forest vegetation by savanna grassland (Fig.4.1). The purpose of imposing such drastic modification in vegetation in the anomaly experiment is to study the upper bounds of climate change that could be expected from the deforestation over Africa. We recognize that the present level of observed deforestation is more modest than the scale depicted in Fig.4.1. It is widely noted that in Africa mature forest is being largely replaced by a mosaic of re-growth forest and shifting agriculture which is different from the situation in the Amazon which is undergoing extensive agricultural colonization (Gurney et al 1993).

The forest vegetation consists of tropical broadleaf evergreen tree type (type 10 in the LSM computer code), while the deforested region is characterized by interrupted woods savanna type of vegetation (type 12 in the LSM computer code). A climatological SST data set archived at NCAR is used to prescribe the lower boundary conditions over the oceans in the model. In each run the model is integrated for ten years and the numerical integrations start from the same initial conditions where the orbital parameters required for computing the solar zenith angle and the initial conditions correspond to the middle of October.

4.3 Intraseasonal variability

The monthly evolution of the simulated rainfall is examined by considering latitude and longitude cross sections through the center of the Congo tropical rain forest, along the

20E meridian and the equator, respectively. Fig.4.2a shows that the model simulates realistic migration of the rainfall belt in the meridional direction. The near equatorial region exhibits rainy conditions nearly through out the year, with two maxima in March-April and October. The lowest rainfall conditions occur in June & July. The southern latitudes have one main rain season, which extends from December through February. Over the northern latitudes corresponding to west Africa and the Sahel, the occurrence of the rainy season during the months of the northern hemispheric summer is realistically reproduced, although the limiting latitude of the rain belt does not extend far enough to the north as observed. Within the longitudinal (10E-30E) band where deforestation mainly occurs in the model, the two rainfall maxima in March and October are clearly evident. July is the only month, which is almost void of rainfall.

Deforestation results in significant reduction in the rainfall, with the axis of minimum rainfall exhibiting south-north migration between 10S & 10N, thus mainly confined to the region of deforestation. The reversal in the sign of the anomaly pattern in Fig.4.2c indicates that deforestation results in delayed onset of the September-October-November rain season. Similar behavior is noted for the February-March-April rain season, although to a lesser extent. Over the Congo deforested region, maximum reduction in rainfall occurs during the driest months of the year, in June through September (Fig. 4.3). This period corresponds to the lowest surface and ground temperatures of the year when the overhead position of the sun is furthest away from the equatorial belt. However, what seems to be even more significant is that this period is also associated with minimum

increase in temperature compared to the rest of the year. Inspection of the primary factors (Fig.4.4) which contribute to the regional hydrological balance indicates that this period is unique compared to the rest of the year, because it experiences a net loss of moisture through horizontal moisture flux divergence in the case of the deforestation run. For the other seasons, moisture flux convergence is positive irrespective of whether deforestation occurs or not. For all the four seasons, the replacement of the tropical rain forest with savanna grassland vegetation results in suppression of precipitation larger than the corresponding reduction in evapotranspiration, implying that the dynamical horizontal convergence of moisture from the surrounding regions also would decrease as a result of deforestation. This outcome is consistent with similar studies conducted in the past to clarify the potential climate impacts of the Amazonian deforestation (Shukla et al 1990).

4.4 Seasonal variability

We have stratified the year into four equal segments, which are normally used to study seasonal climate variability of Africa. These seasons are: December-January-February (DJF), March-April-May (MAM), June-July-August (JJA), and September-October-November (SON). Fig.4.5 shows the model results for the control run for each of the four seasons, and Fig.4.6 gives the corresponding rainfall patterns for the deforestation run. Both the control and deforestation runs yield similar rainfall patterns. The corresponding rainfall patterns are not presented here because they have been discussed comprehensively in other studies (Semazzi et al 1996, Goddard and Graham 1999, and

others). The model faithfully reproduces the migration of the rainfall regimes during the annual cycle. Over complex terrain, such as eastern Africa, the T42 resolution of CCM3 may be too coarse to resolve such important features as, the maximum rainfall over the Ethiopian Highlands. In such cases, it may be necessary to adopt the nested model approach (Semazzi et al 1993, and Sun et al 1999ab).

Fig.4.7 shows the seasonal rainfall differences between the control and the deforestation simulations. Over the deforested region the rainfall deficits occur through out the year. In the seasons of MAM, JJA, and SON the rainfall anomaly patterns are confined to the region of deforestation. However, the DJF season exhibits distinct contrast from the rest of the seasons. The rainfall deficits over the near equatorial region are accompanied by a wave of alternating rainfall centers downstream from their embryonic region over central Africa where most of the deforestation is imposed in the model.

We believe that the wave-like pattern in the rainfall depicted in Fig.4.7 is associated with the suppression of Rossby wave trains (Hoskins and Karoly, 1981; Kalnay and Helem, 1981; Kalnay et al 1986) associated with mid-tropospheric latent heating due to tropical convection over the Congo tropical rain forest. The anomaly pattern manifests itself in form of regional teleconnection and affects remote regions from the deforested area. Over southern Africa, deforestation results in reduction in rainfall over Mozambique, and increase over Botswana, Zambia, the southern region of DRC, and parts of South Africa. Changes in the activity of trapped Rossby wave trains generated by the mid-tropospheric latent heating over the tropical forest region is responsible for this continental

teleconnection climate response.

Fig.4.8 displays the model simulated geopotential anomaly pattern (derived from the pressure field) at the 200mb pressure level. The presence of a high pressure center in the upper levels of the atmosphere seen over southern Africa would correspond to low-level off-shore circulation away from Mozambique toward Madagascar. This flow pattern would suppress the supply of moisture from the Indian ocean and support the rainfall deficits observed in Fig.4.7. The embryonic region for both short Rossby waves and the long Rossby waves is located to the north of the waves and it extends from the tropical forest to the region of the location of the ITCZ during DJF. further north which in turn has been influenced by the replacement of the tropical rain forest. The resulting suppression of rainfall due to the deforestation reduces upper-level divergence which is the primary factor responsible for the generation of wave form disturbances

Many studies have shown that latent heating associated with tropical convection tends to excite Rossby waves (Kalnay et al 1986) downstream from the source region. The meridional structure of the mean zonal flow essentially determines the relationship between the wavelength and trajectories of the ensuing wave patterns (Hoskins and Karoly, 1981). Splitting of forced Rossby wave trains usually observed in connection with tropical forcing, arise because large-scale waves propagate freely polewards and eastwards of the poleward flank of the jet. In the atmosphere, global scale teleconection patterns are the poleward propagating planetary Rossby wave trains predicted by theory (Hoskins and Karoly, 1981). On the contrary, there have been fewer observational

examples of the trapped short scale waves, which are also predicted by theory, largely because of the limited data coverage over the tropics. For the Southern Hemisphere, Kalnay and Helem (1981) were among the first to point out the existence of large amplitude, short wavelength, and stationary Rossby wave trains. These waves, with a dominant scale of wavenumber 7, were prominent over South America during the entire month of January 1979, the first month of FGGE Special Observing Period (SOP-1). Kalnay et al (1986) closely reproduced the observed wave trains using a General Circulation Model and found that convective heating was the primarily responsible for their origin.

The streamline pattern in Fig.4.9 indicates that the anomaly flow (deforestation minus control) promotes offshore transport of moisture thus conducive to the drier conditions in the vicinity of the Mozambique Channel and the adjacent inland region. Streamlines are lines which are everywhere parallel to the instantaneous wind velocity; i.e., 'snapshots' of the flow at an instant or over the period for which the average has been obtained. We also note an increase in westerly flow in the vicinity of the deforested region, which could play a significant opposite role in promoting Rossby wave activity evident in Fig.4.7. Linear analysis based on the potential vorticity equation indicates that the dependence of the Coriolis parameter on latitude creates a dramatic difference between easterly and westerly flow over large-scale sources of wave energy (Holton 1972). When westerly flow intercepts the source region it generated wave trains downstream however, easterly flow results in only localized disturbances in the vicinity of the source.

We believe that the Sahara outflow from the deforested region, which is apparent in Fig.4.9 is a manifestation of the divergence associated with the reduction in surface roughness due to the deforestation as predicted by Charney's hypothesis. In future, this hypothesis should be investigated further.

The apparent opposing roles associated with the increase in westerly flow and the decrease in the mid-tropospheric diabatic latent heating are not entirely clear based on the present model simulations, and they will be the subject of further research investigation to clarify the dynamical reasons for the model results. However, our explanation, based on the role of Rossby wave activity, may have important implications regarding the ENSO teleconnection response over southern Africa. We envisage that the large changes in diabatic latent heating over the central African tropical forest region during ENSO events could be responsible for inducing and maintaining regional climate anomalies through the modulation of the structure and magnitude of trapped Rossby wave trains over the region, similar to the behavior witnessed in the present deforestation study. However, the present design of model experiments is not appropriate to elucidate this hypothesis. If this were the case, then, changes in zonal flow and the intensity of diabatic heating could be important factors in determining the nature of the interannual climate variability over southern Africa in response to ENSO and other forms of ocean forcing scenarios. The wavelength of the resulting wave trains could be a key factor in determining the actual location of the ENSO climate anomalies, thus providing a plausible explanation for the different responses to different ENSO events over southern

Africa.

Inspection of major "outbursts" of convective activity over southern Africa suggests similar structural characteristics, as we have observed in the present model results (personal communication with Dr. Richard Washington, University of Oxford, England). This is consistent with our speculation regarding the possible role of shortwave Rossby waves in providing a link between the near-equatorial anomalies in tropical convection and distant locations further downstream over southern Africa. Indeed the persistent "streaks" of convection usually observed over other tropical regions with widespread organized convection, such as central South America and Indonesia, are potential candidates for supporting similar regional teleconnection climate change in response to deforestation.

4.5 Annual Mean Conditions

We show in Fig.4.10 the simulated annual total rainfall. Comparison with the observed rainfall (Nicholson et al., 1988; and Krishnamurti and Ogallo, 1989) indicates that the model successfully simulates the general features of the African climate. In the control run the model successfully reproduces the transition from the wet conditions over the coastal regions and the drier conditions towards the Sahara desert. The Kalahari desert and the semi-arid region along the coast of Somalia feature prominently. The difference fields, deforestation minus control, in Fig.4.11 shows a distinct region of depleted rainfall over the deforested region. The decrease in rainfall is as large as 300mm/year over the

deforested region. There is some evidence of weak positive anomalies to the south over Namibia and South Africa. Deforestation results in marked changes in surface temperate and ground temperature (Fig.4.12) due to the reduction in evapotranspiration associated with deforestation. The ground and surface temperature increase is primarily confined to the deforested regions of West Africa, the Congo basin, and the eastern Africa evergreen vegetation regions.

4.6 Conclusions

We have investigated the climatic impact of deforestation in Africa. The primary research vehicle in our investigation is the standard version of the NCAR CCM3 GCM with horizontal resolution of Triangular spectral truncation T42 (approximately 2.8 x 2.8 degrees). Two separate ten-year simulations based on climatological sea surface temperature (SST) have been performed. In the control simulation normal vegetation is prescribed. The design of the anomaly experiment is similar to the control run except that the tropical rain forest regions in Africa are replaced by savanna grassland.

CCM3 successfully simulates the primary features of the seasonal mean climate conditions over Africa. The results show that replacement of tropical rain forest vegetation by savanna grassland vegetation produces the following changes in climate over Africa, (i) over the deforested region, we observe significant reduction in the rainfall amounts through out the year. The decrease ranges between 2-3 mm/day during the northern hemispheric summer months when the region experiences the driest conditions

(July-September), to less than 1 mm/day during the wettest months of Autumn and Spring. The changes are as large as 2.5/5F, for the surface/ground temperatures, thus consistent with previous studies in the case of the Amazon deforestation studies (Shukla et al 1990), (ii) over southern Africa deforestation results in rainfall reduction over Mozambique, and increase over Botswana, Zambia, Southern DRC, and parts of South Africa. Changes in the activity of trapped Rossby wave trains generated by the mid-tropospheric latent heating over the tropical forest region is responsible for this continental teleconnection climate response, (iii) over Eastern and Western Africa the impact of deforestation is primarily characterized by reduction in rainfall, however GCM resolution may not be adequate to resolve the large contrasts in terrain and vegetation types, and (iv) in the rest of Africa the response is relatively weak.

The impacts of deforestation simulated by the model for the MAM, SON, and JJA seasons are not too surprising as they may generally be deduced from previous studies where GCMs were employed to study deforestation over other regions. In these seasons, the deforestation results in reduced rainfall which is primarily confined to the deforested region. However, during the SON season, the model results indicate that deforestation may significantly if not dramatically affect distant regions from the region where the rain forest has been cleared. Moreover, the altered circulation at these remote vulnerable regions over Africa could be re-enforced by other sources of climate variability which have not been examined in this chapter. For example, we kept the sea-surface temperature for all the oceans fixed in our model simulations. In reality, it is well known that this is

not the case. Further modeling investigations should therefore be undertaken to investigate how the impacts of deforestation could be modulated by other factors. Moreover, the reduction in vegetation which was prescribed in the model was rather drastic because it was merely designed to explore the outer bounds of the impacts of deforestation on the climate of Africa. Future investigation should apply the best estimates of deforestation levels in the models to arrive at more applicable results.

We postulate that the role of trapped Rossby waves may also apply to other situations when the tropical convection over Africa is enhanced or suppressed by other factors. In particular, we hypothesize that during ENSO the suppression and/or shifting of the convection through the Walker circulation over Central Africa may trigger a similar mechanism as we have seen in this study. In other words, during the El Nino events when tropical convection over the rainforest region is suppressed, the conditions correspond to our present results where the convection was suppressed by deforestation which resulted in reduction of rainfall over Mozambique, and increase over Botswana, Zambia, the southern region of DRC, and parts of Southern Africa. By the same reasoning, during La Nina, we would anticipate the opposite conditions to prevail and expect abundant rainfall for Mozambique. Therefore, trapped Rossby wave activity could be one of the potential mechanisms for explaining the observed relationship between ENSO and the interannual variability of the climate over Southern Africa.

The wavelength of the resulting wave Rossby wave trains could be a key factor in

determining the actual location of the ENSO climate anomalies, thus providing a plausible hypothesis for explaining in part the variations in the response to different ENSO events over southern Africa (ICPO, 2000). The 1991-1992 episode in southern Africa illustrates the degree of nonlinearity and the existence of large gaps in the understanding of the predictability of the ENSO-related climate anomalies over southern Africa (IPCC, 1998). In that episode southern Africa experienced the worst drought of the century, by as much as 80% below normal (Zinyowera and Unganai, 1993), and seasonal grain production dropped by 60% below normal. The drought of 1991-1992 was more severe than that during the 1982-1983 and 1997-1998 ENSO events, although the corresponding Pacific SST anomalies were considerably weaker. Our study indirectly suggests that the trapped large amplitude short-wave Rossby wave trains emanating from the African latent heat source region should be included among the key research question for clarifying the role of and the interaction among the Pacific-Atlantic ENSO teleconnection, the Indian Ocean, the Atlantic Ocean, and the middle-latitude synoptic winter frontal disturbances.

Based on the present results we can infer that, the downscaling would be highly beneficial not only for the immediate region of Eastern and Central Africa where significant removal of tropical forest vegetation cover could occur in the coming decades, but also for the region further south, to infer the projected detailed response of the Southern Africa region to remote deforestation effects.

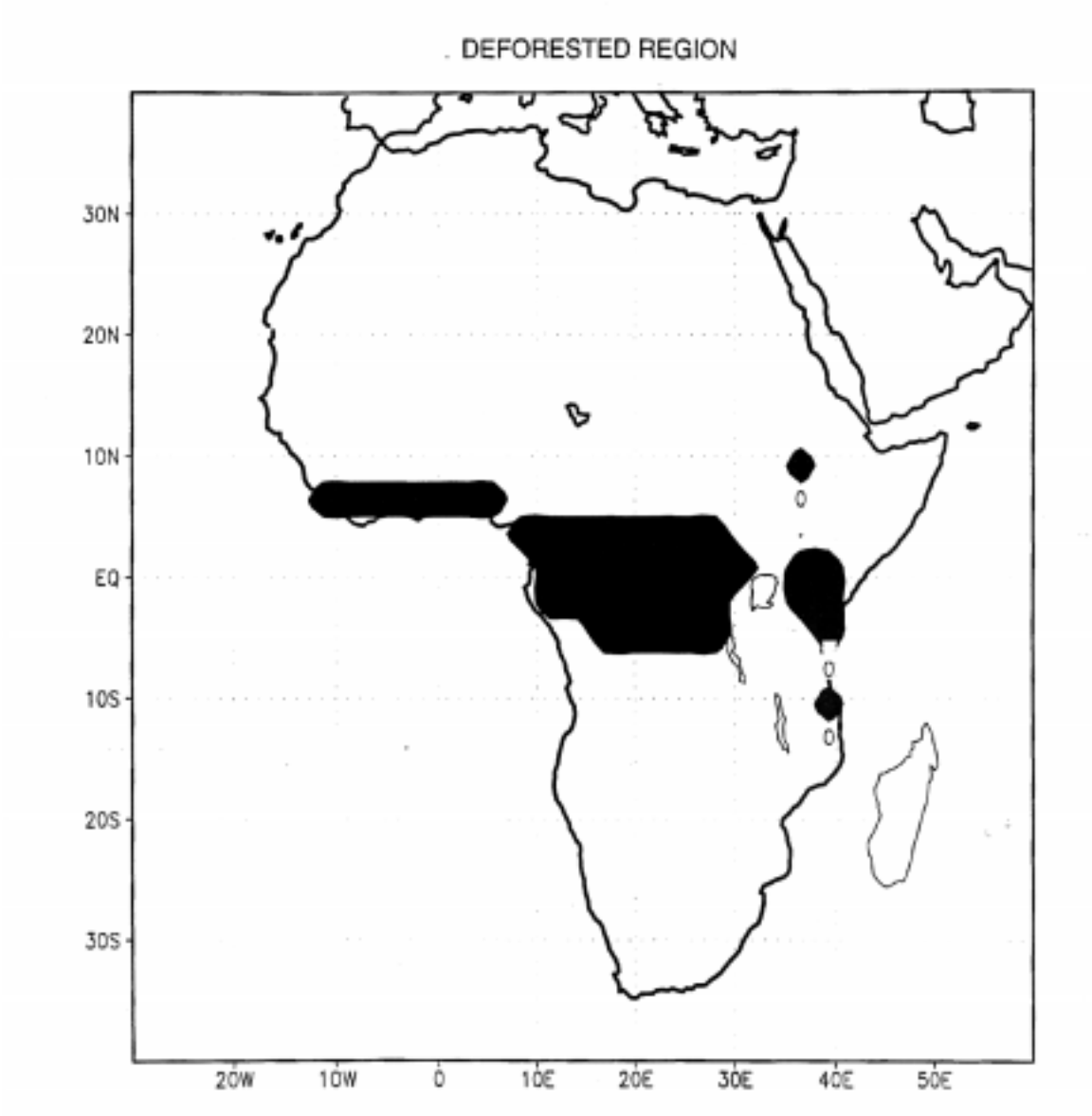

Fig.4.1. Deforested region. The forest vegetation consists of tropical broad leaf evergreen tree type, while the deforested region is savanna type characterized by interrupted woods.

a. RAINFALL (20E) – Control Run

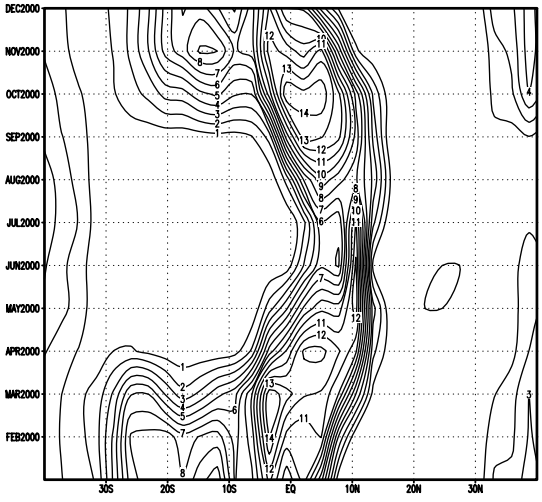

b. RAINFALL (20E) – [DEF-CON]

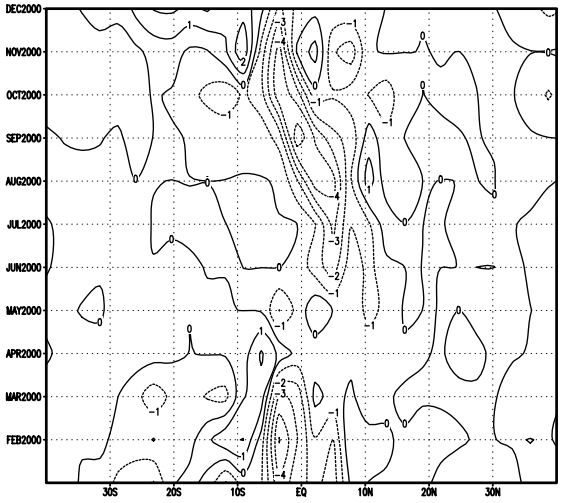

c. RAINFALL (at equator) – Control Run

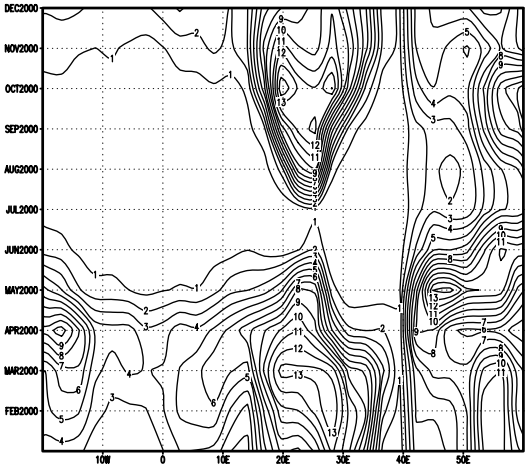

d. Rainfall (at equator) – [DEF-CONT]

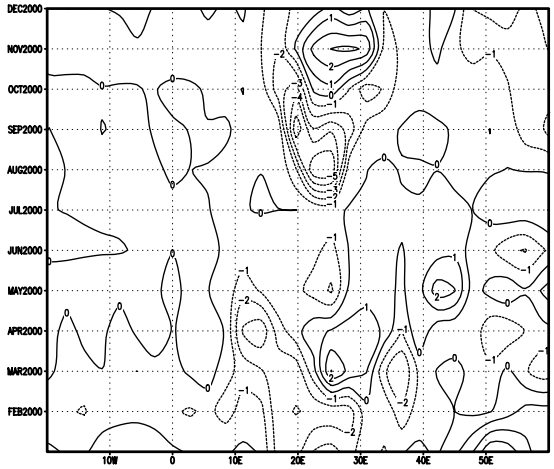

Fig.4.2. (a) Time-latitude cross-section of rainfall (mm/day), for the control run, along 20E, (b) time-latitude cross-section of rainfall, for the deforestation minus control model output, along 20E, (c) time-longitude cross-section of rainfall, for the control run, along the equator, (d) time-longitude cross-section of rainfall, for the deforestation minus control model output, along the equator.

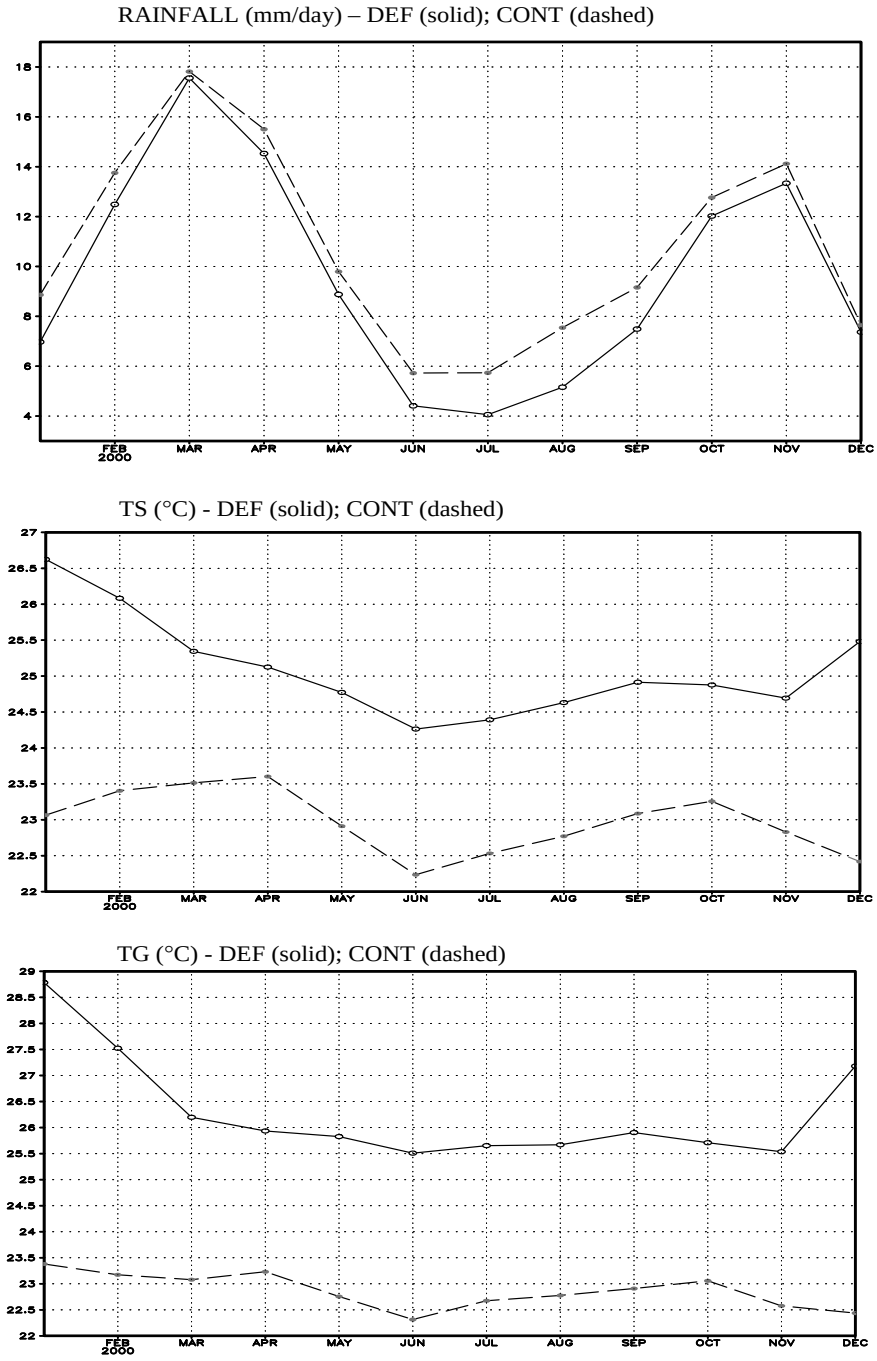

Fig.4.3. (i) Annual evolution of rainfall (mm/day) (top), (ii) annual evolution of surface air temperature (°C) (middle), (iii) annual evolution of ground temperature (°C) (bottom). Area averaging is performed over the primary deforested region [10E-30E, 5S-5N] over the Congo tropical rain forest. Deforestation experiment (solid), and control run (dashed).

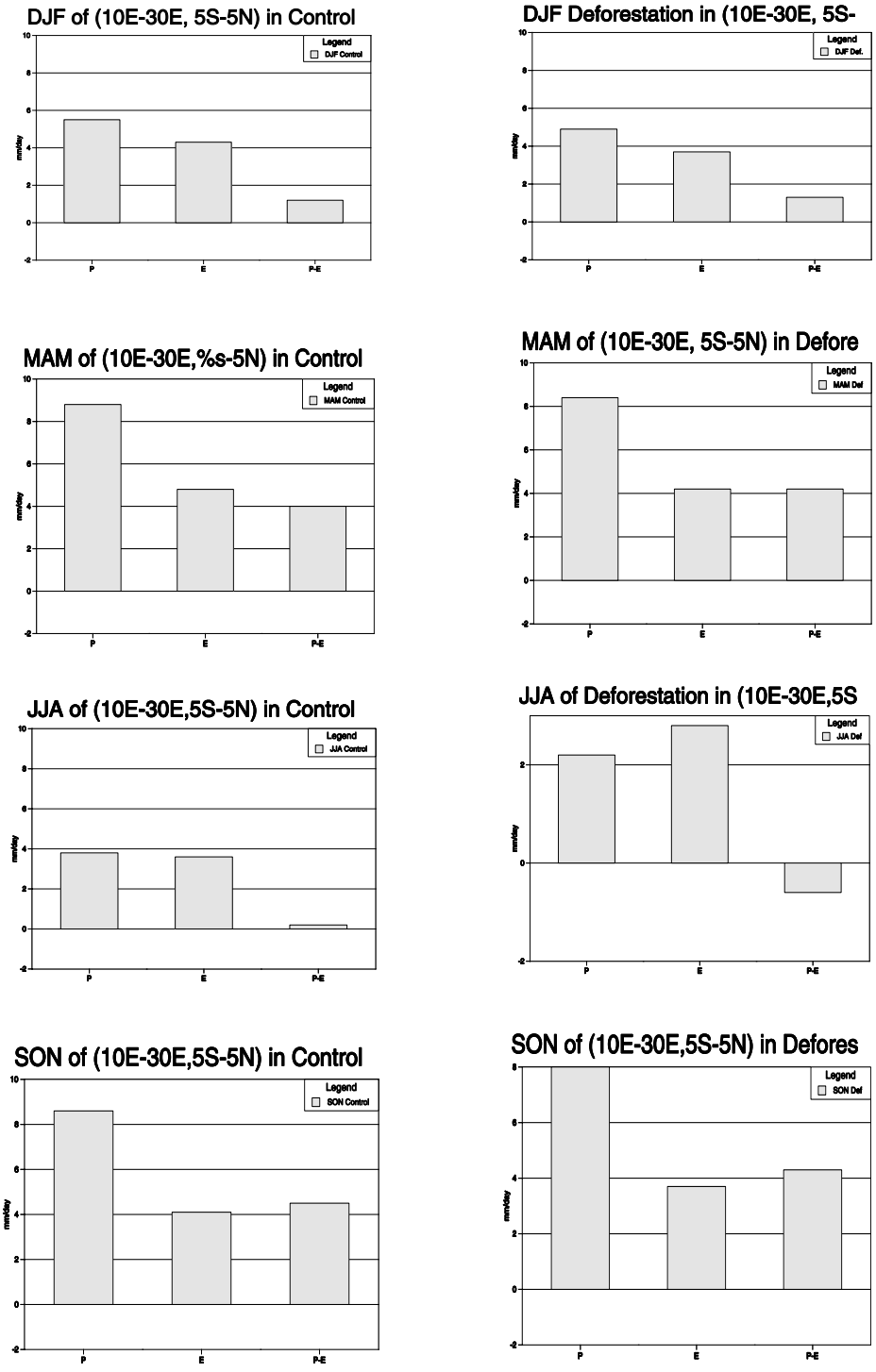

Fig.4.4. Seasonal average rainfall (R), evaporation (E), and (R-E), averaged over the primary deforestation region [10E-30E, 5S-5N] shown in Fig.4.1. Units mm/day.

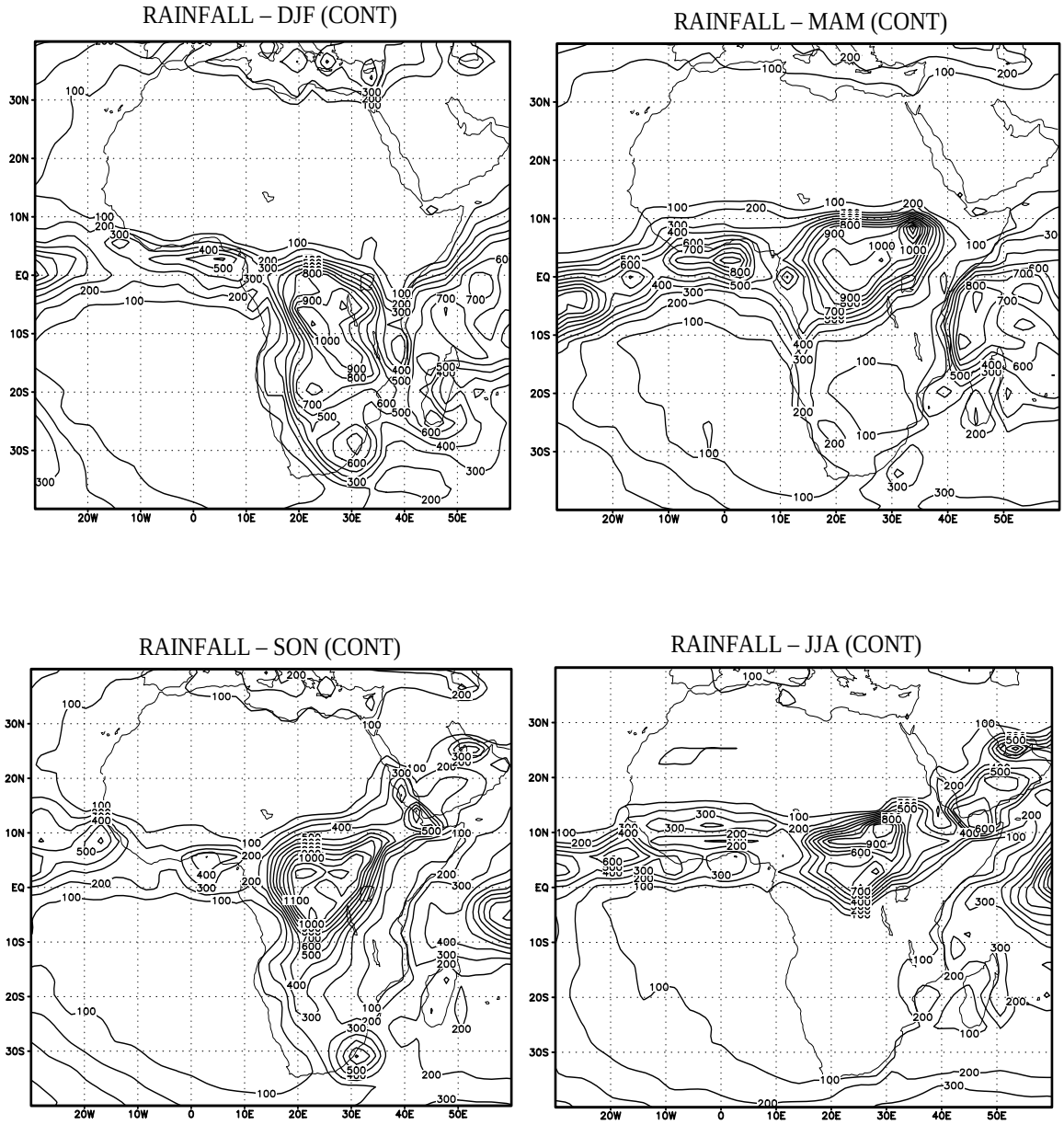

Fig.4.5. December-January-February (DJF; top-left), March-April-May (MAM; top-right), June-July-August (JJA; bottom-right), and September-October-November (SON; bottom-left), total seasonal rainfall (mm) averaged over the 10-years of the model simulation period for the control run.

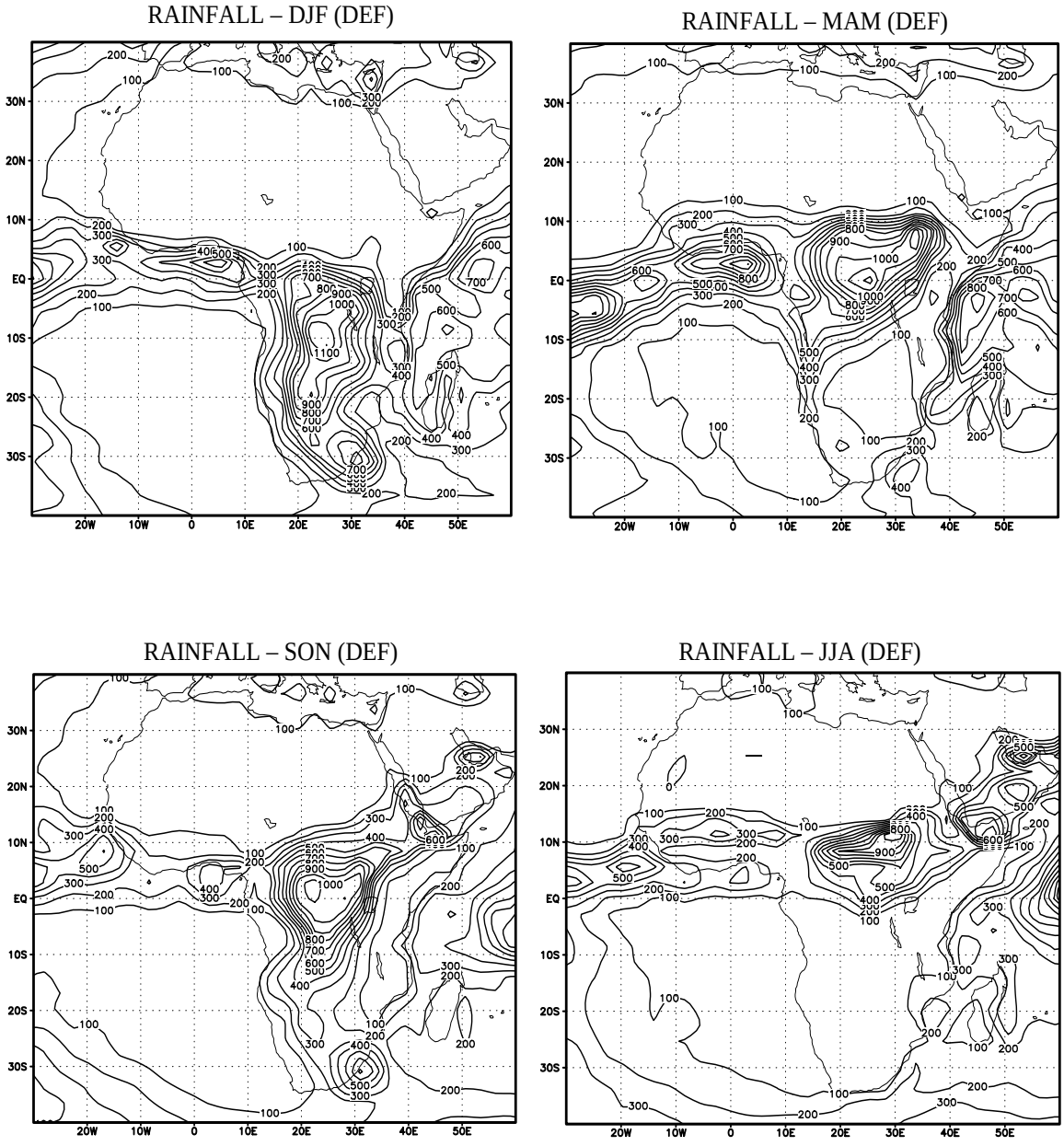

Fig.4.6. December-January-February (DJF; top-left), March-April-May (MAM; top-right), June-July-August (JJA; bottom-right), and September-October-November (SON; bottom-left), total seasonal rainfall (mm) averaged over the 10-years of model simulation period for the deforestation run.

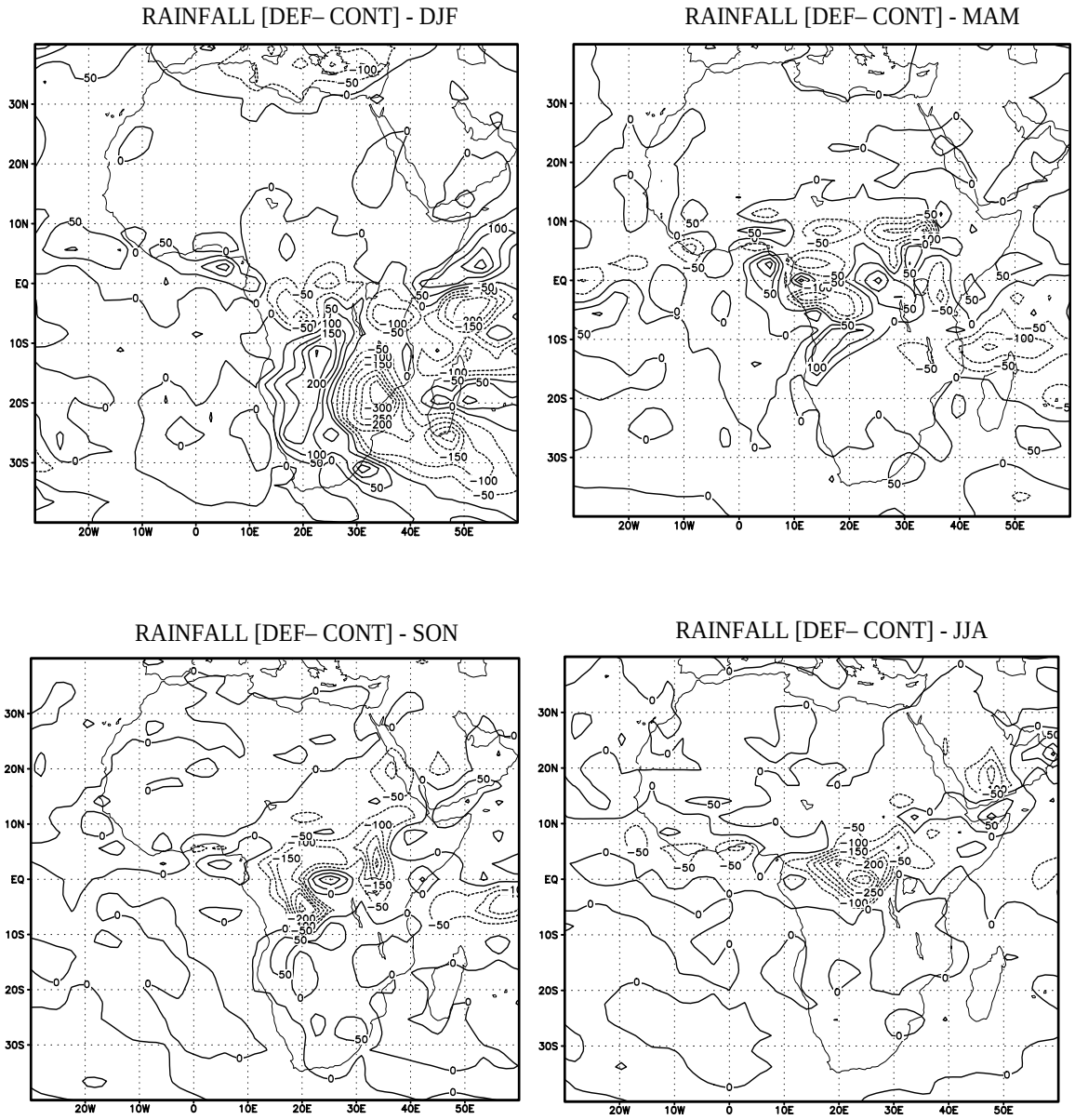

Fig.4.7. December-January-February (DJF; top-left), March-April-May (MAM; top-right), June-July-August (JJA; bottom-right), and September-October-November (SON; bottom-left), total seasonal rainfall (mm) averaged over the 10-years of model simulation period for the deforestation minus control model output.

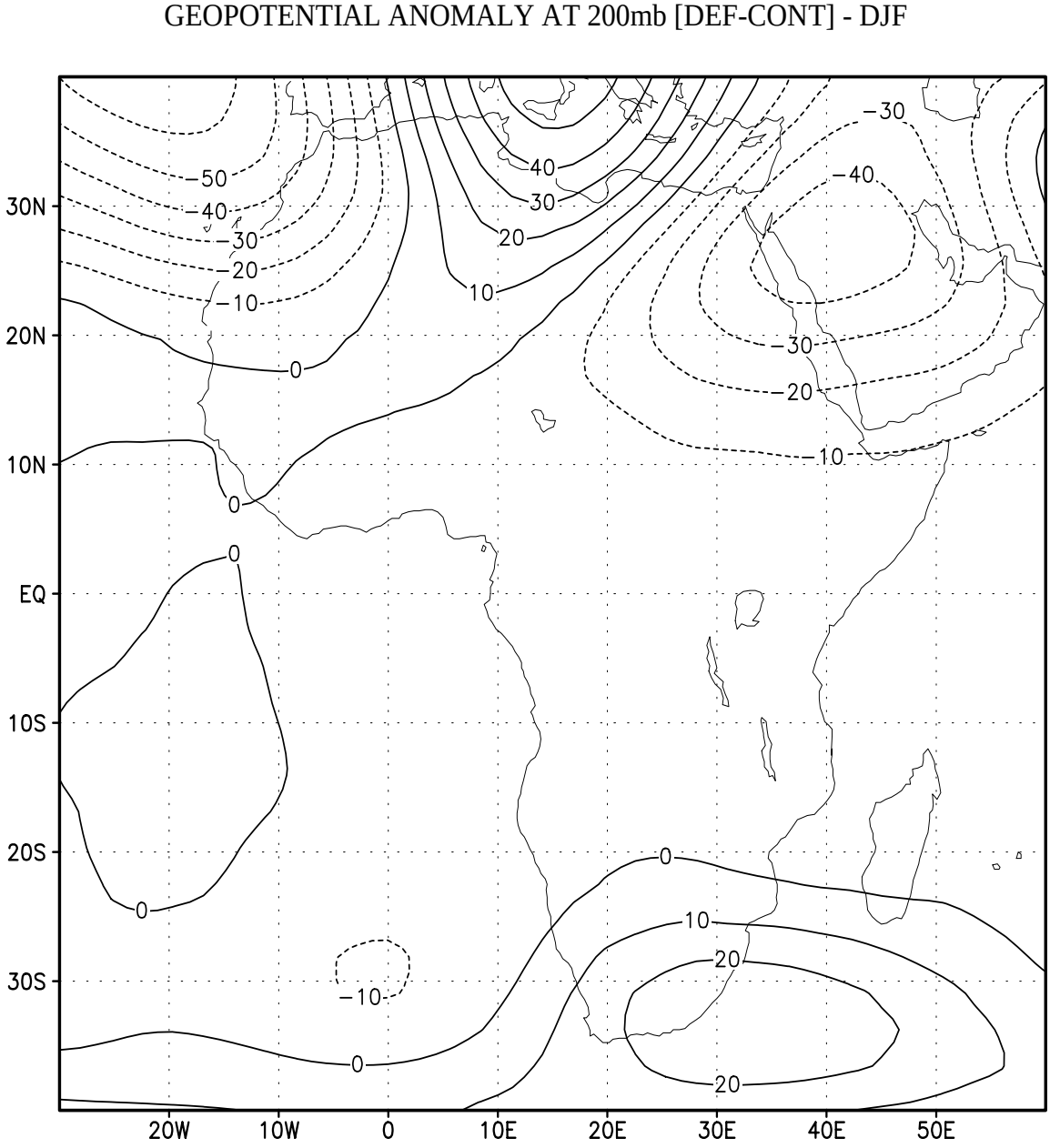

Fig.4.8. December-January-February (DJF) anomaly geopotential at 200mb (meters) for the deforestation minus control model output.

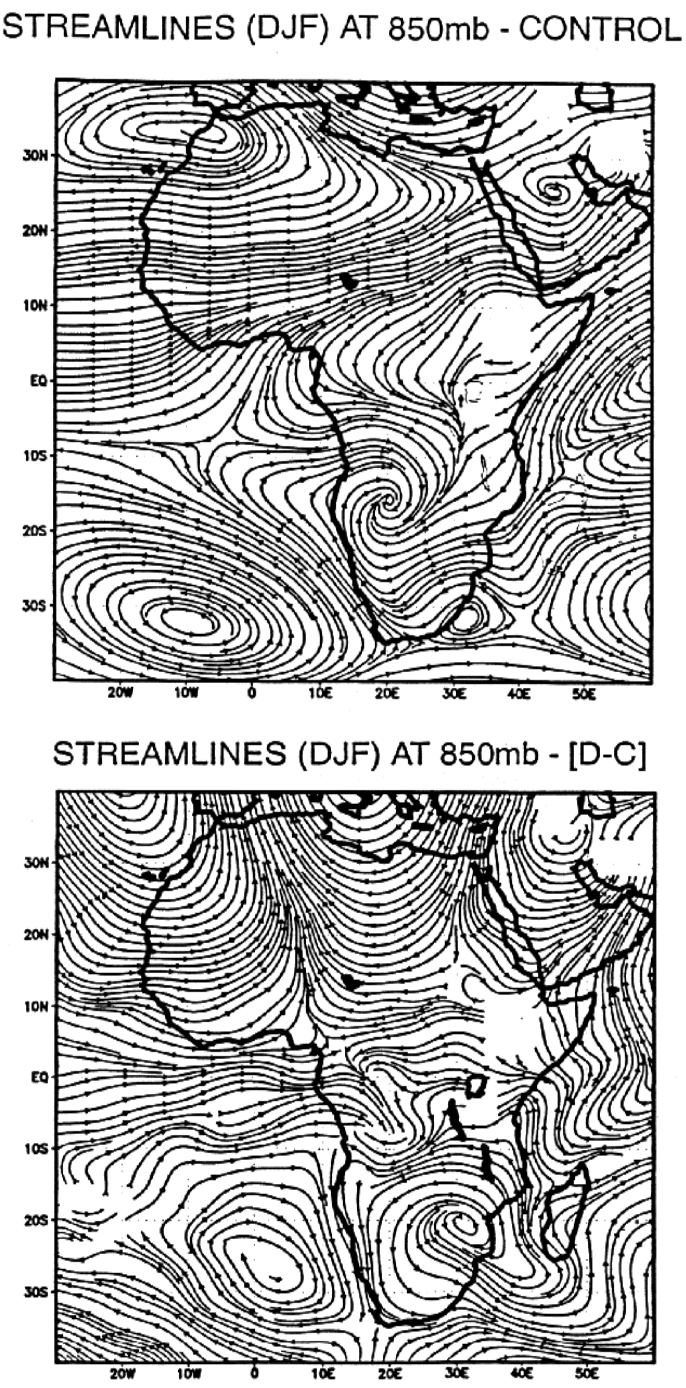

Fig.4.9. December-January-February streamlines at 850mb, Control run (top), and deforestation minus control model output (bottom).

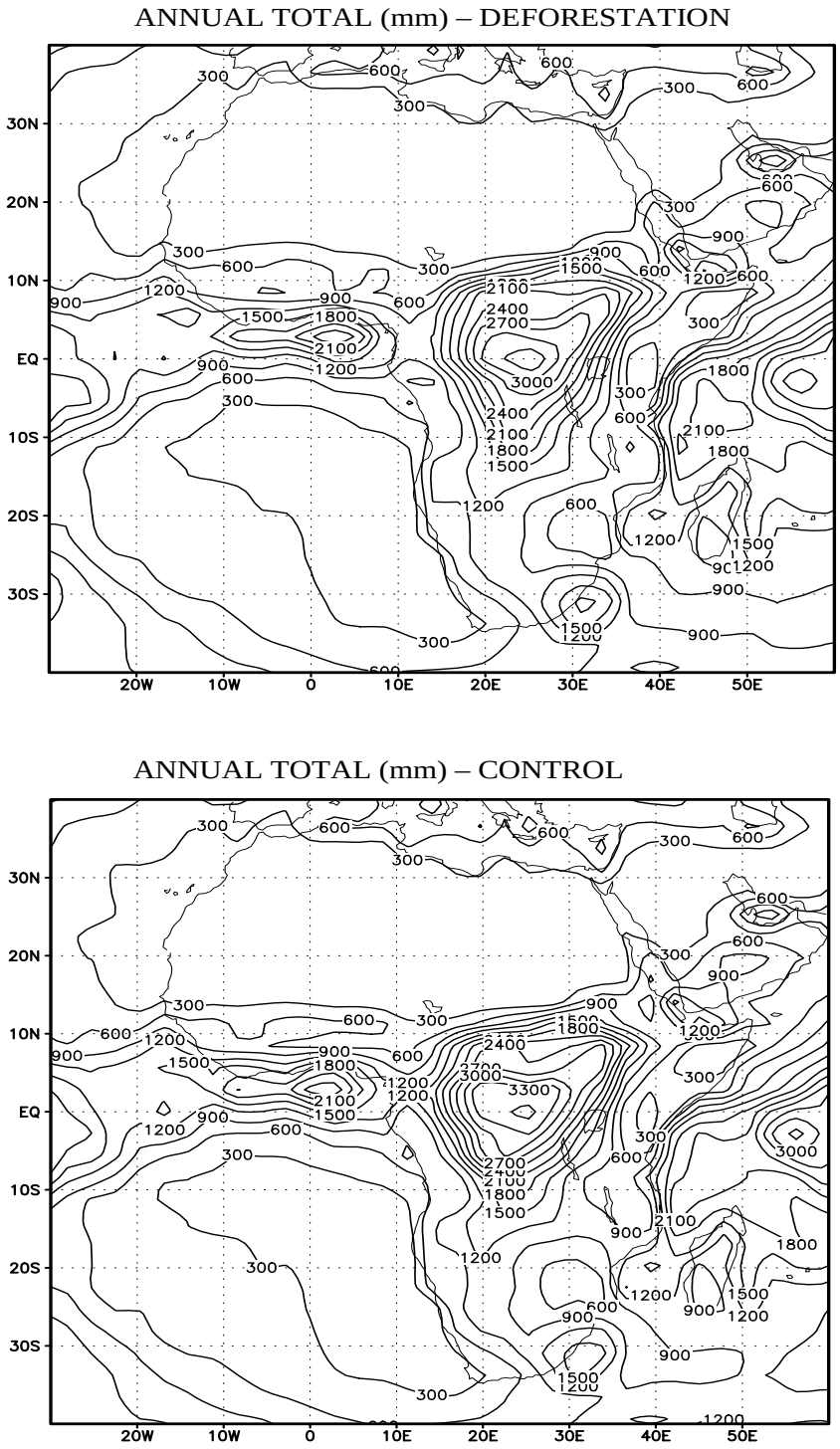

Fig.4.10. Annual mean rainfall (mm) for, the deforestation run (top), and control run (bottom).

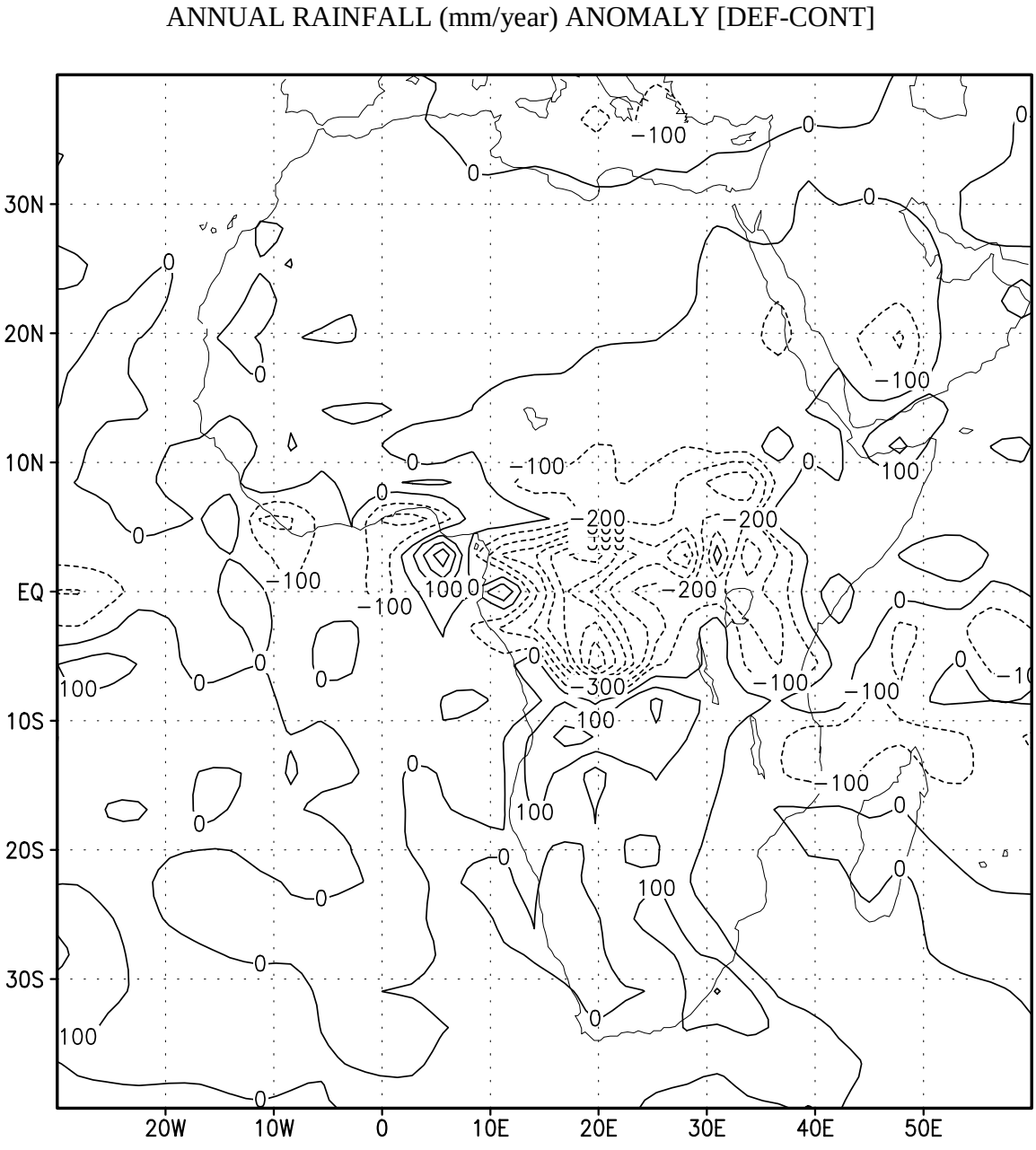

Fig.4.11. Annual mean rainfall (mm) for the deforestation minus control model output.

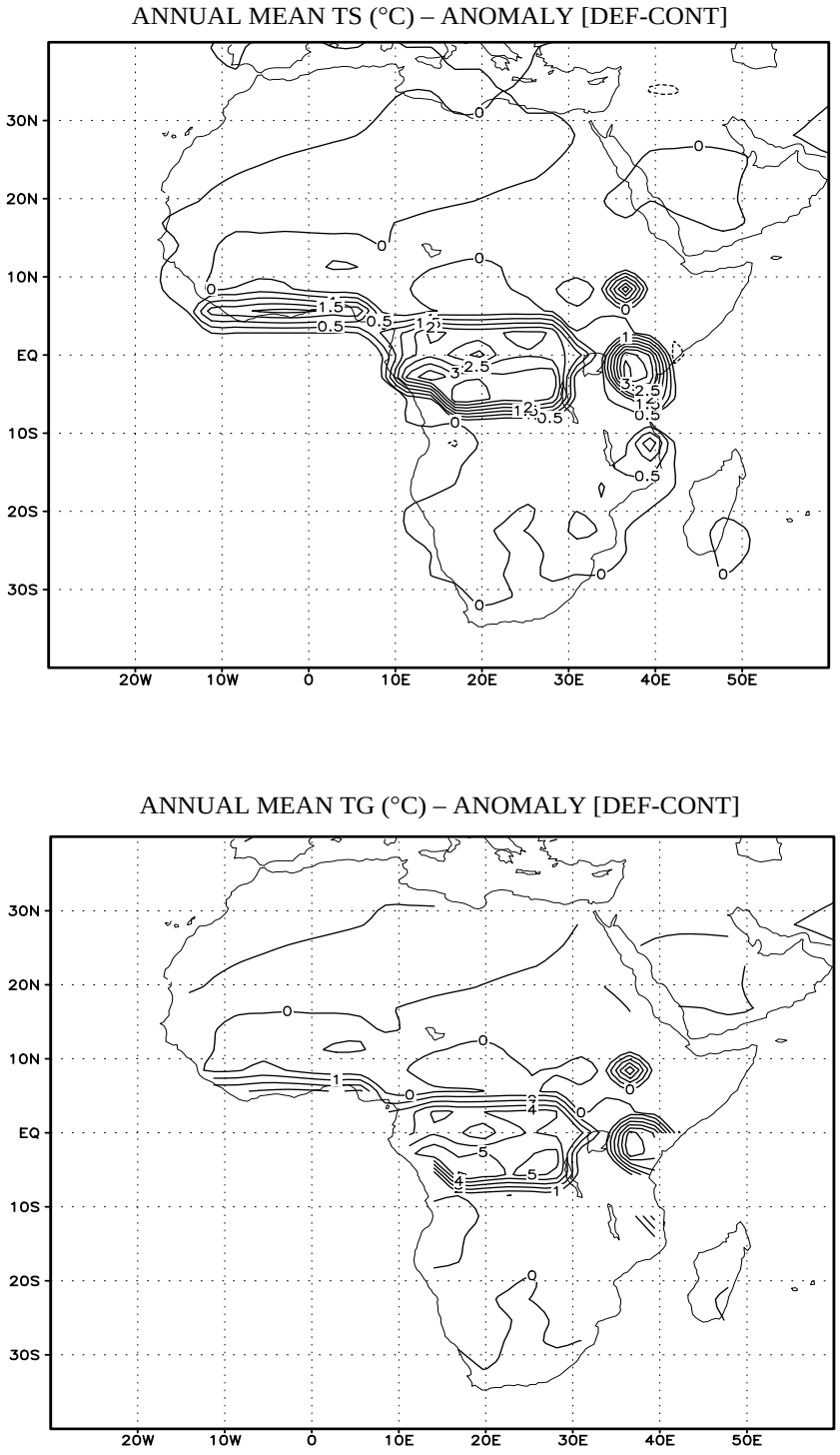

Fig.4.12. Change in annual mean temperature (K), deforestation minus control model output, surface air temperature (top), and ground temperature (bottom).

Chapter 5

Summary and Conclusion

In this study, a 3-dimensional primitive equation lake model was coupled to the NCAR regional climate model and applied to a case study to investigate the mechanisms responsible for the interannual climate variability over the Lake Victoria basin. In contribution to future efforts to apply this approach to climate change investigations, a GCM study based on the NCAR CCM3 climate model has been conducted to understand the role of deforestation of the Congo tropical rain forest.

In Chapter 2, we discuss the configuration of the POM model for Lake Victoria and its coupling with the RegCM2 regional climate model over the Lake Victoria catchment. In this effort a number of simulations have been conducted to investigate the dynamics and thermodynamics of Lake Victoria, and its sensitivity to different forcing specifications. The results show that, (i) the memory in the momentum of lake Victoria is about two weeks, (ii) there exists a 30-day oscillation in Lake Victoria and the water temperature stratification plays a critical role in the development of the oscillations, (iii) these oscillations are trapped above the thermocline along the coast and progress clockwise, (iv) the bythemetry and geometry of the lake play a fundamental role in determining the

climatology of Lake Victoria. The regions of the upwelling or downwelling are determined by wind stress and nearshore bathymetry, (v) the lake surface circulation is characterized by counter clockwise motion in response to the predominantly easterly surface winds, (vi) with time-dependent wind forcing based on the RegCM2 model, in spite of the fact that the diurnal component of the surface winds reverse direction in association with the land/lake breeze, the water circulation maintains the same anti-clockwise circulation throughout the day. This observation re-enforces the proposition that the circulation of the lake is primarily controlled by the large-scale wind pattern rather than the component associated with the land/lake breeze. We postulate that the large inertia associated with water is responsible for the weak response to diurnal cycle that dominates the near-surface wind regime. We find that the mean surface water circulation is primarily determined by wind stress, however heat flux forcing plays the dominant role in modulating its diurnal cycle. Furthermore, the results show that although surface lake temperature is strongly influenced by radiation and heat fluxes at the surface, it is evident that advection within the fluid plays a primary role in determining its spatial structure.

The 3-dimensional model produces a surface temperature pattern indicative of horizontal lake water mixing characterized by a horizontal spiral pattern in the temperature field. This is associated with the spreading of the pool of warm water from the regions of maximum heating in the southeast to the northern section of the lake where the temperature is initially relatively lower due to upwelling and the water column is deeper.

This pattern is not present in the 1-dimensional model. Based on preliminary comparison of the coupled RegCM2-POM model simulation results with the observations, we find that it produces more realistic lake surface temperature and rainfall over and around the lake, than the standard version of the model (RegCM2-1D) which employs simple one dimensional thermal diffusion to represent lakes. We find that the dynamics of the lake plays an important role in determining the coupled variability of the lake circulation and the ambient climatic conditions. Neglecting the lake's hydrodynamics and basing the lake model entirely only on thermodynamics deprives the coupled regional climate model of the ability to transport heat within the lake and influence the climate over the rest of the lake and perhaps the land regions surrounding the lake. Shallow nearshore regions of the lake are breeding areas for warm water and could be a critical factor in the chain of processes which link the fluctuations in the lake level and area, with its surface temperature and ultimately influence on the variability of the climate over the lake basin.

In Chapter 3, the coupled RegCM2-POM model was applied to simulate the climate conditions for the normal year (1988), two contrasting years (the El Nino (1982)) and non El Nino (1987)) to investigate the dynamical and thermodynamical factors responsible for the occurrences of wet and dry conditions over the Lake Victoria basin during the short rainy season. In both surface air temperature and water temperature, the relatively warmer areas are located at the southwestern and central-eastern region of the lake, and cooler area is located further to the northwestern sector. The co-located patterns of the surface air temperature and the lake surface temperature further indicates that there exists

strong atmosphere-lake interaction thus reconfirming the importance of the need for realistic representation of the lake in the model to produce realistic the simulation of the surface lake temperature. Over the lake basin, the regional climate variability is mainly determined by the large-scale circulation. Large-scale convergence anomalies and stronger vertical motion occur during the wet year, while divergence anomaly conditions and weaker vertical motion occur during the dry year. These strong/weak vertical motions associated with the convergence/divergence horizontal circulation intensify/suppress moisture convergence and thus influence precipitation over Lake Victoria during the wet/dry years. Moisture advection contribution is important but secondary to evaporation in explaining the heavy rainfall over the lake. The evaporation is strongly influenced by the wind speed.

The precipitation mainly occurs around midnight to early morning period when the land breeze dominates the lake region. Little or no rainfall occurs during daytime and early evening when the lake breeze is well established over the lake. The divergence/convergence disturbance originates from the eastern part of the lake during day/night time, and then moves toward the southwest. The diurnal oscillation in the atmosphere and the lake thermodynamics interact with each other and modify the regional climatic conditions. The interaction between the lake-land breeze and the prevailing northeasterly flow determines the asymmetry in the distribution of the diurnal rainfall and the southwestward movement of the divergence/convergence disturbances.

In this case study, P-E is positive during the wet year (1982), and negative during the dry (1987) and normal year (1988). These interannual variations in the P-E distribution indicates that Lake Victoria is a water moisture source for the surrounding region during normal and dry years and it is sink during the wet year. Thus the lake moderates the extreme drought and flood conditions. During the wet year, the negative P-E pattern also indicates that the moisture convergence plays an important role in determining the heavy precipitation. The westerly anomaly wind regime during 1982 further suggests that the moisture advection from the Congo tropical rain forest and Atlantic Ocean could be an important factor in explaining the wet anomalies over eastern Africa. Apparently the Indian Ocean did not play a critical role in 1982 El Nino.

The lake circulation variations modulate the LST pattern and thus influence the climate conditions over the lake basin. Transported by the anti-clockwise spiral currents, a warm tongue is formed over the northeastern part and a cold tongue over the northwestern part of the lake. The averaged LST over the entire fluid depth of the lake is higher during both wet and dry years than that during the normal year. The water circulation speed is strong/weak during the wet/dry years in response to the corresponding strong/weak atmospheric momentum forcing. This enhanced/weakened lake circulation and the corresponding horizontal water mixing of warm and cold water, thus results in weak/strong horizontal LST gradients. Consequently, the climatologically higher/lower water temperature over the southwestern/northeastern parts of the lake is reduced/increased during a wet year. The converse is true during a dry year. This LST

pattern further induces weak/strong mesoscale circulation and climatic impacts on the rainfall distribution over the lake during wet/dry years. The schematic illustration regarding the interaction between the large-scale circulation and the mesoscale circulation during the normal and wet years is displayed in Fig. 5.1 and Fig. 5.2, respectively. During the 1982 El Nino when the averaged LST over the lake is higher than that during the normal year, the LST gradient is weakened along the SW-NE axis over the lake. This results in a LST distribution whereby the southwestern region of the lake is cooled while the region of maximum LST shifts to the central-eastern part of the lake from the southwestern region. This LST distribution induces mesoscale convergent flow over the central-eastern part of the lake and divergent flow over the western sector. This mesoscale circulation further intensifies/weakens the large-scale vertical upward motion. The net change in rainfall distribution over the lake during the 1982 EL Nino is therefore a combination of the effect associated with the large-scale convergence pattern and the mesoscale climate changes associated shift of the maximum rainfall toward the central-eastern part of the lake from the western region in response to the LST redistribution. Conversely, the weaker lake circulation enhances the LST gradient over the western part of the lake, especially over the northwestern area, and the relatively heavy rainfall is still located over the northwestern sector of the lake. Therefore, the hydrodynamics of the lake plays an important role in determining the coupled variability of the lake circulation and the lake basin-wide climatic conditions. This conclusion is based on the use of the coupled 3-dimensional lake model however, and it is obscured in the results based on the

coupled 1-dimensional lake model.

In Chapter 4, the climatic impact of deforestation in Africa was investigated based on the standard version of the NCAR CCM3 GCM with horizontal resolution of triangular spectral truncation T42 (approximately 2.8 x 2.8 degrees). The design of the anomaly experiment is similar to the control run except that the tropical rain forest regions in Africa are replaced by savanna grassland.

CCM3 successfully simulates the primary features of the seasonal mean climate conditions over Africa. The results show that replacement of tropical rain forest vegetation by savanna grassland vegetation produces the following changes in climate over Africa, (i) over the deforested region, we observe significant reduction in the rainfall amounts through out the year. The decrease ranges between 2-3 mm/day during the northern hemispheric summer months when the region experiences the driest conditions (July-September), to less than 1 mm/day during the wettest months of Autumn and Spring. The changes are as large as 2.5°/5°C, for the surface/ground temperatures, thus consistent with previous studies in the case of the Amazon deforestation studies (Shukla et al. 1990), (ii) over southern Africa deforestation results in rainfall reduction over Mozambique, and increase over Botswana, Zambia, Southern DRC, and parts of South Africa. Changes in the activity of trapped Rossby wave trains generated by the mid-tropospheric latent heating over the tropical forest region is responsible for this continental teleconnection climate response, (iii) over Eastern and Western Africa the

impact of deforestation is primarily characterized by reduction in rainfall, however GCM resolution may not be adequate to resolve the large contrasts in terrain and vegetation types, the coupled RegCM2-POM model may be used to further investigate this issue in the future, and (iv) in the rest of Africa the response is relatively weak.

The impacts of deforestation simulated by the model for the MAM, SON, and JJA seasons are not too surprising as they may generally be deduced from previous studies where GCMs were employed to study deforestation over other regions. In these seasons, the deforestation results in reduced rainfall which is primarily confined to the deforested region. However, during the DJF season, the model results indicate that deforestation may significantly if not dramatically affect distant regions from the region where the rain forest has been cleared. Moreover, the altered circulation at these remote vulnerable regions over Africa could be re-enforced by other sources of climate variability which have not been examined in this study. For example, we kept the sea-surface temperature for all the oceans fixed in our model simulations. In reality, it is well known that this is not the case. Further modeling investigations should therefore be undertaken to investigate how the impacts of deforestation could be modulated by other factors. Moreover, the reduction in vegetation which was prescribed in the model was rather drastic because it was merely designed to explore the outer bounds of the impacts of deforestation on the climate of Africa. Future investigation should apply the best estimates of deforestation levels in the models to arrive at more applicable results.

The downscaling of the climatic effects of deforestation climatic can be performed by taking the CCM3 GCM output and using it to generate lateral boundary conditions for the RegCM2-POM model. However, that will be the subject of a separate investigation in the future. Based on the present results we can infer that, the downscaling would be highly beneficial not only for the immediate region of Eastern and Central Africa where significant removal of tropical forest vegetation cover could occur in the coming decades, but also for the region further south, to infer the projected detailed response of the Southern Africa region to remote deforestation effects.

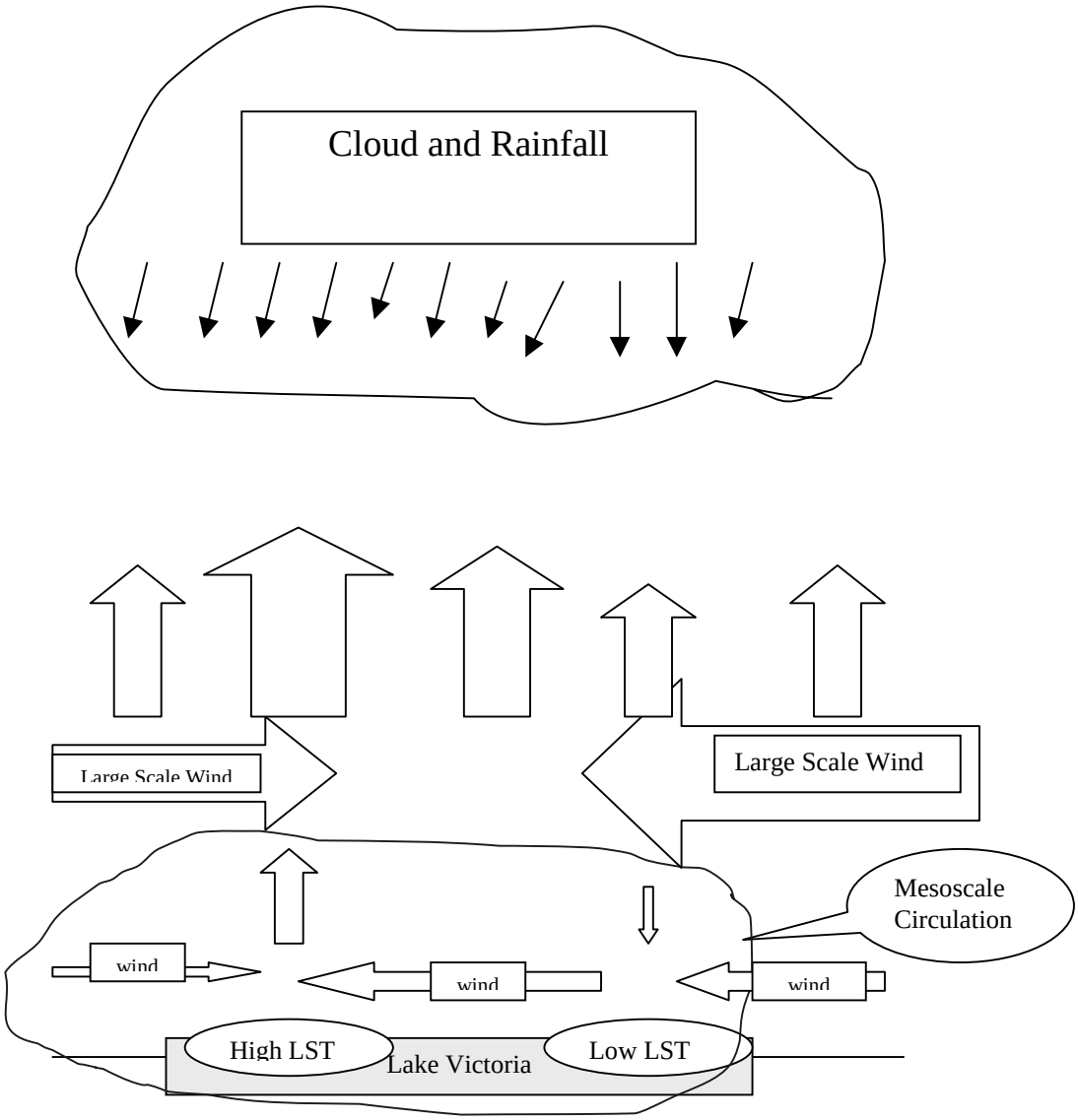

Fig. 5.1 Schematic diagram of interaction between large scale circulation and mesoscale circulation for the normal year

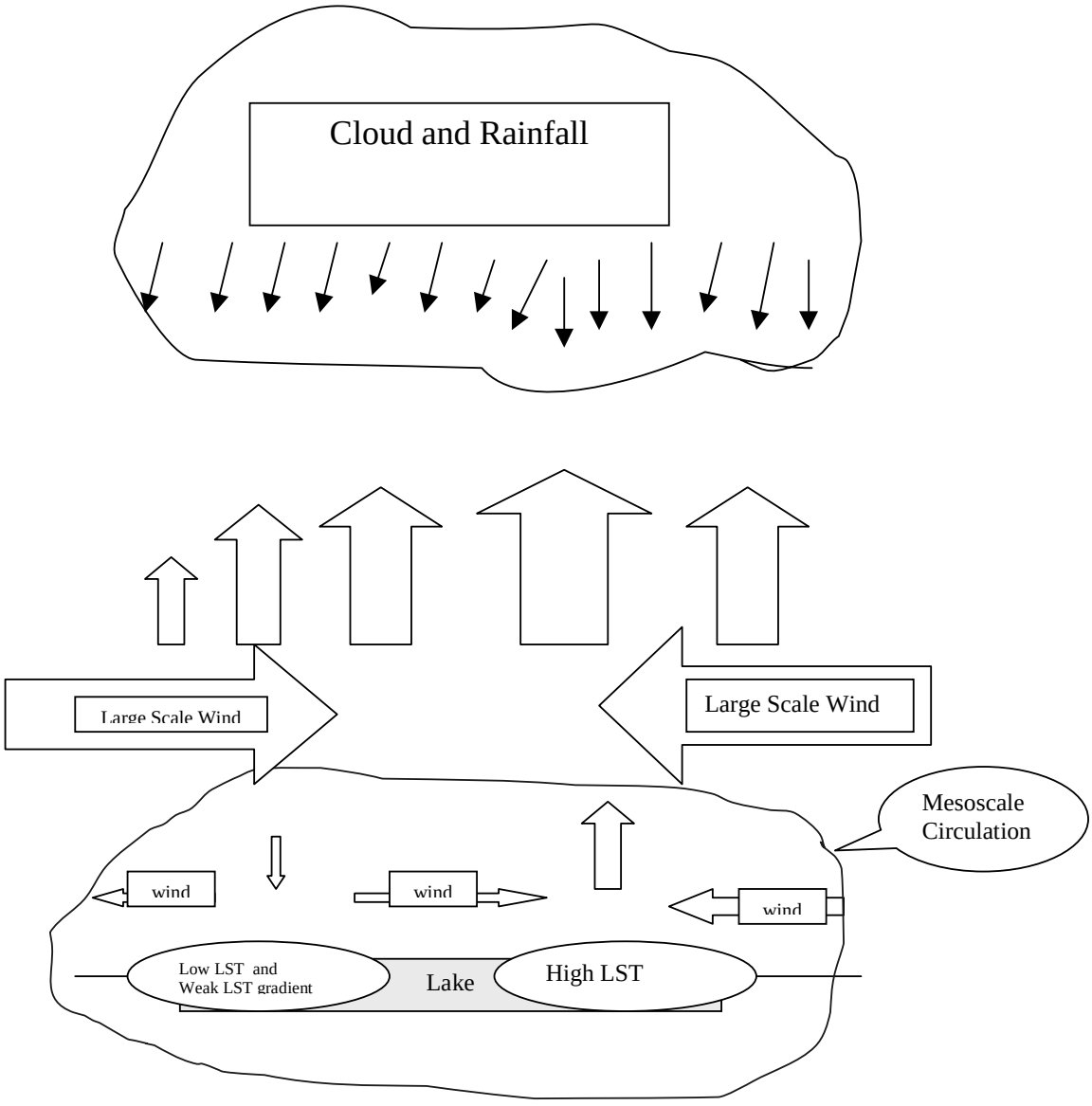

Fig. 5.2 Schematic diagram of interaction between large scale circulation and mesoscale circulation for the wet year

Chapter 6

Recommendations for Future Work

Based on the research undertaken in this thesis we suggest the following investigations as possible areas of future work.

(1) Our coupled RegCM2-POM model results show that the hydrodynamics of Lake Victoria play an important role in determining the coupled variability of the lake and the regional climate. Adopting the traditional modeling approach in which the lake hydrodynamics are neglected and the formulation is entirely based on thermodynamics alone is not satisfactory for eastern Africa. Such a strategy precludes the ability of the coupled regional climate model to transport heat realistically within the lake and thereby results in degraded simulation of the climate downstream over the rest of the lake and the surrounding land regions. Since a large proportion of the surface area of Eastern Africa is occupied by the large lakes of the Great Rift Valley (Malawi, Tanganyika, and Victoria). We recommend extension of the model domain to include the three large lakes of Eastern Africa. In this effort it will be necessary to adopt the double nested approach employed in the present study.

(2) The climate over eastern Africa is highly heterogeneous (Sun et al, 1999ab), and can be divided into 9 homogeneous climate regions based on observational data (Indeje et al, 2000). In our present study, the evaluation of the performance of the coupled model was limited to the basin of Lake Victoria. However, it is evident that the benefits of the using the POM model for Lake Victoria for the coupled model may extend beyond the perimeter of the lake. Future work should extend the evaluation to all the other homogeneous zones adjacent to the lake.

(3) The RegCM2-POM coupled model satisfactorily captures the monthly mean patterns of the short rains, but the performance of the model in simulating the onset and withdraw of the short rains has not been addressed. Knowledge about the onset of rains is critical for determining the planting time of crops, and therefore in crop-farming management to stabilize crop yield. Moreover, the onset and withdraw of the short rains vary with regions. It would be desirable to investigate the onset and withdrawal of the rains for each homogeneous climate region of eastern Africa. To reduce noise in the results, the five-day (pentads) cumulative frequencies of observed rainfall totals could be considered in the determination of the onset/withdrawal of the short rains.

(4) In this study, all the discussions are based on monthly mean conditions of December. However, the results in December do not fully represent the general climate conditions during the short rains. A investigation on intraseasonal

variability of the different sub-regions is recommended. Furthermore, the investigation on interannual variability was based on only a single wet, normal and dry year. Although the wet (1982) year and dry (1987) year represent two extreme years during the 1980s. The results based on these three years represent minimum sampling of the variability and in future work more years should be considered to obtain more robust results.

(5) Our recent studies of lake Victoria based on the POM model have unveiled the existence of a distinct family of wave trains that are sensitive to the vertical density stratification in the lake. These waves are mainly within the thermocline. The oscillations disappear in the case of isothermal lake conditions. They have maximum amplitude near the shoreline and propagate clockwise around Lake Victoria with a period of about 30 days. Lake Tanganyika: Further evidence of well defined wave propagation has also been found in Lake Tanganyika based on observations (personal communication, Pierre-Denis Plisnier, Royal Museum for Central Africa, Belgium). The large and regular fluctuations in temperature (2 degree) in Lake Tanganyika suggest the possibility of large exchanges of energy between the lake and the atmosphere. We hypothesize that this would result in propagating intra-seasonal climate signals over the lake catchment region in response to wave propagation in the lake. Lake Malawi: The similarities of lake-basin shape and temperature distribution in Lakes Tanganyika and Malawi suggest that the waves that have been observed in the case of the former (Coulter

and Spigel, 1991; Eccles, 1974; Degnbol & Mapila, 1982) are also likely to occur in the latter. These waves can influence the evolution of climatic anomalies on seasonal time scales, both over the water and the adjacent terrestrial region. Hence they are the important potential indicators for both seasonal climate and weather prediction over the lake basin. Further investigation of wave dynamics based on both numerical and analytical methods should be undertaken.

(6) Our coupled RegCM2-POM model results indicate that, the lake dynamics exhibit a heat 'pump' effect that takes heat away from the warmest (and shallowest) region of the lake in the southwest and depositing it over the relatively colder regions in the northeast. Consequently, the overall LST of the lake is elevated and the horizontal LST gradient is diminished. The LST pattern induces a strong mesoscale circulation and therefore influence the climate conditions over the lake basin. There exist strong coupling processes between the atmosphere and lake. Understanding the primary factors, which determine this coupled variability of the large lakes is an important prerequisite for understanding the climate predictability over the region. Sensitivity mechanistic experiments, such as altering lake depth and lake domain would be useful in clarifying the primary physical mechanisms involved.

(7) In our investigation on the dynamics and physical mechanisms responsible for the interannual variability over the lake basin, the results show that the climate

conditions are mainly determined by the large scale circulation over Lake Victoria. During the short rains, the prevailing winds over the lake basically consist of easterly flow from Indian Ocean. Therefore, the SSTs over the Indian Ocean are one of the important factors that could be responsible for determining the variability of the climate condition over the region. However, our studies were based on monthly global 1° x 1° Reynolds SST observations that are coarse in both spatial and temporal resolution and may not be adequate in providing enough detail for our study based on 20km resolution. Weekly with spatial resolution can match the coupled lake model may be required. We therefore recommend use of high resolution Ocean models to generate the coastal SSTs, such as the variable resolution MICOM model recently developed at North Carolina State University.

(8) We recommend that future studies should incorporate river inflow and outflow for Lake Victoria to facilitate long term model integrations.

(9) In our simulations, we applied a constant salinity value of 0.2ppt which is used for the Great Lakes (O'Connor et al., 1994). Although it is unlikely that the slight deviations from the present value would result in significant model simulation differences, it is recommended that formal confirmation of this claim should be subject of a future investigation.

(10) In this study we have adopted the same resolution for the lake model and the atmosphere model in the coupled system. Future work should explore if finer resolution for the lake model could result in a improved model results.

Chapter 7

List of References

Acker, T.L., L.E. Buja, J.M. Rosinski, J.E. Truesdale, 1996: User's Guide to NCAR CCM3, NCAR Technical Note/TN-421+IA, Boulder, Colorado.

Allen, J. C., and D. F. Barnes, 1985: The causes of deforestation in developing countries. Annals, Association of American Geographers 75, 163-184.

Anthes, R. A., E. Y. Hsie, and Y. H. Kuo, 1987: Description of the Penn State/NCAR Mesoscale Model Version 4 (MM4). NCAR Tech. Note, NCAR/TN-282+STR.

Anyamba, E.K.,1983: On the monthly mean lower tropospheric circulations during the 1961/62 floods in East Africa, MSc. Thesis, University of Nairobi.

Ba, M. B., and S. E. Nicholson, 1998: Analysis of convective activity and its relationship to the rainfall over the rift valley lakes of east Africa during 1983-90 using the meteosat infrared channel. J. Appl. Meteor., 37, 1250-1264.

Bates, G. T., F. Giorgi, and S. W. Hostetler 1993: Toward the simulation of the effects of the Great Lakes on regional climate. Mon. Wea. Rev., 121, 1373-1387.

Bath, L.M., J. Rosinski, and J. Olson, 1992: User's Guide to NCAR CCM2, NCAR Technical Note/TN-379+IA, Boulder, Colorado.

Beletsky, D., O'Connor, W.P., Schwab, D.J., and Dietrich, D.E., 1997: Numerical Simulation of Internal Kelvin Waves and Coastal Upwelling Fronts. Journal of Physical Oceanography, 27(7), 1197-1215.

Bonan, G.B., 1996: A Land Surface model (LSM version 1.0) for Ecological,

Hydrological, and Atmospheric Studies: Technical Description and User's Guide, NCAR Technical Note/TN-417+STR, Boulder, Colorado.

Birkett, C, 1997: A new global lake and catchment conservation database. IDEAL Bulletin, Spring 1997, 4 pp.

Brown, R., A. Durning, C. Flavin, H. French, J. Jacobson, M. Lowe, S. Postel, M. Starke, and J. Young, 1990: State of the world 1990. A Worldwatch Institute report on progress toward a sustainable society. W. W. Norton and Company, New York - London pp 253.

Brown, L, R., D. Denniston, C. Flavin, H. French, H. Kane, N. Lenssen, M. Renner, D. Roodman, M. Ryan, A. Sachs, L. Starke, P. Weber, and J. Young, 1995: State of the world 1995. A Worldwatch Institute report on progress toward a sustainable society. W. W. Norton and Company, New York - London pp 255.

Bryan, F.O., B. Kauffman, W. Large, and P. Gent, 1996: The NCAR CSM Flux Coupler, NCAR Technical Note NCAR/TN-424+STR, Boulder, Colorado.

Bugenyi, F.W.B., and Magumba, K.M. (1996): The present physicochemical ecology of Lake Victoria, Uganda. In the Limnology, climatology and paleoclimatology of the East African lake, ed. T.C. Johnson and E. Odada. Gordon and Breach, Amsterdam, 141-154.

Charney, J. G., W. J. Quirk, S. H. Chow, and J. Kornfield, 1977: A comparative study of the effects of albedo change on drought in semi-arid regions. J. Atmos. Sci., 34, 1366-1385.

Cogley, J.G. 1991. GGHYDRO - Global Hydrographic Data Release 2.0. Trent Climate Note 91-1, dept. Geography, Trend University, Peterborough, Ontario.

Csanady, G. T., 1984: Circulation in the Coastal Ocean. D. Reidel, 279 pp.

Datta, R. R., 1981: Certain aspects of monsoonal precipitation dynamics over Lake Victoria. Monsoon Dynamics, J. Lighthill and R. P. Pearce, Eds., Cambridge University Press, 333-349.

Dickinson, R. E., and Henderson-Sellers, 1988: Modeling tropical deforestation: A study of GCM land-surface parameterizations. Quart. J. Roy. Meteorol. Soc., 114, 439-462.

Dickinson, R. E., A. Henderson-Sellers, and P. J. Kennedy, 1993: Biosphere-Atmosphere Transfer Scheme (BATS) version 1E as coupled to the NCAR Community Climate Model. NCAR Tech. Note., NCAR/TN-387+STR, 72pp.

Eltahir, E., and C. Gong, 1996: Dynamics of wet and dry years in West Africa. J. Climate, 1030-1042.

Farmer, G., 1988: Seasonal forecasting of the Kenya Coast short-rains. J. Climatol., 8, 489-497.

Flohn, H., 1987: East African rains of 1961/1962 and the abrupt change of the White Nile discharge. Palaeoecology of Africa, 18, 3-18.

Giorgi, F., and L. O. Mearns, 1991: Approaches to the simulation of regional climate changes: A review. Rev. Geophys. 29, 2, 191-216.

Giorgi, F., M. R. Marinnucci, and G. T. Bates, 1993a: Development of a second-generation regional climate model (RegCM2). Part I: Boundary-layer and radiative transfer processes. Mon. Wea. Rev., 121, 2794-2813.

Giorgi, F., M. R. Marinnucci, and G. T. Bates, 1993b: Development of a second-generation regional climate model (RegCM2). Part II: Convective processes and assimilation of lateral boundary conditions. Mon. Wea. Rev., 121, 2814-2832.

Goddard, L., N. E., Graham, 1999: The importance of the Indian ocean for GCM-based climate forecasts over eastern Africa and southern Africa. JGR (in review).

Gurney, R. J., J. L. Foster, and C. L. Parkinson, 1993: Atlas of satellite observations related to global change. Cambridge University Press, pp469.

Hack J.J., B.A. Boville, B.P. Briegleb, J.T. Kiehl, P.J. Rasch, D.L. Williamson, 1993: Description of the NCAR Community Climate Model (CCM2).

Henderson-Sellers, A., and V. Gornitz, 1984: Possible Climatic impacts of land cover transformations with particular emphasis on tropical deforestation. Clim. Change, 6, 231-257.

Holton, J. D., 1972: An introduction to dynamic meteorology. Academic, New York, 319 pp.

Holtslag, A. A. M., E. I. F. de Bruijin, and H. L. Pan, 1990: A high resolution air mass transformation model for short-range weather forecasting. Mon. Wea. Rev., 118, 1561-1575.

Hoskins, B. J. and D. Karoly, 1981: The steady linear response of a spherical atmosphere to thermal and orographic forcing. J. Atmos. Sci. 38, 1179-1196.

Hostetler, S. W., G. T. Bates, and F. Giorgi, 1993: Interactive nesting of a lake thermal model within a regional climate model for climate change studies. J. Geophys. Res., 98, 5045-5057.

Flohn, H., 1987: East African rains of 1961/1962 and the abrupt change of the White Nile discharge. Palaeoecology of Africa, 18, 3-18.

Indeje, M., F. H. M. Semazzi, and L. J. Ogallo, 2000: ENSO Signals in East African Rainfall Seasons. Int. J. Climatol. 20, 19-46.

Indeje, M., and F. H. M. Semazzi, 2000: Relationships between QBO in the lower equatorial stratospheric zonal winds and East African seasonal rainfall. Meteorol. Atmos. Phy. 73, 227-244.

Indeje, M., 2000: Prediction and Numerical Simulation of the Regional Climate of Equatorial Eastern Africa. PhD thesis, North Carolina State University.

Ininda, J. M., 1994: Simulation of the impact of sea surface temperature anomalies on the short rains over East Africa. J. African. Met. Soc., 3, 127-138.

International CLIVAR Project Office Report (ICPO), 2000: Climate Research for Africa. WCRP Informal Report No. 16/1999; ICPO Publication Series No. 29.

IPCC, WGII 1998: The regional impacts of climate change. An Assessment of vulnerability, R. T. Watson, M. C. Zinyowera, and R. H. Moss (eds.), Cambridge University Press, New York, USA.

Johnson, T. C., 1997: Personal Communication.

Kalnay, E., and M. Halem, 1981: Large amplitude stationary Rossby waves in the southern hemisphere. Proc. Int. Conf. Early results of FGGE and Large scale aspects of its Monsoon Experiments, Tallahassee, ICU/WMO 3.5-3.15.

Kalnay, E., M. Kingtse, and J. Peagle, 1986: Large-scale amplitude short-scale stationary Rossby waves in the southern hemisphere: Observations and mechanistic experiments to determine their origin. J. Atmos. Sci., 252-275.

Kelly, J. G. W., J. S. Hobgood, K. W. Bedford and D. J. Schwab, 1998: Generation of three-dimensional lake model forecasts for Lake Erie. Weather and Forecasting, 13, 659-687.

Kendall R. L., 1969: The ecological history of the lake Victoria basin. Ecological Monographs, 39, 121-176.

Kiehl, J.T., J. Hack, G. Bonan, B. Boville, B. Briegleb, D. Williamson, and P. Rasch, 1996: Description of the NCAR Community Climate Model (CCM3), NCAR Technical Note NCAR/TN-420+STR, Boulder, Colorado.

Krishnamurti, T. N., and L. J. Ogallo, 1989: Recent African Climate. Report No. FSU-89-13.

Lehman J. T., 1997: How climate change is shaping Lake Victoria. IDEAL Bulletin, Spring 1997, 1-2.

Livingstone, D. A., 1994: Evolution of African climate. Biological relationships between Africa and South America., P. Goldblatt, ed., Yale University Press, New Haven.

Malingreau, J. P., C. J. Tucker, and N. Laporte, 1989: AVHRR for monitoring global tropical deforestation. Int. J. Remote Sensing, 10, 866-867.

Matthews, E . 1983: Global vegetation and land use. Journal of Climate and Applied Meteorology 22, 474-487.

Mellor, G. L., 1991: An equation of state for numerical models of oceans and estuaries. J. Atmos. Ocean Tech., 8, 609-611.

Mellor, G. L., and Yamada, T., 1974: A heirachy of turbulence closure models for planetary boundary layers. J. Atmos. Sci., 31, 1791-1806.

Moura, A. D., L. Bengtsson, J. Buizer, A. Busalacchi, M. A. Cane, P. Lagos, A. Leetma, T. Matsuno, K. Mooney, P. Morel, E. S. Sarachick, J. Shukla, A. Sumi and M. Petterson, 1992: 'International Research Institute for Climate Prediction'. A proposal.

Muwonge M., 1994: Water Hyacinth in lake Victoria and other environmental problems. The Uganda American Focus, vol. 4, Number 2.

Nicholson, E. N., 1986: The nature of rainfall variability in Africa south of the equator. J. Climatol., 6, 515-530.

Nicholson, S. E. and Entekhabi, D., 1986. 'The quasi-periodic behavior of rainfall variability in Africa and its relationship to the Southern Oscillation', Arch., Met. Geoph. Biocl., Seri. A, 34, 311.

Nicholson, S. E., J. Kim and J. Hoopingarner, 1988: Atlas of African rainfall and its interannual variability. Dept. of Meteorology. The Florida State University, Tallahassee, Florida 32306. pp. 237.

Nicholson, S. E. and B. S. Nyenzi, 1990. 'Temporal and spatial variability of SSTs in the tropical Atlantic and Indian Oceans', Archives for Meteorology, Geophysics, and Bioclimatology, Seri. A, p. 138-146. Nicholson, S. E., 1996. A review of Climate Dynamics and Climate Variability in Eastern Africa. Johnson and Odada, op. cit., p. 57-78.

Nicholson, S. E., 1996: Victoria lake-level modeling aims to predict basin rainfall. IDEAL Bulletin, Spring 1996, 5pp.

Nobre, C., P. J. Sellers, and J. Shukla, 1991: Amazonian deforestation and regional climate change. J. Clim., 4, 957-988.

Ochumba, P.B.O. (1996): Measurement of water currents, temperature, dissolved oxygen and winds on the Kenyan Lake Victoria. In The limnology, climatology and paleoclimatology of the East African lake, ed. T.C. Johnson and E. Odada. Gordon and Breach, Amsterdam, p. 155-167.

O'Connor, W.P., and Schwab, D.J., 1994: Sensitivity of Great Lakes Forecasting System Nowcasts to Meteorological Fields and Model Parameters, in: M.L. Spaulding, K. Bedford, A. Blumberg, R. Cheng, and C. Swanson (eds.), Estaurine and Coastal Modeling III, Proceedings of the 3rd International Conference, Sept. 8-10, 1993, Oak Brook, IL, American Society of Civil Engineers, New York, NY, 149-157.

Ogallo, L.J., 1988: Relationships between seasonal rainfall in East Africa and the South Oscillation. Int. J. Climatol. 8, 31-43.

Ogallo, L.J., 1989: The spatial and temporal patterns of the East African seasonal rainfall derived from principal component analysis. Int. J. Climatol. 9, 145-167.

Okeyo, A.E; 1987: The influence of Lake Victoria on the convective activities over the Kenya highlands. J. Meteor. Soc. Japan, Special Volume , 689-695.

Olson, J. S., J. A. Watts and Allison, L.J. 1983. Carbon in live vegetation of major world ecosystems. ORNL-5862. Oak Ridge National Laboratory, Oak Ridge, TN.

Schwab, D.J., 1977: Internal free oscillations in Lake Ontario. Limnol. Oceanogr., 22,700-708

Schwab, D.J., O'Connor, W.P., and Mellor, G.L., 1995: On the Net Cyclonic Circulation in Large Stratified Lakes, Journal of Physical Oceanography, 25(6), Part II, 1516-1520.

Schwab, D.J., Beletsky, D., O'Connor, W.P., and Dietrich, D.E., 1996: Numerical Simulation of Internal Kelvin Waves with z-level and Sigma Level Models, in: M.L. Spaulding and R.T. Cheng (eds.), Estaurine and Coastal Modeling,

Proceedings of the 4th International Conference, Oct. 26-28, 1995, San Diego, CA, American Society of Civil Engineers, New York, NY, 298-312.

Semazzi, H. F. M., 1980a: Stationary barotropic flow induced by a mountain over a tropical belt. Mon. Mea. Rev., 108, 922-930.

Semazzi, H. F. M., 1980b: Numerical experiments on the orographic dynamic phenomenon over a tropical belt. Arch. Met. Geoph. Biokl., Ser. A., 29, 55-65.

Semazzi, H. F. M., 1985: An investigation of the equatorial orographic dynamic mechanism. J. Atmos. Sci., 42, 38-83.

Semazzi, H.F.M., N.-H. Lin, Y.-L. Lin and F. Giorgi, 1993. A CCM1-MM4 nested model study of the influence of sea-surface temperature anomalies on the Sahelian Climate. JGL, 20, 2897-2900.

Semazzi, H. F. M., B. Burns, N. H. Lin and J. E. Schemm, 1996: A GCM Study of the Teleconnections Between the Continental Climate of Africa and Global Sea-Surface Temperature Anomalies. Journal of Climate, 9, 2480-2497.

Semazzi, H.F.M., and L. Sun, 1997: The role of orography in determining the Sahelian climate. Intern. J. Climatolo. 17, 581-596.

Semazzi, H. F. M., and M. Indeje, 1999: Inter-seasonal variability of ENSO rainfall signal over Africa. J. Afri. Meteorol. Soc. 4, 81-94.

Semazzi, H. F. M., 1999: Development of a regional climate prediction model for the Lake Victoria basin. IDEAL Bulletin, Summer, 1999, p. 10-11.

Shukla, J., Nobre, and P. J. Sellers, 1990: Amazon deforestation and climate change. Science, 247, 1322-1325.

Song, Y., F. H. M. Semazzi and L. Xie, 2000: Development of a Coupled Regional Climate Simulation Model for the Lake Victoria Basin. Chapter in IDEAL book, in review.

Spigel, R. H., and G. W. Coulter, 1996: Comprison of hydrology and physical limnology of the east African great lakes: Tanganyika, Malawi, Victoria, Kivu and Turkana (with reference to some North American Great Lakes), The Limnology, Climatology and Paleoclimatology of the east African lakes, Gordon and Breach Publishers, 103-139.

Stager J. C., P. N. Reinthal, and D. A. Livingstone, 1986: A 25,000-year history for lake Victoria, East Africa, and some comments on its significance for the evolutiopn of cichlid dishes. Freshwater Biology, 16, 15-19.

Sud, Y.C. and W.E. Smith, 1985: The influence of surface roughness of deserts on the July circulation. Boundary-Layer Meteorol., 33, 15-49.

Sud, Y.C., J. Shukla and Y. Mintz, 1988: Influence of land surface roughness on atmospheric circulation and precipitation: A sensitivity study with a general circulation model. J. Appl. Meteorol., 27, 1036-1054.

Sun, L., F. H. M. Semazzi, F. Giorgi and L. Ogallo, 1998a. 'Application of NCAR Regional Climate Model to eastern Africa. Part I: Simulation of the Autumn rains of 1988', J. Geoph. Res., 104, 6529-6548.

Sun, L., F. H. M. Semazzi, F. Giorgi and L. Ogallo, 1998b. 'Modeling study of the interannual variability of the Autumn rains over eastern Africa', J. Geoph. Res., 104, 6549-6562.

Talling, J. F. (1969) The incidence of vertical mixing, and some biological and chemical consequences, in tropical African lakes. Verh. Int. Ver. Limnol., 17, 998-1012.

Tucker, C. J., B. N. Holben, and T. E. Goff, 1984: Intensive forest clearing in Rondonia, Brazil, as detected by remote sensing. Remote Sensing of Environment, 15, 255-262.

Webb, R.S., C.E. Rosenzweig and E.R. Levine, 1993: Specifying land surface characteristics in general circulation models: soil profile data set and derived water-holding capacities. Global Biogeochemical cycles 7:97-108.

Williamson, D.L. and P.J. Rasch, 1989: Two-Dimensional Semi-Lagrangian Transport

with Shape Preserving Interpolation, Mon. Wea. Rev., 117, 102-129.

Williams, M., 1990: Forests transformed by human action: global and regional changes in the biosphere over the past 300 years. Eds. B.L. Turner et al., Cambridge University Press, New York pp 179-201.

Xie, L., L.J. Pietrafesa, E. Bohm, C. Zhang and X. Li, 1998: Evidence and mechanism of hurricane Fran-induced ocean cooling in the Charleston trough. Geophysical Research Letters, 25, 769-772.

Yin, X., and S. E. Nicholson, 1998: The water balance of Lake Victoria. Hydrological Sciences Journal, 43, 789-811.

Zhang, H., A. Henderson-Sellers, and K. McGuffie, 1996a: Impacts of tropical deforestation. Part I: Process analysis of local climate change. J. Climate, 9, 1497-1517.

Zhang, H., K. McGuffie, and A. Henderson-Sellers, 1996b: Impacts of tropical deforestation. Part II: The role of large scale dynamics. J. Climate, 9, 2498-2521.

Zheng, X., and E. Eltahir, 1998: The role of vegetation in the dynamics of West African monsoons. J. Climate, 2078-2096.

Zinyowera, M. C., and S. L. Unganai, 1993: Drought in southern Africa. An update on the 1991-92 drought. Drought Network News Int., 4(3), 3-4.